

Constraining spherically symmetric metrics by the gap between photon rings

Fabio Aratore,^{1,2,*} Oleg Yu. Tsupko,^{3,4,†} and Volker Perlick^{3,‡}

¹*Dipartimento di Fisica “E.R. Caianiello”, Università degli studi di Salerno,
Via Giovanni Paolo II 132, I-84084 Fisciano SA, Italy*

²*Istituto Nazionale di Fisica Nucleare (INFN), Sezione di Napoli -
Gruppo collegato di Salerno, Via Cintia, 80126 Napoli NA, Italy*

³*ZARM, University of Bremen, 28359 Bremen, Germany*

⁴*Space Research Institute of Russian Academy of Sciences, Profsoyuznaya 84/32, Moscow 117997, Russia*

(Dated: February 23, 2024)

Gravitational lensing of luminous matter that surrounds a black hole or some other sufficiently compact object produces an infinite sequence of images. Besides the direct (or primary) image, it comprises demagnified and deformed replicas of the original known as photon rings which are progressively nearing the boundary of the so-called shadow. In the present paper, we present analytical approximation formulas for higher-order photon rings for an asymptotically flat, static, spherically symmetric spacetime that admits a photon sphere. We consider a geometrically thin disk of light sources in the equatorial plane and an observer at arbitrary inclination far away from the center. Fixing the emission radius and leveraging the strong deflection limit, which provides an analytical logarithmic approximation for the deflection angle, we find the deformed shape of higher-order photon rings in the form of a polar equation on the observer’s screen. It has been suggested by other authors to use the relative size of photon rings for characterizing the underlying spacetime. In particular, the relative separation between two neighboring photon rings, which we call “gap parameter”, was considered. We analytically calculate the gap parameter of higher-order photon rings for metrics of the considered class that may depend on multiple parameters. The advantage of using this quantity is in the fact that, to within the assumed approximations, it is independent of the mass of the central object (or of some other characteristic parameter if the mass is zero) and of the distance of the observer. Measurements of the gap parameter, which may become possible in the near future, will restrict the spacetime models that are in agreement with the observations. Even without knowing the inner and outer radii of the shining disk, it will conclusively rule out some metrics. We exemplify our calculations of the gap parameter with the Schwarzschild, Reissner-Nordström, Janis-Newman-Winicour and Ellis wormhole metrics.

I. INTRODUCTION

Black holes and other sufficiently compact objects can cause arbitrarily large deflections of light rays. In particular, photons can loop around a black hole arbitrarily many times. In the case of a spherically symmetric and static spacetime, this leads to the formation of a *photon sphere*, which is a sphere $r = \text{const.}$ such that every light ray remains on this sphere if it starts tangentially to it. If the spacetime is asymptotically flat, the outermost photon sphere is necessarily unstable in the sense that other light rays can approach it from above in an asymptotic spiral motion; this can be easily verified with the help of the standard effective potential for lightlike geodesics. This leads to the formation of an infinite sequence of images of each light source. These images can be labeled by a natural number 0, 1, 2, 3, etc., called its *order*, which counts how often the orbit meets the axis, that is the straight line through the observer position and the origin of the coordinate system. (This definition is unambiguous and convenient, but it is restricted to spherically symmetric and static spacetimes. In the case of the

Kerr spacetime and an observer off the equatorial plane, the images are sometimes labeled by counting how often the corresponding light ray crosses the equatorial plane.) The image of order 0 is called the *primary* (or *direct*) image, the image of order 1 is called the *secondary* image and all other images are called *higher-order* images. (For an illustration of images of a thin accretion disk, see, e.g., Fig. 1 in Ref.[1]). In the case of perfect alignment the observer sees an infinite sequence of *Einstein rings* [2–7]. (Einstein rings are sometimes called *Chwolson rings*, referring to a pioneering paper by Chwolson [8].) The existence of a photon sphere and the formation of higher-order images are closely related to the fact that a black hole or another sufficiently compact object casts a *shadow* [9, 10]: it displays a dark disk on the sky of an observer whose boundary corresponds to past-oriented light rays from the observer position that spiral towards the photon sphere, for reviews see [11, 12]. With increasing order the images of a light source become fainter and fainter and approach the boundary of the shadow.

The existence of a photon sphere and the resulting observational phenomena have firstly been discussed for the Schwarzschild metric: In this case the existence of a photon sphere, at $r = 3m$ in standard notation, is known since the early days of general relativity, see Hilbert [13]. Much later, Darwin [14] observed that this leads to the formation of an infinite sequence of images and that the

* faratore@unisa.it

† tsupkooleg@gmail.com; tsupko@cosmos.ru

‡ perlick@zarm.uni-bremen.de



Article submitted to journal

Subject Areas:Particle physics, gauge symmetries,
cosmology**Keywords:**Cosmological constant, Emergent
gauge symmetry, Hierarchy puzzle,
Higgs boson, Dark matter**Author for correspondence:**

Steven D. Bass

e-mail: Steven.Bass@cern.chThe cosmological constant
and scale hierarchies with
emergent gauge symmetriesSteven D. Bass^{1,2}¹Kitzbühel Centre for Physics, Kitzbühel Austria²Marian Smoluchowski Institute of Physics,
Jagiellonian University, Kraków, Poland

Motivated by the stability of the electroweak Higgs vacuum we consider the possibility that the Standard Model might work up to large scales between about 10^{10} GeV and close to the Planck scale. A plausible scenario is an emergent Standard Model with gauge symmetries originating in some topological like phase transition deep in the ultraviolet. In this case the cosmological constant scale and neutrino masses should be of similar size, suppressed by factor of the large scale of emergence. The key physics involves a subtle interplay of Poincaré invariance, mass generation and renormalisation group invariance. The Higgs mass would be environmentally selected in connection with vacuum stability. Consequences for dark matter scenarios are discussed.

Baryogenesis and leptogenesis with relativistic bubble walls

Miguel Vanvlasselaer^{a,*}

^a*Theoretische Natuurkunde and IIHE/ELEM, Vrije Universiteit Brussel, & The International Solvay Institutes, Pleinlaan 2, B-1050 Brussels, Belgium*

E-mail: *miguel.vanvlasselaer@vub.be

In this talk, we study the impact of first order phase transitions with fast bubble walls on mechanisms of leptogenesis and baryogenesis. We begin our exploration with the usual leptogenesis where the breaking of $B - L$ occurs via a PT with fast walls. Then we move to a more exotic case where the $B - L$ breaking phase transition creates heavy particles in the plasma and catalyzes the leptogenesis. Finally, we apply the same production mechanism to the EWPT at low energy and build a new model of EWBG. Those models are all original and contain crucial new phenomenological aspects like the emission of large amount of Gravitational waves.

Corfu Summer institute 2023: "Workshop on Theoretical Particle Cosmology in the Early and Late Universe"

APRIL 30 - MAY 6, 2023

Corfu, Greece.

*Speaker

© Copyright owned by the author(s) under the terms of the Creative Commons Attribution-NonCommercial-NoDerivatives 4.0 International License (CC BY-NC-ND 4.0).

<https://pos.sissa.it/>

Baryogenesis and leptogenesis with relativistic bubble walls

Miguel Vanvlasselaer

1. Introduction

One of the greatest puzzles of the early universe cosmology is the origin of the observed excess of matter over anti-matter, which is commonly parameterized by

$$Y_B \equiv \frac{n_B - n_{\bar{B}}}{s} \Big|_0 = (8.75 \pm 0.23) \times 10^{-11} \quad (1)$$

with n_B , $n_{\bar{B}}$ and s respectively the number density of baryons, anti-baryons and the entropy density. The second equality comes from Planck data and evolution models of the early universe[1]. Within the inflationary paradigm, this asymmetry calls for an explanation in terms of early universe dynamics, a dynamics which is called *baryogenesis*. For a successful baryogenesis scenario, the well-known Sakharov requirements should be satisfied [2], namely the violation of the baryon number, violation of C and CP symmetries, and the presence of an out-of-equilibrium process. Many different mechanisms can fulfil those requirements, see [3, 4] for extensive reviews. On the top of this, baryogenesis mechanisms can be broadly classified into two different categories, depending of the SM sectors where the asymmetry originally forms: in the baryon sector, in the case of the original *baryogenesis scenario* or in the lepton sector, in the case of the so-called *leptogenesis scenario*[5].

First order phase transitions are very efficient ways to fulfil the out-of-equilibrium criterion, and it is used namely in the case of *electroweak baryogenesis* [6, 7]. Several BSM models could make the EWPT first order[8–12] (see [13] for review). However, relativistic bubble walls were believed to *suppress* the final baryon asymmetry[14–17].

In this paper we propose to reconsider this belief by discussing situations in which ultra-relativistic bubble walls actually can enhance the baryon/lepton asymmetry. We will discuss three different types of models taking advantage of fast walls: in section 3, we study the usual leptogenesis catalized by a phase transition (see also [18] for another viable model). The Right-Handed Neutrinos (RHN) abruptly receive a large mass upon crossing the bubble wall, and decay all together, suppressing the wash-outs.

In section 4, we study another model of leptogenesis catalized via the production of heavy states, which we identify with Majorana neutrinos. The idea is based on the observation in[19] that an ultra-relativistic bubble wall with Lorentz factor $\gamma_w \gg 1$, can produce in the plasma particles with mass up to $M \lesssim \sqrt{\gamma_w T_{\text{nuc}} \times v}$, where T_{nuc} and v are the nucleation temperature of FOPT and the scale of the symmetry breaking respectively. Beside being an out-of-equilibrium production channel, we will also show that this production mechanism can be naturally CP-violating. We confirm the statements above by analyzing the CP-violating effects in the interference of tree and one loop level processes.

Finally, in section 5, we study a model for which the Electroweak phase transition, again with fast bubble walls, produces heavy states and catalyzes EWBG.

One of the interesting feature of the class of models we discuss in this paper is that it requires ultra-relativistic bubble wall velocities and strong phase transition, and then is generically accompanied with strong gravitational waves signal.

High Frequency Gravitational Wave Bounds from Galactic Neutron Stars

V. Dandoy^a T. Bertólez-Martínez^b F. Costa^c

^a*Service de Physique Theorique, C.P. 225, Université Libre de Bruxelles, Boulevard du Triomphe, B-1050 Brussels, Belgium*

^b*Departament de Física Quàntica i Astrofísica and Institut de Ciències del Cosmos, Universitat de Barcelona, Diagonal 647, E-08028 Barcelona, Spain*

^c*Institute for Theoretical Physics, Georg-August University Göttingen, Friedrich-Hund-Platz 1, Göttingen, D-37077 Germany*

E-mail: virgile.dandoy@ulb.be, antoni.bertolez@fqa.ub.edu, francesco.costa@theorie.physik.uni-goettingen.de

ABSTRACT: High-Frequency Gravitational Waves (HFGWs) constitute a unique window on the early Universe as well as exotic astrophysical objects. If the current gravitational wave experiments are more dedicated to the low frequency regime, the graviton conversion into photons in a strong magnetic field constitutes a powerful tool to probe HFGWs. In this paper, we show that neutron stars, due to their extreme magnetic field, are a perfect laboratory to study the conversion of HFGWs into photons. Using realistic models for the galactic neutron star population, we calculate for the first time the expected photon flux induced by the conversion of an isotropic stochastic gravitational wave background in the magnetosphere of the ensemble of neutron stars present in the Milky Way. We compare this photon flux to the observed one from several telescopes and derive upper limits on the stochastic gravitational wave background in the frequency range 10^8 Hz - 10^{25} Hz. We find our limits to be competitive in the frequency range 10^8 Hz - 10^{15} Hz.

Upper Bound on the Speed of Sound in Nuclear Matter from Transport

Mauricio Hippert,^{1,2} Jorge Noronha,^{1,2} and Paul Romatschke^{3,4}

¹*Illinois Center for Advanced Studies of the Universe,
University of Illinois Urbana-Champaign, Urbana, IL 61801, USA*

²*Department of Physics, University of Illinois Urbana-Champaign, Urbana, IL 61801, USA*

³*Department of Physics, University of Colorado, Boulder, Colorado 80309, USA*

⁴*Center for Theory of Quantum Matter, University of Colorado, Boulder, Colorado 80309, USA*

We point out that there is an upper bound on the speed of sound squared given by $c_s^2 \leq 0.781$ valid for all known systems described by relativistic transient hydrodynamics where calculations of certain ratios of hydrodynamic transport coefficients can be performed from first principles. Assuming this bound is valid for ultradense matter implies that the maximum mass of isolated (non-rotating) neutron stars cannot be larger than 2.7 solar masses.

I. INTRODUCTION

The measurements of neutron stars with masses $\gtrsim 2 M_\odot$ (where M_\odot is the mass of the sun) [1–3] suggest that the cold neutron star equation of state (EoS) is stiff enough such that its speed of sound, c_s , surpasses its conformal limit, $c_s \leq 1/\sqrt{3}$, at a given density [4]. This is also supported by the binary neutron-star merger gravitational-wave event GW170817 [5–7], which further constrained the masses and effective tidal deformability of the inspiraling neutron stars [8–16]. Further support to a supraconformal speed of sound may come from the observation of gravitational waves from the merger of a black hole with a compact object of mass $2.6 M_\odot$ [17], if the latter is a neutron star [18–23].

Due to asymptotic freedom [24, 25], the speed of sound in QCD is expected to approach the conformal limit from below at sufficiently large densities [26, 27]. This fact, combined with the knowledge about the nuclear physics equation of state at low densities [8, 28–30] and the recent observation of large neutron star masses, implies that c_s in QCD is not monotonic as this quantity must display at least one peak as a function of density (when taking into account the region of asymptotically large density). Assuming there is only a single peak, essential questions are: (i) How large is c_s at the peak? (ii) At what density does c_s peak? (iii) What is the correct effective theory of ultradense matter that explains the answers to (i) and (ii)? Ultimately, future observations [31–34] will constrain the answer to (i) and (ii) [35–41] and provide useful guidance towards answering (iii).

Relativistic causality and covariant stability [42] impose that the speed of sound cannot surpass the speed of light, i.e., $c_s \leq 1$. At high temperatures and zero baryon chemical potential, lattice QCD calculations [43, 44] and holographic models [45–48] find that the conformal limit for the speed of sound is respected, $c_s \leq 1/\sqrt{3}$. At nonzero baryon density, however, discussions concerning the (subluminal) upper bound to the speed of sound go back several decades [49–52]. It is now known that the speed of sound can surpass the conformal result in a variety of systems such as QCD at large isospin density [53], two-color QCD [54], holographic models [55–59], re-

summed perturbation theory [60, 61], quarkyonic matter [62–66], and other models at high density [67–82]. However, despite recent progress [83, 84], very little is known about the transport properties of ultradense matter when the speed of sound nears the speed of light.

In this work, we point out that ultradense matter with nearly luminal speed of sound must have very unusual transport properties. We discuss a scenario where fundamental properties of thermodynamics and transport in relativity can constrain the equation of state of ultradense matter. Assuming the validity of relativistic transient hydrodynamics in which dissipative stresses obey additional relaxation equations [85], we argue that causality and stability of matter imply that there is an upper bound on the speed of sound squared given by $c_s^2 \leq 0.781$ in all known systems¹ where calculations of certain ratios of first-order hydrodynamic transport coefficients and their corresponding relaxation times can be performed from first principles. In this case, a violation of the bound implies that such systems either exhibit very unusual transport coefficients or cannot be consistently described by transient fluid dynamics², signaling the presence of exotic transport behavior that simple relaxation dynamics cannot describe.³ Given current astrophysical constraints, we show that imposing this bound on c_s implies that the maximum mass of an isolated neutron star is bound by $M < 2.7 M_\odot$, assuming chiral effective theory is valid up to two times saturation density. Therefore, the new transport bound provides further support to the claim that the $2.6 M_\odot$ compact object observed to merge with a $23 M_\odot$ black hole causing the GW190814 event [17] can be a neutron star.

¹ We only consider systems where the equilibrium state is unique and the correlation length is finite.

² This is not connected to the non-analytic behavior induced by the backreaction of sound waves [86].

³ While unusual transport coefficients can be expected from superfluid phases, the onset of superfluidity leads to multiple sound modes [87], which makes causality and stability analyses considerably more convoluted [88]. Therefore, we leave the exploration of superfluid states to future work. However, we note that our bound holds even in the case of a pion condensate, where a global $U(1)$ symmetry is spontaneously broken [53, 89, 90] (see Fig. 1).

New Mass Window for Primordial Black Holes as Dark Matter from Memory Burden Effect

Ana Alexandre,^{1,2,*} Gia Dvali,^{1,2} and Emmanouil Koutsangelas^{1,2,†}

¹ *Arnold Sommerfeld Center, Ludwig-Maximilians-Universität, Theresienstraße 37, 80333 München, Germany,*

² *Max-Planck-Institut für Physik, Föhringer Ring 6, 80805 München, Germany*

(Dated: Friday 23rd February, 2024, 2:05am)

The mass ranges allowed for Primordial Black Holes (PBHs) to constitute all of Dark Matter (DM) are broadly constrained. However, these constraints rely on the standard semiclassical approximation which assumes that the evaporation process is self-similar. Quantum effects such as memory burden take the evaporation process out of the semiclassical regime latest by half-decay time. What happens beyond this time is currently not known. However, theoretical evidence based on prototype models indicates that the evaporation slows down thereby extending the lifetime of a black hole. This modifies the mass ranges constrained, in particular, by BBN and CMB spectral distortions. We show that previous constraints are largely relaxed when the PBH lifetime is extended, making it possible for PBHs to constitute all of DM in previously excluded mass ranges. In particular, this is the case for PBHs lighter than 10^9 g which enter the memory burden stage before BBN and are still present today as DM.

I. INTRODUCTION

Since it was first proposed that black holes could form from primordial fluctuations [1–3], the possibility of Primordial Black Holes (PBH) constituting all or part of the Dark Matter (DM) in the Universe has been considered [4]. This possibility has recently seen a renewed interest as a result of the LIGO detection of merging black hole binaries with masses around $1 - 50M_\odot$ [5] whose formation is not easily explained by astrophysical processes. Although at the moment there is no observational evidence for their existence, several constraints have been put on the fraction of DM in the form of PBHs [6–8], defined as

$$f_{PBH}(t) \equiv \frac{\rho_{PBH}(t)}{\rho_{DM}(t)}, \quad (1)$$

for different values of the PBH mass M in terms of physical time t . Currently, there are only a few mass ranges of interest that still leave the door open for $f_{PBH} = 1$ (for a review on PBHs, see [9]).

Another important point of interest is that PBHs are the only ones that can be small enough for Hawking radiation to be relevant [10]. For a PBH forming from primordial fluctuations, its mass should be comparable to the horizon mass at the time of its formation, t_f . Assuming this takes place during radiation domination, we

can estimate it as

$$M \sim \rho V \Big|_{t_f} \sim \frac{M_{\text{P}}^2}{H} \Big|_{t_f} \sim M_{\text{P}} t_f. \quad (2)$$

Here, ρ denotes the total energy density of the universe, H , the Hubble parameter and, $V(t) \sim H(t)^{-3}$, the Hubble volume.

The standard Hawking evaporation time, which describes the lifetime of a PBH of mass M , can be expressed as

$$t_H \sim r_g S \sim \frac{M^3}{M_{\text{P}}^4}, \quad (3)$$

where

$$r_g \sim \frac{M}{M_{\text{P}}^2}, \quad S \sim \left(\frac{M}{M_{\text{P}}} \right)^2, \quad (4)$$

denote the gravitational radius and entropy of the black hole, respectively. In this scenario, for a PBH to be present in the Universe today, its mass must be larger than $M \sim 10^{14}$ g, meaning that smaller PBHs cannot account for any DM.

However, this estimate is based on the semi-classical evaporation scenario which relies on the assumption of self-similarity. That is, during its evaporation, a black hole gradually shrinks in size while maintaining the standard semi-classical relations between its parameters, such as its mass, the radius and the temperature. Notice that this is a very strong assumption, since the evaporation rate has been reliably derived exclusively for a black hole of a fixed radius and in exact-zero back-reaction limit: there exists no reliable semi-classical calculation

*Electronic address: alexand@mpp.mpg.de

†Electronic address: emi@mpp.mpg.de

Perturbative reheating and thermalization of pure Yang-Mills plasma

Kyohei Mukaida^{◦,△}, Masaki Yamada^{•,▲}

[◦] *Theory Center, IPNS, KEK, 1-1 Oho, Tsukuba, Ibaraki 305-0801, Japan*

[△] *Graduate University for Advanced Studies (Sokendai),
1-1 Oho, Tsukuba, Ibaraki 305-0801, Japan*

[•] *FRIS, Tohoku University, Sendai, Miyagi 980-8578, Japan*

[▲] *Department of Physics, Tohoku University, Sendai, Miyagi 980-8578, Japan*

Abstract

We investigate the thermalization of high-energy particles injected from the perturbative decay of inflaton during the pre-thermal phase of reheating in detail. In general, thermalization takes a relatively long time in a low-temperature plasma; therefore, the instantaneous thermalization approximation is not justified, even for the reheating of the Standard Model (SM) sector. We consider a pure Yang–Mills (YM) theory as an approximation of the SM sector or a possible dark sector, considering the Landau–Pomeranchuk–Migdal effect, a quantum interference effect in a finite temperature plasma. We perform the first numerical calculation to solve the time evolution of the system, including the redshift due to the expansion of the Universe, and show the details of the temperature evolution near the maximum and the behavior of the quasi-attractors at later times. The maximal temperature T_{\max} and time scale t_{\max} are determined quantitatively, such as $T_{\max} \simeq 0.05 \times (\Gamma_I M_{\text{Pl}}^2 / m_I^3)^{2/5} m_I$ and $t_{\max} \simeq 2 \times 10^3 \times (\Gamma_I M_{\text{Pl}}^2 / m_I^3)^{-3/5} m_I^{-1}$ in the SM-like system, where m_I and Γ_I are the mass and decay rate of inflaton. We also provide a similar formula for pure $SU(N)$ and $SO(N)$ YM theories for general values of N and coupling constant α , including $T_{\max} \propto \alpha^{4/5}$ and $t_{\max} \propto N^{-2} \alpha^{-16/5}$ behaviors and their numerical coefficients. The thermalization occurs in a finite time scale, resulting in a lower maximal temperature of the Universe after inflation than that under the instantaneous thermalization approximation.

Quark stars in massive gravity might be candidates for the mass gap objects

J. Sedaghat^{1*}, B. Eslam Panah^{2,3,4†}, R. Moradi^{5‡}, S. M. Zebarjad^{1§}, and G. H. Bordbar^{1¶}

¹ *Department of Physics, Shiraz University, Shiraz 71454, Iran*

² *Department of Theoretical Physics, Faculty of Science, University of Mazandaran, P. O. Box 47415-416, Babolsar, Iran*

³ *ICRANet-Mazandaran, University of Mazandaran, P. O. Box 47415-416, Babolsar, Iran*

⁴ *ICRANet, Piazza della Repubblica 10, I-65122 Pescara, Italy*

⁵ *Key Laboratory of Particle Astrophysics, Institute of High Energy Physics, Chinese Academy of Sciences, Beijing 100049, China.*

We have investigated the structural properties of strange quark stars (SQSs) in a modified theory of gravity known as massive gravity. In order to obtain the equation of state (EOS) of strange quark matter, we have employed a modified version of the Nambu-Jona-Lasinio model (MNJL) which includes a combination of NJL Lagrangian and its Fierz transformation by using weighting factors $(1 - \alpha)$ and α . Additionally, we have also calculated dimensionless tidal deformability (Λ) in massive gravity. To constrain the allowed values of the parameters appearing in massive gravity, we have imposed the condition $\Lambda_{1.4M_\odot} \lesssim 580$. Notably, in the MNJL model, the value of α varies between zero and one. As α increases, the EOS becomes stiffer, and the value of Λ increases accordingly. We have demonstrated that by softening the EOS with increasing the bag constant, one can obtain objects in massive gravity that not only satisfy the constraint $\Lambda_{1.4M_\odot} \lesssim 580$, but they also fall within the unknown mass gap region ($2.5M_\odot - 5M_\odot$). To establish that the obtained objects in this region are not black holes, we have calculated Schwarzschild radius, compactness, and $\Lambda_{M_{TOV}}$ in massive gravity.

I. INTRODUCTION

The gravitational wave (GW) events offer new insights into compact stars. The binary merger GW170817 [1] and its electromagnetic counterpart [2] have led to new constraints on the maximum mass of neutron stars (NSs). Based on GW170817, the upper bound of M_{TOV} for NSs is predicted as $\sim (2.3 - 2.4)M_\odot$ [3, 4]. However, there are other observations of pulsars and binary mergers with masses greater than these values such as PSR J0952-0607 [5], the secondary component of GW190814 [6, 7] and the remnants of GW170817 [8] and GW190425 [9] which fall within the unknown mass gap region ($2.5M_\odot \lesssim M \lesssim 5M_\odot$). This region was called a mass gap because analysis of observations of X-ray binaries revealed a small number of compact objects in this region [10–12]. Recent observed systems within this interval, show a relative gap instead of an absolute gap [13]. There are arguments that the presence or absence of mass gap objects can constrain the properties of the core-collapse supernova engine and the compact objects in the mass gap region can be created by merging lighter compact objects [14, 15]. There are two crucial reasons why objects in the mass gap region are unlikely to be neutron stars. The first reason is that for non-rotating NSs, the equation of state (EOS) must be very rigid to get such massive objects (the speed of sound is greater than 0.6 of

the speed of light) [16, 17]. Such EOSs contrast dimensionless tidal deformability (Λ) constraints obtained from GW178017, which require softer EOSs. The second reason is that for a rotating NS, the rotation rate should be close to the keplerian limit [16, 18–20]. Now, the question arises whether these objects are the smallest black holes or other forms of compact stars, like hybrid stars and self-bounded strange quark stars (SQSs).

Theoretically, strange quark matter (SQM) is formed in two classes of compact stars. i) Hybrid stars with a quark core and hadronic shells [21–26] and ii) SQSs composed of pure quark matter from the core up to the upper layers of the star [27–31]. Ever since Trazawa [32], Witten [33], and Bodmer [34] proposed SQM as the ground state of QCD, until now when the GWs have found so many binaries, the study of SQM in compact stars has always been of interest. Many studies on hybrid and quark stars have focused on recent discoveries of GWs. Refs. [35–37] study hybrid stars with constraints obtained from GW190814, GW170817, and PSR J0030+0451 [38, 39]. In Ref. [40], the properties of SQM in the bag model and non-newton gravity are investigated by the constraints obtained from GW170817 and PSR J0740+6620. In Ref. [41], the EOS of quark matter is constrained by using the bayesian statistical model and the mass and radius measurements of PSR J0030+0451 [42]. Refs. [7, 16, 43] investigate whether the secondary component of GW190814 could be a SQS. In Refs. [44, 45] the structural features of the SQSs have also been investigated using the data obtained from GWs.

GR is a successful theory of gravity. However, at large scales, it cannot explain why our universe is undergoing an accelerated cosmic expansion. This is one of the reasons why GR needs to be modified. Among various mod-

*J.Sedaghat@shirazu.ac.ir

†eslampanah@umz.ac.ir

‡Rahim.Moradi@icranet.org

§zebarjad@shirazu.ac.ir

¶ghbordbar@shirazu.ac.ir

Isotropic and anisotropic neutron star structure in 4D Einstein-Gauss-Bonnet Gravity

Gholam Hossein Bordbar*, Mohammad Mazhari and Ahmad Poostforush
Physics Department and Biruni Observatory, Shiraz University, Shiraz 71454, Iran

With regards to the coupling constant and the strong magnetic field of neutron stars, we have studied these stars in the 4D Einstein-Gauss-Bonnet (4D EGB) gravity model in order to grasp a better understanding of these objects. In this paper, we have shown that the neutron stars properties are considerably affected by the coupling constant and magnetic field. We have found that as a consequence of the strong magnetic field and the coupling constant, the maximum mass and radius of a neutron star are increasing functions of the coupling constant, while Schwarzschild radius, compactness, surface gravitational redshift, and Kretschmann scalar are decreasing functions. Additionally, our study has shown that the physical properties of a magnetized neutron star not only are greatly influenced by the strong magnetic field, but also by the anisotropy. Moreover, we have shown that to obtain the hydrostatic equilibrium configuration of the magnetized material, both the local anisotropy effect and the anisotropy due to the magnetic field should be considered. Finally, we have found that in the anisotropic magnetized neutron stars, the maximum mass and radius do not always increase with increasing the internal magnetic field.

I. INTRODUCTION

A neutron star is an ideal astrophysical laboratory for testing condensed matter physics theories and making connections between nuclear physics, particle physics, and astrophysics [1, 2]. This makes the neutron star as a valuable system to study its various properties. The purpose of present work is to evaluate the structural characteristics of isotropic and anisotropic magnetized neutron stars containing pure neutron matter. Recent observations have revealed that the neutron stars have a mass $M \geq 2.5M_{\odot}$ [3, 4].

Owing to the existence of a strong magnetic field, there is anisotropy in the magnetized neutron star pressure; therefore, the pressure is different in the radial (P_r) direction from the tangential (P_t) direction. According to available evidence [5–7], it is difficult to obtain the strength of the magnetic field inside the magnetized neutron stars, prompting researchers to develop theoretical models that can be used to analyze the influence of strong magnetic fields on the physical parameters of magnetized neutron stars. Magnetized neutron stars are classified into two groups based on their surface magnetic field. Pulsars and magnetars have different magnetic fields on their surface. Pulsars are found to have surface magnetic fields of approximately $10^{13}G$ to $10^{15}G$ [8], and magnetars are found to have surface magnetic fields of approximately $10^{16}G$ to $10^{17}G$ [9].

Einstein-Gauss-Bonnet gravity is a natural generalization of general relativity. As the most general torsion-free theory of gravity, this leads to stable second-order equations of motion in higher dimensions. A version of this theory was proposed by Lanczos [10], and later confirmed by David Lovelock [11, 12]. Because this theory shares Einstein's principle of gravity, the Einstein-Gauss-Bonnet (EGB) gravity is more suitable than other higher-curvature gravity theories. Einstein's and GB's terms are included in Lovelock's Lagrangian theory. As a result, the famous EGB gravity was proposed, which is the most straightforward nontrivial generalization of Einstein's gravity. It has been shown that static wormhole solutions in the EGB theory of gravity with higher dimensions can be found [13, 14].

A notable feature of EGB gravity in the 4-dimensional case is that the Euler-Gauss-Bonnet term becomes a topological invariant that contributes neither to equations of motion nor gravitational dynamics [15]. A recent paper by Glavan and Lin [16] proposes a modified general covariant theory of gravity in 4-spacetime dimensions ($D = 4$) that propagates only the massless graviton and bypasses Lovelock's theorem. The Einstein gravity theory with the cosmological constant is the only gravity theory that meets several conditions; metricity, diffeomorphism invariance, and second-order equations of motion. Essentially, this theory is formulated in higher dimensions, $D > 4$, and has Einstein-Hilbert terms with cosmological constants, as well as GB coupling rescaled as $\alpha/(D-4)$. 4D theory is defined as $D \rightarrow 4$. As a result, the GB invariance gives rise to the nontrivial contributions in gravitational dynamics, at the same time preserving the graviton degrees of freedom and retaining the freedom from Ostrogradsky instability [15]. This new theory is called 4D EGB gravity (see Ref. [16] for more details).

In other gravities such as $f(\mathcal{R})$ gravity, it is specifically discussed the mass-radius diagram for static neutron star models obtained by the numerical solution of modified Tolman-Oppenheimer-Volkoff equations [17]. This study explores the impact of different Lagrangians, including quadratic and cubic corrections, on the mass-radius relation.

* email address: ghbordbar@shirazu.ac.ir

Automated chemical reaction network generation and its application to exoplanet atmospheres

JEEHYUN YANG ¹ AND RENYU HU ^{1,2}

¹*Jet Propulsion Laboratory, California Institute of Technology, Pasadena, CA 91109, USA*

²*Division of Geological and Planetary Sciences, California Institute of Technology, Pasadena, CA 91125, USA*

ABSTRACT

Along with the advent of JWST and spectroscopic characterization of exoplanet atmospheres with unprecedented detail, there is a demand for a more complete picture of chemical and photochemical reactions and their impact on atmospheric composition. Traditionally, building reaction networks for (exo)planetary atmospheres involves manually tracking relevant species and reactions, a time-consuming and error-prone process. This approach's applicability is also often limited to specific conditions, making it less versatile for different planetary types. (i.e., photochemical networks for Jupiters may not be directly applicable to water-rich exoplanets). We introduce an automated approach using a computer-aided chemical reaction network generator, combined with a one-dimensional photochemical kinetic-transport model, offering significant advantages. This approach automatically selects reaction rates through a rate-based iterative algorithm and multiple refinement steps, enhancing model reliability. Also, this approach allows for the efficient simulation of diverse chemical environments, from hydrogen to water, carbon dioxide, and nitrogen-dominated atmospheres. Using WASP-39b and WASP-80b as examples, we demonstrate our approach's effectiveness, showing good agreement with recent JWST data. Our WASP-39b model aligns with prior studies and JWST observations, capturing photochemically produced sulfur dioxide. The WASP-80b model reveals an atmosphere influenced by deep interior thermochemistry and vertical mixing, consistent with JWST NIRC*am* observations. Furthermore, our model identifies a novel initial step for the N₂-NH₃-HCN pathway that enhances the efficiency of the conversion in high-temperature/pressure environments. This automated chemical network generation offers a novel, efficient, and precise framework for studying exoplanetary atmospheres, marking a significant advancement over traditional modeling techniques.

Keywords: Astrochemistry (75) — Exoplanet atmospheres (487) — Planetary atmospheres (1244) — Exoplanet atmospheric composition (2021) — Theoretical models (2107)

1. INTRODUCTION

Our knowledge of other stellar systems and their accompanying planets has been expanding significantly since the exoplanet surveys of Kepler, K2, and Transiting Exoplanet Survey Satellite (TESS) satellites. Over 5500 exoplanets have been confirmed (NASA's [Exoplanet Archive 2023](#)). Adding to this, the recent launch of JWST has provided us with a deluge of high-quality spectroscopic data. This allows for the characterization of exoplanet atmospheres with unprecedented detail, exemplified by the detection of SO₂ in the hot-Jupiter

WASP-39 b's atmosphere, which indicates active photochemistry (Tsai et al. 2023). Another example is the detection of CO₂ in the temperate sub-Neptune K2-18 b's atmosphere (Madhusudhan et al. 2023), which supports the hypothesis of a water-rich interior (Madhusudhan et al. 2021; Hu et al. 2021), but can also be potentially explained by a high-metallicity atmosphere (Yu et al. 2021; Hu et al. 2021; Tsai et al. 2021; Wogan et al. 2024).

As shown above, JWST enables detailed atmospheric measurements of diverse types of exoplanets from Jupiter-sized to Earth-sized, from cool to hot atmospheres, on which one may expect diverse atmospheric composition and redox conditions. 1-D photochemical atmospheric modeling is crucial for interpreting the JWST observations as well as guiding future observations. Thus, enhancing 1-D photochemical atmospheric

Antisymmetric galaxy cross-correlations in and beyond Λ CDM

Eleonora Vanzan,^{1,2,*} Alvise Raccanelli,^{1,2,3,4,†} and Nicola Bartolo^{1,2,3,‡}

¹*Dipartimento di Fisica Galileo Galilei, Università di Padova, I-35131 Padova, Italy*

²*INFN Sezione di Padova, I-35131 Padova, Italy*

³*INAF-Osservatorio Astronomico di Padova, Italy*

⁴*Theoretical Physics Department, CERN, 1 Esplanade des Particules, 1211 Geneva 23, Switzerland*

Many different techniques to analyze galaxy clustering data and obtain cosmological constraints have been proposed, tested and used. Given the large amount of data that will be available soon, it is worth investigating new observables and ways to extract information from such datasets. In this paper, we focus on antisymmetric correlations, that arise in the cross-correlation of different galaxy populations when the small-scale power spectrum is modulated by a long-wavelength field. In Λ CDM this happens because of nonlinear clustering of sources that trace the underlying matter distribution in different ways. Beyond the standard model, this observable is sourced naturally in various new physics scenarios.

We derive, for the first time, its complete expression up to second order in redshift space, and show that this improves detectability compared to previous evaluations at first order in real space. Moreover, we explore a few potential applications to use this observable to detect models with vector modes, or where different types of sources respond in different ways to the underlying modulating long mode, and anisotropic models with privileged directions in the sky. This shows how antisymmetric correlations can be a useful tool for testing exotic cosmological models.

I. INTRODUCTION

Current and future galaxy surveys are expected to map the Large-Scale Structure (LSS) of the Universe with unprecedented detail, providing us with catalogs of different tracers of the underlying dark matter field. Observing different types of sources will allow for the use of the multi-tracer approach, which promises to be a winning strategy to beat down cosmic variance [1–6].

Recently, there have been many efforts to improve the available statistical tools for analyzing the LSS, through a more accurate modeling of e.g., observational, small-scale and general-relativistic corrections. However, it is also worth investigating completely new avenues, which may both complement existing observables and be better-suited to test specific cosmological models. A recently developed observable [7], searches for imprints on the two-point statistics from primordial fossil fields. These fields could be either scalar, vector, or tensor modes, and they would induce local departures from an otherwise statistically isotropic two-point function.

An extension to this observable has been proposed in [8], to exploit the benefits of the multitracer technique: the antisymmetric part of the galaxy cross-correlation, which will be non-vanishing in the presence of two different tracers. If one considers two galaxies drawn from the same population, separated by a distance \mathbf{r} , the two-point auto-correlation function is symmetric under the inversion $\mathbf{r} \mapsto -\mathbf{r}$. But if the two galaxies belong to different populations, with different biasing and evolution properties, then their cross-correlation function may not be symmetric under this exchange. Such an antisymmetric term is generated in standard Λ CDM, as shown in [8], because of biased nonlinear clustering: it arises from the fact that the two populations trace the dark matter field in different ways, i.e., they have different bias parameters.

An antisymmetric contribution can also arise from exotic new physics, e.g., the presence of vector fields that leave an imprint on the galaxy clustering. This work, starting from the idea sketched in [8], derives a more complete expression for the antisymmetric part of galaxy correlations, including redshift-space distortions, a more detailed modeling for the galaxy bias, and the effect of primordial non-Gaussianity. Then, for the first time, it investigates the detectability of such an observable by future galaxy surveys. Furthermore, it explores a few possible exotic physics models that could be tested using this new observable.

*Electronic address: eleonora.vanzan@phd.unipd.it

†Electronic address: alvise.raccanelli.1@unipd.it

‡Electronic address: nicola.bartolo@pd.infn.it

High-resolution spectroscopic analysis of four unevolved barium stars*

M. P. RORIZ ¹, N. HOLANDA ¹, L. V. DA CONCEIÇÃO ², S. JUNQUEIRA,¹ N. A. DRAKE ^{1,3}, A. SONALLY,¹ AND
C. B. PEREIRA¹

¹*Observatório Nacional/MCTI, Rua General José Cristino, 77, 20921-400, Rio de Janeiro, Brazil*

²*Department of Physics and Astronomy, University of Manitoba, Winnipeg, MB, R3T 2N2, Canada*

³*Laboratory of Observational Astrophysics, Saint Petersburg State University, Universitetski pr. 28, 198504, Saint Petersburg, Russia*

(Received xxxx; Revised yyyy; Accepted zzzz)

Submitted to AJ

ABSTRACT

A classical Local Thermodynamic Equilibrium analysis, based on high-resolution spectroscopic data, is performed for a sample of three potential barium dwarf candidates and one star already recognized as such. We derived their atmospheric parameters, estimated their masses and luminosities, and determined chemical abundances for a set of 21 elements, including CNO. Some elemental abundances are derived for the first time in HD 15096, HD 37792, and HD 141804. The program stars are dwarfs/subgiants with metallicities typical of disc stars, exhibiting moderate carbon enhancements, with [C/Fe] ratios ranging from +0.29 to +0.66 dex, and high levels of *slow* neutron-capture (*s*-process) elements, with [s/Fe] \gtrsim +1.0 dex. As spectroscopic binaries, their peculiarities are attributable to mass transfer events. The observed neutron-capture patterns were individually compared with two sets of *s*-process nucleosynthesis models (Monash and FRUITY), yielding dilution factors and masses estimates for the former polluting Asymptotic Giant Branch stars. Low-mass ($\lesssim 3.0 M_{\odot}$) models successfully reproduce the observations. In addition, we estimated mean neutron exposures of the order of 0.6 – 0.7 mb⁻¹ for the *s*-processed material observed in their envelopes. Applying an empirical initial-final mass relation, we constraint in $\sim 0.7 M_{\odot}$ the mass of their dim white-dwarf companions. Moreover, our kinematic study revealed that the program stars are members of the thin disk, with probabilities greater than 70%. Hence, we identified HD 15096 and HD 37792 as new barium dwarfs and confirmed that HD 141804 is a barium dwarf. Thus, the number of barium dwarfs identified in the literature from high-resolution spectroscopy increases to 71 objects.

Keywords: stars: fundamental parameters — stars: atmospheres — stars: abundances — stars: chemically peculiar — stars: individuals (HD 15096, HD 37792, HD 141804, HD 207585) — techniques: spectroscopy

1. INTRODUCTION

Barium (Ba) stars (Bidelman & Keenan 1951) and their Population II analogues, CH stars (Keenan 1942), were initially recognized as red giants enriched in car-

bon and elements synthesized mostly through the *slow* neutron-capture mechanism (*s*-process; Burbidge et al. 1957; Käppeler et al. 2011; Lugaro et al. 2023). However, the *s*-process nucleosynthesis is expected to take place in the interiors of Thermally-Pulsing Asymptotic Giant Branch (TP-AGB) stars (Gallino et al. 1998; Busso et al. 1999; Straniero et al. 2006; Karakas & Lattanzio 2014). Consequently, as first ascent giants, Ba and CH stars are not able to produce *in loco* and self-enriched their envelopes with the *s*-processed material. Until the discovery of their binary nature (McClure et al. 1980; McClure

Corresponding author: M. P. Roriz
michelle@on.br

* HD 15096, HD 37792, and HD 141804 were observed under the program ID 097.A-9024(A). HD 207585 was observed under the agreement between Observatório Nacional (Brazil) and European Southern Observatory (ESO).

Birth of Rapidly Spinning, Overmassive Black Holes in the Early Universe

KOHEI INAYOSHI ¹ AND KOHEI ICHIKAWA ^{2,3}

¹*Kavli Institute for Astronomy and Astrophysics, Peking University, Beijing 100871, China*

²*Global Center for Science and Engineering, Faculty of Science and Engineering, Waseda University*

³*Department of Physics, School of Advanced Science and Engineering, Faculty of Science and Engineering, Waseda University, 3-4-1, Okubo, Shinjuku, Tokyo 169-8555, Japan*

ABSTRACT

The James Webb Space Telescope (JWST) has unveiled numerous massive black holes (BHs) in faint, broad-line active galactic nuclei (AGNs). The discovery highlights the presence of dust-reddened AGN populations, referred to as “little red dots (LRDs)”, more abundant than X-ray selected AGNs, which are less influenced by obscuration. This finding indicates that the cosmic growth rate of BHs within this population does not decrease but rather increases at higher redshifts beyond $z \sim 6$. The BH accretion rate density deduced from their luminosity function is remarkably higher than that from other AGN surveys in X-ray and infrared bands. To align the cumulative mass density accreted to BHs with the observed BH mass density at $z \simeq 4 - 5$, as derived from the integration of the BH mass function, the radiative efficiency must be doubled from the canonical 10% value, achieving significance beyond the $> 2\sigma$ confidence level. This suggests the presence of rapid spins with 96% of the maximum limit among these BHs, maintained by prolonged mass accretion instead of chaotic accretion with randomly oriented inflows. Moreover, we derive an upper bound for the stellar mass of galaxies hosting these LRDs, ensuring consistency with galaxy formation in the standard cosmological model, where the host stellar mass is limited by the available baryonic reservoir. Our analysis gives a lower bound for the BH-to-galaxy mass ratio that exceeds the typical value known in the nearby universe and aligns with that for JWST-detected unobscured AGNs. Accordingly, we propose a hypothesis that the dense, dust-rich environments within LRDs facilitate the emergence of rapidly spinning and overmassive BH populations during the epoch of reionization. This scenario predicts a potential association between relativistic jets and other high-energy phenomena with overmassive BHs in the early universe.

Keywords: Galaxy formation (595); High-redshift galaxies (734); Quasars (1319); Supermassive black holes (1663)

1. INTRODUCTION

The cosmic evolution of massive black hole (BH) populations is predominantly driven by mass accretion, powering active galactic nuclei (AGNs) (e.g., Lynden-Bell 1969). Multi-wavelength observations have consistently shown that AGN activity peaks around $z \sim 2$ and declines toward higher redshifts (e.g., Ueda et al. 2014; Delvecchio et al. 2014). The analysis of AGN activity offers insights into the radiative efficiency of accreting BHs by comparing it with the local mass density of relic BHs (Soltan 1982; Yu & Tremaine 2002).

Recent observations by the James Webb Space Telescope (JWST) have revealed a new category of dust-reddened, broad-line AGNs, often referred to as “little red dots” (hereafter LRDs, Matthee et al. 2023). These AGNs are characterized by their compact morphology and moderate dust obscuration ($A_V \approx 3$) in the spectra (Barro et al. 2023; Kocevski et al. 2023; Harikane et al. 2023; Labbe et al. 2023). Investigations into the AGN luminosity function of LRDs at $z = 4-8$ found an abundance of $\Phi \sim 10^{-5} - 10^{-4} \text{ Mpc}^{-3} \text{ mag}^{-1}$ in the observed UV absolute magnitude range of $-22 \lesssim M_{UV} \lesssim -18$ (e.g., Kokorev et al. 2024), significantly exceeding those predicted by extrapolations from the unobscured AGN luminosity function in ground-based surveys (e.g., Niida et al. 2020). Moreover, spectroscopic analysis of LRDs, facilitating direct measurement of broad H α emissions

Internal magnetic field structures observed by PSP/WISPR in a filament related coronal mass ejection

G.M. Cappello¹, M. Temmer¹, A. Vourlidas², C. Braga², P.C. Liewer³, J. Qiu⁴,
G. Stenborg², A. Kouloumvakos², A.M. Veronig^{1,5}, V. Bothmer⁶

¹ Institute of Physics, University of Graz, Universitätsplatz 5, 8010 Graz, Austria
e-mail: greta.cappello@uni-graz.at

² The Johns Hopkins University Applied Physics Laboratory, 11101 Johns Hopkins Road, Laurel, MD 20723, USA.

³ Jet Propulsion Laboratory, California Institute of Technology, Pasadena, CA, 91109, USA

⁴ Department of Physics, Montana State University, Bozeman, MT, 59717, USA

⁵ Kanzelhöhe Observatory for Solar and Environmental Research, University of Graz, 9521 Treffen, Austria

⁶ Institut für Astrophysik und Geophysik, Georg-August-Universität, Göttingen, Germany

Received February 14, 2024; accepted

ABSTRACT

Context. We track and investigate from white-light data taken with the Wide-field Instrument for Solar PRobe (WISPR) aboard Parker Solar Probe (PSP), localized density enhancements, reflecting small-scale magnetic structures belonging to a filament-related coronal mass ejection (CME).

Aims. We aim to investigate the 3D location, morphology and evolution of the internal magnetic fine structures of CMEs. Specifically, we ask: what is the physical origin of the small-scales in the WISPR images? How do these structures evolve over time? What is their relationship with the filament/source region and the flux rope?

Methods. The fast tangential motion of the PSP spacecraft during its perihelion permits viewing the same event from multiple angles in short times relative to the event's evolution. Hence, we can derive the three-dimensional information of selected CME features from a single spacecraft using triangulation techniques.

Results. We group small-scale structures with roughly similar speeds, longitude and latitude, into three distinct morphological groups. We find twisted magnetic field patterns close to the eastern leg of the CME that may be related to 'horns' outlining the edges of the flux-rope cavity. Aligned thread-like bundles are identified close to the western leg. They may be related to confined density enhancements evolving during the filament eruption. High density blob-like features (magnetic islands) are widely spread in longitude ($\sim 40^\circ$) close to the flanks and rear part of the CME. We also note that the large-scale outer envelope of the CME, seen clearly from 1 AU, is not well observed in PSP.

Conclusions. We demonstrate that CME flux ropes may comprise different morphological groups with a cluster behavior, apart from the blobs which instead span a wide range of longitudes. This may hint either to the three-dimensionality of the post-CME current sheet (CS) or to the influence of the ambient corona in the evolutionary behavior of the CS. Importantly, we show that the global appearance of the CME can be very different in WISPR (0.11–0.16 AU) and instruments near 1 AU because of shorter line-of-sight integration of WISPR.

Key words. coronal mass ejections – triangulation – 3D reconstruction – small scale features – internal structures – parker solar probe

1. Introduction

Coronal mass ejections (CMEs) refer to the substantial expulsion of plasma and magnetic flux from the solar corona into interplanetary space. Their driver is a magnetic flux rope structure, which may not necessarily contain cold filamentary material (e.g., Chen 2011), accelerated outward by magnetic reconnection through the Lorentz force (Forbes 2000; Vršnak 2001). Using multiple viewpoints of CMEs through stereoscopic coronagraph images from the Solar TERrestrial RELations Observatory (STEREO, Kaiser et al. 2008), we have gained valuable insights about their three-dimensionality when observed from 1 AU. Typically, but not always, we observe a CME morphology that includes a faint front (a shock sheath if the CME is fast enough) followed by a bright loop-like leading edge, and then a dim region corresponding to a low plasma-beta structure delineating the flux rope (Vourlidas et al. 2013; Temmer & Both-

mer 2022). When interacting with the near-Earth environment, CMEs can drive a variety of space weather effects, such as geomagnetic storms, disruption of satellite communication systems or ground-induced currents (see reviews by e.g., Pulkkinen 2007; Gopalswamy 2022). Hence, the evolution of CMEs from Sun to Earth has received particular attention over the years. Several recent reviews give an overview of our current understanding of the physics of CME evolution, their interaction with the ambient solar wind, state-of-the-art modeling and analysis methods, and the gaps that we need to fill in the future (e.g., Green et al. 2018; Temmer 2021; Zhang et al. 2021; Gopalswamy 2022; Mishra & Teriaca 2023; Temmer et al. 2023).

There are clear associations of CMEs with phenomena observed on the solar disk, such as flares, filament/prominence eruptions, coronal waves, or dimming regions, etc. (see e.g., Chen 2011). Note that in this manuscript we will use the terms 'filament' and 'prominence' interchangeably, since we study ob-

An upper limit to differential magnification effects in strongly gravitationally lensed galaxies

STEPHEN SERJEANT¹

¹*School of Physical Sciences
The Open University, Milton Keynes, MK7 6AA UK*

Submitted to AAS Journals

ABSTRACT

Differential magnification is now well-known to distort the spectral energy distributions of strongly gravitationally lensed galaxies. However, that does not mean that any distortions are possible. Here I prove an analytic upper bound to differential magnification effects. For example, a thermal or sub-thermal CO ladder cannot be made to appear super-thermal just from gravitational lensing, and the Balmer decrement emission line ratio $H\alpha:H\beta$ cannot reduce below the case B prediction just from differential magnification. In general, if a physical model of a galaxy predicts upper and/or lower bounds to an emission line ratio, then those bounds also apply to the differentially magnified strongly gravitationally lensed case. This applies not just for velocity-integrated emission lines, but also for the line emission in any rest-frame velocity interval.

1. INTRODUCTION

The landmark discovery that bright submm and mm-wave galaxies are mainly strongly gravitationally lensed (Negrello et al. 2010) has led to a glut of strongly lensed systems (e.g. Negrello et al. 2017; Reuter et al. 2020; Urquhart et al. 2022). Taken in conjunction with optical and near-infrared strong lensing catalogues, there are now of the order a thousand confirmed or candidate strong lensing systems, and future dark energy missions are expected to increase these numbers by two orders of magnitude (e.g. Collett 2015). Many spectroscopic or continuum studies currently rely either on low angular resolution data or integrated fluxes across the system (e.g. Urquhart et al. 2022; Bendo et al. 2023; Hagimoto et al. 2023; Cox et al. 2023; Ismail et al. 2023; Berta et al. 2023). Therefore studies have been made to assess the effects of differential gravitational lensing magnification on the observed integrated spectral energy distributions of strongly lensed galaxies (e.g. Serjeant 2012; Hezaveh et al. 2012). These effects are now widely cited and recognised, but sometimes anomalies in observations are wrongly attributed to differential magnification. This paper therefore sets out to address this by proving an analytic bound on differential magnification effects.

2. METHOD

The formalism is a continuum generalisation of the discrete argument we presented in Appendix E of Hagimoto et al. (2023). I consider two emission lines, numbered 1 and 2, and line 2 is always brighter than line 1. For example, line 2 could be the $H\alpha$ emission line, and line 1 could be $H\beta$

PRODIGE - Planet-forming disks in Taurus with NOEMA.

I. Overview and first results for ^{12}CO , ^{13}CO , and C^{18}O .

D. Semenov^{1,2}, Th. Henning¹, S. Guilloteau^{3,4}, G. Smirnov-Pinchukov¹, A. Dutrey^{3,4}, E. Chapillon⁵, V. Piétu⁵, R. Franceschi¹, K. Schwarz¹, S. van Terwisga¹, L. Bouscasse⁵, P. Caselli⁶, C. Ceccarelli⁷, N. Cunningham⁷, A. Fuente⁸, T.-H. Hsieh⁶, A. Lopez-Sepulcre^{5,7}, D. M. Segura-Cox^{9,6*}, J. E. Pineda⁶, M. J. Maureira⁶, Th. Möller¹⁰, M. Tafalla⁸, and M. T. Valdivia-Mena⁶

¹ Max-Planck-Institut für Astronomie (MPIA), Königstuhl 17, D-69117 Heidelberg, Germany
e-mail: semenov@mpia.de

² Department of Chemistry, Ludwig-Maximilians-Universität, Butenandtstr. 5-13, D-81377 München, Germany

³ LAB, Université de Bordeaux, B18N, Allée Geoffroy, Saint-Hilaire, CS 50023, 33615 Pessac Cedex

⁴ CNRS, Université de Bordeaux, B18N, Allée Geoffroy, Saint-Hilaire, CS 50023, 33615 Pessac Cedex

⁵ IRAM, 300 Rue de la Piscine, F-38046 Saint Martin d'Hères, France

⁶ Max-Planck-Institut für extraterrestrische Physik (MPE), Gießenbachstr. 1, D-85741 Garching bei München, Germany

⁷ IPAG, Université Grenoble Alpes, CNRS, F-38000 Grenoble, France

⁸ Centro de Astrobiología (CAB), CSIC-INTA, Ctra Ajalvir Km 4, Torrejón de Ardoz, 28850 Madrid, Spain

⁹ Department of Astronomy, The University of Texas at Austin, 2500 Speedway, Austin, TX, 78712, USA

¹⁰ I. Physikalisches Institut, Universität zu Köln, Zùlpicher Str. 77, 50937 Köln, Germany

February 23, 2024

ABSTRACT

Context. Physics and chemistry of planet-forming disks are far from being fully understood. To make further progress, both broad line surveys and observations of individual tracers in a statistically-significant number of disks are required.

Aims. We are performing a line survey of 8 planet-forming Class II disks in Taurus with the IRAM Northern Extended Millimeter Array (NOEMA), as a part of the MPG-IRAM Observatory Program PRODIGE (PROtostars and Disks: Global Evolution; PIs: P. Caselli and Th. Henning).

Methods. Compact and extended disks around T Tauri stars CI, CY, DG, DL, DM, DN, IQ Tau, and UZ Tau E are observed in ~ 80 lines from > 20 C-, O-, N-, and S-bearing species. The observations in four spectral settings at 210-280 GHz with 1σ rms sensitivity of $\sim 8 - 12$ mJy/beam at $0.9''$ and 0.3 km s⁻¹ resolution will be completed in 2024. The uv -visibilities are fitted with the DiskFit model to obtain key stellar and disk properties.

Results. In this first paper, the combined ^{12}CO , ^{13}CO and C^{18}O $J = 2 - 1$ data are presented. We find that the CO fluxes and disk masses inferred from dust continuum tentatively correlate with the CO emission sizes. We constrain dynamical stellar masses, geometries, temperatures, the CO column densities and gas masses for each disk. The best-fit temperatures at 100 au are $\sim 17 - 37$ K, and decrease radially with the power-law exponent $q \sim 0.05 - 0.76$. The inferred CO column densities decrease radially with the power-law exponent $p \sim 0.2 - 3.1$. The gas masses estimated from ^{13}CO (2-1) are $\sim 0.001 - 0.2 M_{\odot}$.

Conclusions. Using NOEMA, we confirm the presence of temperature gradients in our disk sample. The best-fit CO column densities point to severe CO freeze-out in these disks. The DL Tau disk is an outlier, and has either stronger CO depletion or lower gas mass than the rest of the sample. The CO isotopologue ratios are roughly consistent with the observed values in disks and the low-mass star-forming regions. The high $^{13}\text{CO}/\text{C}^{18}\text{O}$ ratio of ~ 23 in DM Tau could be indicative of strong selective photodissociation of C^{18}O in this disk.

Key words. ISM: individual objects: CI Tau, CY Tau, DG Tau, DL Tau, DM Tau, DN Tau, IQ Tau, UZ Tau - Line: profiles - Protoplanetary disks - Radio lines: planetary systems - Stars: variables: T Tauri - Techniques: interferometric

1. Introduction

A diversity of discovered exoplanets calls for better understanding of the physical and chemical processes in their natal planet-forming disks (e.g. Mordasini et al. 2012; Turrini et al. 2021; Mollière et al. 2022). Recently, young planets have been for the first time imaged inside the gas-rich PDS 70 disk (e.g. Keppler et al. 2018; Haffert et al. 2019; Facchini et al. 2021). However, despite extensive progress achieved with the powerful Very Large Telescope (VLT), *Spitzer*, James Webb Space Telescope

(JWST), *Herschel*, Atacama Large Millimeter/Submillimeter Array (ALMA), extended Jansky Very Large Array (eVLA), and NOEMA, our understanding of the disk physics and chemical composition is still limited. Among key disk properties, we have only begun getting their (1) mass measurements, (2) dust-to-gas ratios, (3) temperature structures, and (4) elemental ratios and molecular abundances in the gas and ice phases (e.g., Andrews 2020; Öberg et al. 2021; Benisty et al. 2023; Manara et al. 2023; Miotello et al. 2023; Öberg et al. 2023).

The majority of the disk masses has been inferred from the dust continuum data, often by using fixed dust emissivities

* NSF Astronomy and Astrophysics Postdoctoral Fellow

Cool and Data-Driven: An Exploration of Optical Cool Dwarf Chemistry with Both Data-Driven and Physical Models

Adam D. Rains,^{1,2*} Thomas Nordlander,^{2,3} Stephanie Monty,⁴ Andrew R. Casey,^{3,5} Bárbara Rojas-Ayala,⁶ Maruša Žerjal,^{2,7,8} Michael J. Ireland,² Luca Casagrande,^{2,3} and Madeleine McKenzie^{2,3}

¹Department of Physics and Astronomy, Uppsala University, Box 516, 75120 Uppsala, Sweden

²Research School of Astronomy and Astrophysics, Australian National University, Canberra, ACT 2611, Australia

³ARC Centre of Excellence for Astrophysics in Three Dimensions (ASTRO-3D), Australia

⁴Institute of Astronomy, University of Cambridge, Madingley Rd, Cambridge, CB3 0HA, UK

⁵School of Physics & Astronomy, Monash University, Wellington Road, Clayton 3800, Victoria, Australia

⁶Instituto de Alta Investigación, Universidad de Tarapacá, Casilla 7D, Arica, Chile

⁷Instituto de Astrofísica de Canarias, E-38205 La Laguna, Tenerife, Spain

⁸Universidad de La Laguna, Dpto. Astrofísica, E-38206 La Laguna, Tenerife, Spain

Accepted XXX. Received YYY; in original form ZZZ

ABSTRACT

Detailed chemical studies of F/G/K—or Solar-type—stars have long been routine in stellar astrophysics, enabling studies in both Galactic chemodynamics, and exoplanet demographics. However, similar understanding of the chemistry of M and late-K dwarfs—the most common stars in the Galaxy—has been greatly hampered both observationally and theoretically by the complex molecular chemistry of their atmospheres. Here we present a new implementation of the data-driven *Cannon* model, modelling T_{eff} , $\log g$, [Fe/H], and [Ti/Fe] trained on low–medium resolution optical spectra (4 000 – 7 000 Å) from 103 cool dwarf benchmarks. Alongside this, we also investigate the sensitivity of optical wavelengths to various atomic and molecular species using both data-driven and theoretical means via a custom grid of MARCS synthetic spectra, and make recommendations for where MARCS struggles to reproduce cool dwarf fluxes. Under leave-one-out cross-validation, our *Cannon* model is capable of recovering T_{eff} , $\log g$, [Fe/H], and [Ti/Fe] with precisions of 1.4%, ± 0.04 dex, ± 0.10 dex, and ± 0.06 dex respectively, with the recovery of [Ti/Fe] pointing to the as-yet mostly untapped potential of exploiting the abundant—but complex—chemical information within optical spectra of cool stars.

Key words: methods: data analysis – techniques: spectroscopic – stars: fundamental parameters – stars: low-mass

1 INTRODUCTION

The Solar Neighbourhood—and indeed the Universe more broadly—is dominated by cool dwarf stars of spectral types K and M (e.g. Henry et al. 1994; Chabrier 2003; Henry et al. 2006; Winters et al. 2015; Henry et al. 2018). While Milky Way stars in general are expected to host at least one planet on average (Cassan et al. 2012), cool dwarfs are actually more likely to host small planets as compared to more massive stars (Howard et al. 2012; Dressing & Charbonneau 2015) with many yet undiscovered (Morton & Swift 2014). Enabled by the space-based Kepler (Borucki et al. 2010), K2 (Howell et al. 2014), and TESS (Ricker et al. 2015) missions, exoplanetary astrophysics now has a large and ever-growing set of such systems to study both individually in detail, as well as collectively in a demographic sense.

When presented as such, it is easy to come to the conclusion that cool dwarfs and their planets are as well-understood as their prevalence might imply. In reality though, these stars are intrinsically

faint—especially at optical wavelengths—and possess complex spectra blanketed by innumerable overlapping molecular absorption features. In the infrared (IR) this absorption is dominated by molecules like H₂O, CO, FeH, and OH; and in the optical from oxides like TiO, ZrO, and VO, as well as hydrides like MgH, CaH, AlH, and SiH. Such complexity renders the spectral energy distribution (SED) not just a strong function of temperature, as with Solar-type stars, but also chemistry, making it difficult to ascribe an accurate or unique set of stellar parameters to any given star. This intense molecular absorption makes ‘true’ continuum normalisation impossible at optical wavelengths, and poses severe challenges for traditional spectroscopic analysis techniques. As a result, our understanding of the chemistry of cool dwarfs and their planets typically lags far behind those of Solar-type stars.

This atmospheric complexity and the large impact a single molecular species can have on an emergent spectrum means that the generation of model spectra that accurately match observations has been, and continues to be, a challenge. While model spectra at cool temperatures demonstrate reasonable performance in the near infrared (NIR, e.g. Allard et al. 1997; Baraffe et al. 1997, 1998; Allard et al. 2012),

* E-mail: adam.rains@physics.uu.se (ADR)

A thermodynamic criterion for the formation of Circumplanetary Disks

LEONARDO KRAPP ¹, KAITLIN M. KRATTER ¹, ANDREW N. YOUNG ^{2,3}, PABLO BENÍTEZ-LLAMBAY ⁴,
FRÉDÉRIC MASSET ⁵ AND PHILIP J. ARMITAGE ^{6,7}

¹*Department of Astronomy and Steward Observatory, University of Arizona, Tucson, Arizona 85721, USA*

²*Department of Astronomy and Steward Observatory, University of Arizona, Tucson, AZ 85721, USA*

³*The Lunar and Planetary Laboratory, University of Arizona, Tucson, AZ 85721, USA*

⁴*Facultad de Ingeniería y Ciencias, Universidad Adolfo Ibáñez, Av. Diagonal las Torres 2640, Peñalolén, Chile*

⁵*Instituto de Ciencias Físicas, Universidad Nacional Autónoma de México, Av. Universidad s/n, 62210 Cuernavaca, Mor., Mexico*

⁶*Center for Computational Astrophysics, Flatiron Institute, 162 Fifth Avenue, New York, NY 10010, USA*

⁷*Department of Physics and Astronomy, Stony Brook University, Stony Brook, NY 11794, USA*

(Received; Revised; Accepted)

Submitted to ApJ

ABSTRACT

The formation of circumplanetary disks is central to our understanding of giant planet formation, influencing their growth rate during the post-runaway phase and observability while embedded in protoplanetary disks. We use 3D global multifluid radiation hydrodynamics simulations with the FARGO3D code to define the thermodynamic conditions that enable circumplanetary disk formation around Jovian planets on wide orbits. Our simulations include stellar irradiation, viscous heating, static mesh refinement, and active calculation of opacity based on evolving dust fluids. We find a necessary condition for the formation of circumplanetary disks in terms of a mean cooling time: when the cooling time is at least one order of magnitude shorter than the orbital time scale, the specific angular momentum of the gas is nearly Keplerian at scales of $R_{\text{Hill}}/3$. We show that the inclusion of multifluid dust dynamics favors rotational support because dust settling produces an anisotropic opacity distribution that favors rapid cooling. In all our models with radiation hydrodynamics, specific angular momentum decreases as time evolves in agreement with the formation of an inner isentropic envelope due to compressional heating. The isentropic envelope can extend up to $R_{\text{Hill}}/3$ and shows negligible rotational support. Thus, our results imply that young gas giant planets may host spherical isentropic envelopes, rather than circumplanetary disks.

Keywords: planet formation

1. INTRODUCTION

In the dominant planet formation paradigm of core accretion (Pollack et al. 1996), gas giants grow through accretion of solids and gas from the protoplanetary disk. At early times mass accretion onto the envelope is limited by Kelvin-Helmholtz cooling, which radiates away energy from gravitational contraction and accretion of solids; as the planet cools, more mass can become bound. In this phase, the outer boundary of the planetary atmosphere is matched to either the Hill Radius or Bondi Radius, whichever is smaller (e.g., Pollack et al. 1996; Ayliffe & Bate 2009a; Tanigawa et al. 2012;

Ormel et al. 2015; Cimerman et al. 2017; Kurokawa & Tanigawa 2018; Lambrechts & Lega 2017; Béthune & Rafikov 2019; Zhu et al. 2021). A sharp transition in the evolution to the so-called “runaway” phase occurs when the envelope becomes strongly self-gravitating (Pollack et al. 1996; Hubickyj et al. 2005; Rafikov 2006; D’Angelo & Lubow 2008; Piso & Youdin 2014; Lee & Chiang 2015; D’Angelo et al. 2021). The envelope contraction rate accelerates, allowing mass to accrete onto the envelope at an increasing rate. This phase of growth is expected to continue until limited by the supply of gas from the disk.

Subsequent to the runaway phase, the envelope is thought to accrete at the rate supplied by the disk, which depends upon disk processes including gap opening and photoevaporation that reduce the mass supply (Lissauer et al. 2009; Mordasini et al. 2012; D’Angelo & Bodenheimer 2013). The accretion of angular mo-

Upper Limits of ^{44}Ti Decay Emission in Four Nearby Thermonuclear Supernova Remnants

Jianbin Weng,^{1*} Ping Zhou,^{1,2*} Hagai B. Perets,^{3,4} Daniel R. Wik⁵ and Yang Chen^{1,2*}

¹*School of Astronomy and Space Science, Nanjing University, 163 Xianlin Avenue, Nanjing 210023, China*

²*Key Laboratory of Modern Astronomy and Astrophysics, Nanjing University, Ministry of Education, China*

³*Physics Department, Technion – Israel Institute of Technology, Haifa 3200003, Israel*

⁴*Department of Natural Sciences, The Open University of Israel, 1 University Road, Ra'anana 4353701, Israel*

⁵*Department of Physics & Astronomy, The University of Utah, 115 South 1400 East, Salt Lake City, UT 84112, USA*

Accepted XXX. Received YYY; in original form ZZZ

ABSTRACT

To identify progenitors and investigate evidence of He burning, we searched for decay radiation of freshly synthesized ^{44}Ti in four young nearby thermonuclear supernova remnants: Kepler, SN 1885, G1.9+0.3 and SN 1006, by analysing the up-to-date NuSTAR archival data. No apparent flux excess from the 68 and 78 keV line emissions accompanying decay was detected above the power law continuum applied for the remnants and the absorbed stray light. By comparing the inferred upper limits of the line flux and the initial ^{44}Ti masses with a wide variety of supernova nucleosynthesis models, we placed constraints on the supernova progenitors. We derived the first NuSTAR line flux upper limit for Kepler and ruled out most of the double-detonation scenarios with a thick He layer under low density. We estimated, for the first time, the upper limit for SN 1885, which is high because of the large distance yet still remains consistent with the He shell detonation. The new flux and mass limit of G1.9+0.3 derived from a longer total exposure is lower than the results from previous studies and evidently excludes explosive burning of He-rich matter. The relatively advanced age and the large spatial extent of SN 1006 have prevented meaningful constraints.

Key words: ISM: supernova remnants – nuclear reactions, nucleosynthesis, abundances – X-rays: general

1 INTRODUCTION

A thermonuclear supernova (SN) is the drastic explosion of a white dwarf (WD) powered by the runaway fusion of carbon and oxygen. Thermonuclear SNe were always considered the synonym of Type Ia SNe until recent advances in SN survey revealed several subclasses with distinct photometric and spectral properties (see Jha et al. 2019 for a review). It is also generally accepted that no single progenitor system or explosion mechanism could account for the whole thermonuclear SN family. Many models have been proposed to explain the distinct observational characteristics of each subtype.

The existing thermonuclear SN models can be classified based on their distinctions in specific details of the explosion. In the binary progenitor scenario, the models can be divided into the single degenerate channel, where the companion of the exploding WD is a main sequence star or an evolved star (Nomoto 1982; Whelan & Iben 1973), and the double degenerate channel, where the companion is another WD (Iben & Tutukov 1984; Webbink 1984). Regarding the propagation of the combustion fronts, thermonuclear SN models can be characterised by detonation with supersonic shock waves (Arnett 1969), pure deflagration with subsonic flame fronts (Nomoto et al. 1984; Fink et al. 2014), or their combinations, e.g., delayed detonation (Khokhlov 1991; Seitenzahl et al. 2013) and gravitationally

confined detonation (Plewa et al. 2004; Seitenzahl et al. 2016). Another fundamental factor for the outcome of a thermonuclear SN is the mass of the primary exploding WD, and it also changes how the fusion runaway is set off. Near the centre of a WD close to the Chandrasekhar mass limit (near- M_{Ch}), the extreme density and temperature spontaneously lead to a runaway carbon fusion (Nomoto et al. 1984). Alternatively, a WD below the Chandrasekhar limit (sub- M_{Ch}) can be detonated by the detonation in the accreted He shell (double-detonation, Livne 1990; Woosley & Weaver 1994; Shen & Bildsten 2014) or by the violent interactions during the merger process of the double degenerate scenario (violent merger, Pakmor et al. 2010, 2012, 2013). Other newly proposed methods for ignition include WD-WD head-on collisions (Kushnir et al. 2013; Papish & Perets 2016) and ^{235}U fission chain reactions (Horowitz & Caplan 2021).

Some unconventional models have also been put forward for some unusual thermonuclear SNe. For example, the He shell detonation model has been proposed for Ca-rich transients, where the He shell detonation does not lead to a secondary detonation in the CO WD core (Perets et al. 2010; Waldman et al. 2011). Weng et al. (2022) suggested the supernova remnant (SNR) G306.3-0.9 is likely the first found Galactic Ca-rich transient remnant based on its metal abundances. Another interesting model is the core-degenerate merger, which is also suggested as the progenitor of the Kepler SNR and SN PTF 11kx (Tsebrenko & Soker 2013; Soker et al. 2013). In this scenario, a hot massive core of an asymptotic giant branch (AGB)

* E-mail: jianbin.weng@smail.nju.edu.cn, pingzhou@nju.edu.cn, ygchen@nju.edu.cn

Quenching-driven equatorial depletion and limb asymmetries in hot Jupiter atmospheres: WASP-96b example

Maria Zamyatina¹★, Duncan A. Christie^{1,2}, Eric Hébrard¹, Nathan J. Mayne¹,
 Michael Radica³, Jake Taylor^{3,4}, Harry Baskett¹, Ben Moore¹, Craig Lils¹, Denis Sergeev¹,
 Eva-Maria Ahrer², James Manners⁵, Krisztian Kohary¹ and Adina D. Feinstein⁶†

¹Department of Physics and Astronomy, Faculty of Environment, Science and Economy, University of Exeter, Exeter EX4 4QL, UK

²Max Planck Institute for Astronomy, Königstuhl 17, 69117 Heidelberg, Germany

³Institut Trotier de Recherche sur les Exoplanètes and Département de Physique, Université de Montréal, 1375 Avenue Thérèse-Lavoie-Roux, Montréal, QC, H2V 0B3, Canada

⁴Department of Physics (Atmospheric, Oceanic and Planetary Physics), University of Oxford, Parks Rd, Oxford OX1 3PU, UK

⁵Met Office, Fitzroy Road, Exeter EX1 3PB, UK

⁶Laboratory for Atmospheric and Space Physics, University of Colorado Boulder, UCB 600, Boulder, CO 80309

Accepted 2024 February 16. Received 2024 February 16; in original form 2023 December 15

ABSTRACT

Transport-induced quenching in hot Jupiter atmospheres is a process that determines the boundary between the part of the atmosphere at chemical equilibrium and the part of the atmosphere at thermochemical (but not photothermochemical) disequilibrium. The location of this boundary, the quench level, depends on the interplay between the dynamical and chemical timescales in the atmosphere, with quenching occurring when these timescales are equal. We explore the sensitivity of the quench level position to an increase in the planet’s atmospheric metallicity using aerosol-free 3D GCM simulations of a hot Jupiter WASP-96b. We find that the temperature increase at pressures of $\sim 10^4$ – 10^7 Pa that occurs when metallicity is increased could shift the position of the quench level to pressures dominated by the jet, and cause an equatorial depletion of CH₄, NH₃ and HCN. We discuss how such a depletion affects the planet’s transmission spectrum, and how the analysis of the evening-morning limb asymmetries, especially within ~ 3 – 5 μm , could help distinguish atmospheres of different metallicities that are at chemical equilibrium from those with the upper layers at thermochemical disequilibrium.

Key words: planets and satellites: atmospheres – planets and satellites: composition – planets and satellites: gaseous planets

1 INTRODUCTION

Hot Jupiters, i.e. close-in extrasolar gas giant planets, were, are and in the near future will be the best targets for exoplanet atmospheric characterisation. These planets host large and often anomalously inflated atmospheres (e.g., Tremblin et al. 2017; Komacek et al. 2022), which aid the detection and identification of atoms and molecules present in these atmospheres. One of the tools used to study hot Jupiter atmospheres is general circulation models (GCMs, e.g., Showman et al. 2009; Rauscher & Menou 2010; Dobbs-Dixon & Agol 2013; Mayne et al. 2014; Mendonça et al. 2016; Sainsbury-Martinez et al. 2019; Carone et al. 2020; Helling et al. 2020; Lee et al. 2021; Menou 2020). GCMs simulate the thermodynamic and chemical structure of a planetary atmosphere, and can predict different planetary climates depending on the choice of model parameters. One such parameter is the planet’s atmospheric metallicity.

Atmospheric metallicity is the abundance of elements heavier than helium in a planetary atmosphere. Atmospheric metallicity affects many aspects of the planetary climate, e.g., the thermal structure,

atmospheric circulation and emitted flux (Drummond et al. 2018), however, the value of atmospheric metallicity for hot Jupiters is uncertain by several orders of magnitude (e.g., Welbanks et al. 2019). To correctly determine the atmospheric metallicity of a hot Jupiter, one, ideally, needs to fully understand the planet’s observed thermochemical state. While achieving such an understanding is an active area of research, hot Jupiters that have “aerosol-free” limbs at observable pressures, meaning that the opacities of aerosols constituting condensate clouds and/or photochemical hazes contribute little to the planet’s transmission spectrum, can aid such research. WASP-96b was historically considered one of “aerosol-free” hot Jupiters.

WASP-96b is a highly inflated hot Jupiter, with a mass of $0.48 \pm 0.03 M_J$ and a radius of $1.20 \pm 0.06 R_J$ (Hellier et al. 2014). It orbits a G8-type star at a distance of 0.0453 AU in 3.425 days, which results in it likely being tidally-locked and having an equilibrium temperature of 1285 ± 40 K (Hellier et al. 2014). WASP-96b was observed with transit photometry with the Transiting Exoplanet Survey Satellite (TESS, 0.60–1.00 μm , Yip et al. 2021; Nikolov et al. 2022) and the Infrared Array Camera on the Spitzer Space Telescope (Spitzer/IRAC, 3.6 and 4.5 μm , Yip et al. 2021; Nikolov et al. 2022) as well as with ground- and space-based transit spectroscopy with the FOCal Reducer/low dispersion Spectrograph 2 on the Very Large

★ E-mail: m.zamyatina@exeter.ac.uk

† NHFP Sagan Fellow

Mid-Infrared Properties of Narrow-Line Seyfert 1 Galaxies Detected by LoTSS DR2

XU-LIANG FAN^{1,2}

¹*School of Mathematics, Physics and Statistics, Shanghai University of Engineering Science, Shanghai 201620, China*

²*Center of Application and Research of Computational Physics, Shanghai University of Engineering Science, Shanghai 201620, China*

Submitted to ApJ

ABSTRACT

Narrow-line Seyfert 1 galaxies (NLS1s), a subclass of active galactic nuclei (AGNs) at early stage of accretion process, are also found to host relativistic jets. However, currently known jetted NLS1s are rare. The majority of NLS1s are undetected at radio band. The radio detection rate of NLS1s raises with the LOFAR Two-metre Sky Survey (LoTSS), which gives a good opportunity to find more jetted NLS1s. The better sensitivity brings another question of whether the radio emission of NLS1s with low radio luminosity originates from jet activity. In order to clarify the origin of radio emission for NLS1s, and search for more jetted NLS1s, we explore the mid-infrared properties of LoTSS detected NLS1s by comparing them with known jetted AGNs and star forming galaxies (SFGs), which locate above and on the well studied radio/far-infrared correlation, respectively. The majority of NLS1s show mid-infrared (MIR) excess compared with SFGs. Their radio emission shows significant correlation with MIR emission. In MIR color-color diagram, NLS1s are overlapped with flat spectrum radio quasars, but well separated from SFGs and optically selected radio galaxies. The flux ratio between radio and MIR emission of these NLS1s is also similar with a radio quiet quasar with weak jet. These results imply substantial contributions from AGN activities for both radio and MIR emission of NLS1s. A small fraction of NLS1s with relatively higher radio luminosity locate in similar region with blazars in radio-MIR diagram, which suggests that the radio emission of these NLS1s is dominated by jet. We obtain a sample of jetted NLS1 candidates through their radio excess in radio-MIR diagram.

Keywords: *Unified Astronomy Thesaurus concepts:* Active galactic nuclei (16); Radio AGNs (2134); Low-luminosity active galactic nuclei (2033)

1. INTRODUCTION

Dust Accumulation near the Magnetospheric Truncation of Protoplanetary Discs. II. The Effects of Opacity and Thermal Evolution

Rixin Li¹ (李日新) ^{★†}, Yi-Xian Chen² (陈逸贤), and Douglas N. C. Lin^{3,4} (林潮)

¹Department of Astronomy, University of California, Berkeley, Berkeley, CA 94720, USA

²Department of Astrophysical Sciences, Princeton University, Princeton, NJ 08544, USA

³Department of Astronomy, University of California, Santa Cruz, CA 95064, USA

⁴Institute for Advanced Studies, Tsinghua University, Beijing, 100084, People's Republic of China

Accepted 2024 February 19. Received 2024 February 15; in original form 2023 September 30

ABSTRACT

Dust trapping in the global pressure bump induced by magnetospheric truncation offers a promising formation mechanism for close-in super-Earths/sub-Neptunes. These planets likely form in evolved protoplanetary discs, where the gas temperature at the expanding truncation radius become amiable to refractory solids. However, dust accumulation may alter the disc opacity such that thermal evolution is inevitable. To better understand how thermodynamics affects this planet formation pathway, we conduct a suite of local dust evolution simulations in an idealized inner disc model. Our calculations take into account self-consistent opacity-dependent temperature changes as well as dust evaporation and vapour condensation. We find that disc thermal evolution regulates dust growth and evolution, discouraging any accumulation of small particles that drives the increase of opacity and temperature. Significant retention of dust mass takes place when the disc environments allow runaway growth of large solids beyond the fragmentation barrier, where small particles are then swept up and preserved. Our results further validate dust accumulation near disc truncation as a promising mechanism to form close-in planets.

Key words: protoplanetary discs – planets and satellites: formation – accretion – solid state: refractory

1 INTRODUCTION

Short-period super-Earths (also referred to as sub-Neptunes or Kepler planets) are the most common type of currently observable exoplanets (e.g., Howard et al. 2010; Dressing & Charbonneau 2015). However, their distinct properties (e.g., tight orbital configurations, insensitivity to host metallicities, mass-radius valley) and the lack of their analogues in the Solar System challenge the conventional planet formation theory (Petigura et al. 2017; Johnson et al. 2017; Fulton et al. 2017; Petigura et al. 2018; Zhu et al. 2018; Kunimoto & Matthews 2020; Reiners et al. 2022; Stefánsson et al. 2023).

Several formation channels for such super-Earths have been proposed over the years, with a broad consensus that super-Earths are most likely formed out of materials originated from the external disc (i.e., *ex situ* formation) (Morbidelli & Raymond 2016, see also their Fig. 5 and references therein; Izidoro et al. 2021). The remaining key question is when and where growth takes place during inward migration of solids. If the initial growth of planetary embryos is efficient, they may form in the external disc and then migrate into the tight orbits (e.g., Ida & Lin 2010; Kley & Nelson 2012). Pebble accretion may help embryos grow much further during and after migration (e.g., Lambrechts et al. 2014; Bitsch et al. 2015; Johansen & Lambrechts 2017; Lambrechts et al. 2019).

Alternatively, rapid inward drift of dust into traps induced by pressure bumps at short-period orbits may retain solid mass fast

enough to form embryos and supply their further growth. The dead zone inner boundary (DZIB) may serve this purpose, but recent disc modeling suggested that the DZIB either locates far out or may not induce a pressure bump at all (e.g., Chatterjee & Tan 2014; Hu et al. 2016, 2018; Jankovic et al. 2021, 2022).

In Li et al. (2022, hereafter Paper I), we proposed and demonstrated that the global pressure maxima induced by magnetospheric truncation in evolved discs may trap dust efficiently, providing a promising formation pathway for close-in super-Earths. Specifically, two sub-pathways for effective dust retention operate at different parameter regimes. When the turbulent relative velocity between dust (correlated with the Shakura–Sunyaev α -parameter (Shakura & Sunyaev 1973) and the gas sound speed c_s) is relatively low and the threshold velocity for fragmentation u_f is high (e.g., due to the sticky surface layer on dust at a high temperature), or when large solids can be rapidly delivered from the outer disc, a fraction of particles may grow fast and surpass the fragmentation barrier. This process triggers an accelerated accumulation of progressively larger particles, eventually reaching the typical size of planetesimals (referred to as the *breakthrough scenario*). Conversely, in a different scenario characterized by a high turbulent relative velocity and a low threshold velocity for fragmentation, coagulation growth beyond small grains is highly suppressed. However, when the dust supply from the outer disc is substantial enough to counteract the removal through funnel flows, the overall dust mass can still gradually rise, eventually reaching a point where gravitational instability (GI) produces planetesimals (referred to as the *feedback+GI scenario*).

Dust retention at the truncation radius R_T , which converges with

[★] Contact e-mail: rixin@berkeley.edu

[†] 51 Pegasi b Fellow

X-ray observations of Isolated Neutron Stars

Michela Rigoselli^{a,*}

^a*INAF, IASF Milano,
Via Alfonso Corti 12, I-20133 Milano, Italy
E-mail: michela.rigoselli@inaf.it*

Pulsars are rapidly spinning neutron stars, that radiate at the expense of their strong magnetic field and their high surface temperature. Five decades of multi-wavelength observations showed a large variety of physical parameters, such as the spin period, the magnetic field and the age, and of observational properties, especially in the radio and X-ray band. Isolated neutron stars have been classified according to the presence of thermal or non-thermal emission, and whether they show a constant flux, rapid flares and bursts or long-standing outbursts. One of the current challenges in the study of such objects is to explain these different manifestations in the context of a unified evolutionary picture. On the other hand, recent findings show that the classes of isolated neutron stars are more connected than previously thought, and that non only magnetars hold a complex magnetic field topology in the crust and above the surface.

*Multifrequency Behaviour of High Energy Cosmic Sources - XIV
12–17 June 2023
Palermo, Italy*

*Speaker

© Copyright owned by the author(s) under the terms of the Creative Commons Attribution-NonCommercial-NoDerivatives 4.0 International License (CC BY-NC-ND 4.0).

<https://pos.sissa.it/>

X-ray observations of INS

Michela Rigoselli

1. The Isolated Neutron Stars zoology

Neutron stars have been detected for the first time as radio pulsating sources in 1967 [1], and in the subsequent fifty years more than 3300 have been registered¹ [2]. They have mainly been discovered thanks to the detection of their pulsed non-thermal emission, at wavelengths spanning from radio to γ -rays, and they can be isolated stars or members of a binary system.

The energy that sustains pulsar emission is supplied by their fast rotation (Section 1.1), via the braking operated by their intense magnetic field, that is assumed to be dipolar. Under these very simple assumptions, three characteristic quantities can be inferred from the period P and its derivative \dot{P} : the so-called spin-down luminosity

$$\dot{E}_{\text{rot}} = 4\pi^2 I_{\text{NS}} \dot{P} P^{-3}, \quad (1)$$

where $I_{\text{NS}} \approx 10^{45}$ g cm² is the moment of inertia, the dipolar magnetic field on the surface

$$B_{\text{dip}} \approx 3.2 \times 10^{19} (P\dot{P})^{1/2} \text{ G}, \quad (2)$$

and the characteristic age

$$\tau_c = \frac{P}{2\dot{P}}, \quad (3)$$

that takes this form if the current period is way larger than the initial period P_0 .

With the advent of X-ray satellites and all-sky surveys, several thermally emitting isolated neutron stars (INSs) have been discovered at the center of supernova remnants (SNRs) (Section 1.3), or as serendipitous sources with a very soft X-ray stable spectrum (Section 1.4), or as extremely flaring sources (Section 1.2).

P and \dot{P} play a fundamental role in characterizing the pulsar properties, and the neutron star population is usually represented in the $P - \dot{P}$ diagram (shown in Figure 1), as the ordinary stars are represented in the Hertzsprung-Russell diagram; the different classes of INSs are placed on different zones of the diagram.

In the following, I will review the main X-ray properties of INSs and the links that are emerging among the different classes. On this topic, see also [3–6].

1.1 Rotation-powered pulsars

The rotation-powered pulsars (RPPs) are the bulk of INSs and are detected because of their pulsed emission. Nowadays more than 3000 RPPs are known, and they have been detected from the radio band to the very-high energy γ -rays (see e.g. the recent result on Vela pulsating emission at 20 TeV [8]). They also show optical/UV/X-ray thermal emission from the cooling surface and from hot spots heated by returning currents [9, and references therein].

RPPs fill the central region of the $P - \dot{P}$ diagram (Figure 1, black dots); a newborn pulsar appears in the top-left corner and, according to the magnetic-dipole braking model, it evolves along the B_{dip} constant lines (dashed), crossing the τ_c constant lines (dotted). The bottom-right corner of the plot is empty because when pulsars cross the so-called “death line” [7], they are too old and too slow to maintain the required potential difference for pair production in the vacuum gap [10, 11].

¹<https://www.atnf.csiro.au/research/pulsar/psrcat/>.

Luminosity class of the symbiotic stars 4U1954+319 and ZZ CMi

R. Zamanov¹, K. A. Stoyanov¹, G. Latev¹, J. Marti², A. Takey³, E. G. Elhosseiny³,
M. D. Christova⁴, M. Minev¹, V. Vujčić⁵, M. Moiseev¹, and V. Marchev¹¹*Institute of Astronomy and National Astronomical Observatory, Bulgarian Academy of Sciences, 72 Tsarigradsko Chaussee Blvd., 1784 Sofia, Bulgaria*

E-mail: rkz@astro.bas.bg, kstoyanov@astro.bas.bg

²*Departamento de Física, Escuela Politécnica Superior de Jaén, Universidad de Jaén, Campus Las Lagunillas s/n, A3-420, 23071, Jaén, Spain*³*National Research Institute of Astronomy and Geophysics (NRIAG), 11421 Helwan, Cairo, Egypt*⁴*Department of Applied Physics, Technical University of Sofia, blvd. Kl. Ohridski 8, 1000 Sofia, Bulgaria*⁵*Astronomical Observatory, Volgina 7, 11060 Belgrade 38, Serbia*

(Received: February 7, 2024; Accepted:, 2024)

SUMMARY: We performed optical photometry and spectral observations of the symbiotic stars 4U1954+319 and ZZ CMi. For 4U1954+319 using high-resolution spectra we measure the equivalent widths of diffuse interstellar bands (DIBs) and estimate the interstellar reddening $E(B - V) = 0.83 \pm 0.09$. Using *GAIA* distances and our photometry, we find (1) absolute V band magnitude of 4U1954+319 $M_V = -5.23 \pm 0.08$ and that the mass donor is a supergiant of luminosity class Ib, and (2) for ZZ CMi $M_V = -0.27 \pm 0.2$ and that the mass donor is a giant of luminosity class III.

Key words. stars: binaries: symbiotic – stars: individual: 4U1954+319, ZZ CMi

1. INTRODUCTION

Symbiotic stars are long-period interacting binary systems composed of a hot component, a cool giant and a nebula formed from material lost by the donor star and ionized by the radiation of the hot component (Mikołajewska 2012). The hot component can be a white dwarf, neutron star, or main-sequence star. In the majority, the donor star is a red giant but occasionally it could be an asymptotic giant branch star. The spectrum of symbiotic stars is a combination of emission lines from the hot component and the nebula, and absorption lines from the donor star. The donor star loses mass through stellar wind or Roche-lobe overflow. The hot component accretes matter and produces high-energy emission and the symbiotic phenomenon (Mikołajewska 2007).

To the current moment (January 2024) SIMBAD Astronomical database (Wenger et al. 2000) gives: for 4U1954+319 spectral type M4/5III (Masetti et al. 2006), and for ZZ CMi spectral type M6I-IIep (Shenavrin et al. 2011). We performed spectral observations and optical photometry, aiming to find the luminosity classes of these symbiotic stars.

2. Observations

Five optical spectra of 4U1954+319 and two of ZZ CMi were secured with the ESpeRo Echelle spectrograph (Bonev et al. 2017) on the 2.0-m telescope of the Rozhen National Astronomical Observatory, Bulgaria. The journal of observations is presented in Table 1, where are given the start of the observation, exposure time, signal-to-noise ratio around 6570 Å,

Can Early Dark Energy be Probed by the High-Redshift Galaxy Abundance?

Liu, Weiyang,^{1,2*} Zhan, Hu,^{1,3} Gong, Yan,^{1,2} and Wang, Xin^{1,2}

¹Key Laboratory of Space Astronomy and Technology, National Astronomical Observatories, Chinese Academy of Sciences, Beijing, 100101, China P.R.

²School of Astronomy and Space Science, University of Chinese Academy of Sciences, Beijing, 100049, China P.R.

³The Kavli Institute for Astronomy and Astrophysics, Peking University, Beijing, 100871, China P.R.

Accepted XXX. Received YYY; in original form ZZZ

ABSTRACT

The Hubble tension and σ_8 tension are two of the major issues of the standard Λ Cold Dark Matter (Λ CDM) model. The analysis of the Cosmic Microwave Background (CMB) data acquired by the Atacama Cosmology Telescope (ACT) and the large-scale ($\ell \lesssim 1300$) Planck Telescope manifest their preference for the Early Dark Energy (EDE) theory, which was set to alleviate the Hubble tension by decreasing the sound horizon r_s , and gives $H_0 \approx 72 \text{ km s}^{-1} \text{ Mpc}^{-1}$. However, the EDE model is commonly questioned for exacerbating the σ_8 tension on top of the Λ CDM model, and its lack of preference from the late-time matter power spectrum observations, e.g., Baryon Oscillation Spectroscopic Survey (BOSS). In light of the current obscurities, we inspect if the high redshift galaxy abundance, i.e., Stellar Mass Function/Density (SMF/SMD) and Luminosity Function (LF), can independently probe the EDE model and ameliorate the challenges it encounters. Our result shows that the EDE model produces more observable galaxies than Λ CDM at $z > 8$. The LF and SMD, in particular, are consistent with the recent unexpectedly high results observed by the James Webb Space Telescope (JWST), which may posit another observational hint of EDE. This result also implies an efficient suppression mechanism of the galaxy formation rate that leads to the conversion between EDE- and Λ CDM-like Universe around $z \sim 7 - 10$, and that σ_8 tension could be more of a tension of galaxy evolution than cosmology, hence diminishing its impact on EDE or Λ CDM theory.

Key words: cosmology – dark energy – galaxies: high-redshift – galaxies: abundances

1 INTRODUCTION

The discovery of the accelerating expansion of the Universe and the resulting cosmological constant dark energy (Riess et al. (1998); Perlmutter et al. (1999)) led to the transition of the cosmological model from Einstein de Sitter ($\Omega_m = 1$) to Λ CDM Universe. This was later recognised as the standard model of cosmology for it was endorsed by numerous follow-up observations. However, despite the success, the last decade witnessed growing doubts regarding this model, due to the appearance of the (third) Hubble tension that implies the values of the Hubble constant measured from the early and late Universe are inherently inconsistent. For instance, when assuming Λ CDM, Planck Collaboration et al. (2020a) derived $H_0 = 67.36 \pm 0.54 \text{ km s}^{-1} \text{ Mpc}^{-1}$ from CMB, while the direct local observational result from Riess et al. (2022) showed that $H_0 = 73.30 \pm 1.04 \text{ km s}^{-1} \text{ Mpc}^{-1}$. Although many efforts have been made to check whether the inconsistency between the local direct and early indirect measurement of H_0 is caused by some statistical flukes or overlooked observational errors, the consensus still has not been reached as yet. Instead, the rising concern is that the modification of the cosmological model itself is required to alleviate the tension.

On top of the Hubble tension, the Λ CDM model is also challenged by the anomaly on the matter clustering, dubbed as the S_8 tension.

The factor $S_8 \equiv \sigma_8 \sqrt{\Omega_m/0.3}$ measures the amplitude of the matter clustering and is closely related to the growth rate of the large-scale structure via $f\sigma_8$, where $f = [\Omega_m(z)]^{0.55}$. The observed result of this factor from the Weak Lensing (WL), e.g., Kilo-Degree Survey (KiDS), is $S_8 \approx 0.759$ (Asgari et al. (2021)), about $2 - 3\sigma$ lower than the expected value from CMB that gives $S_8 \approx 0.834$ (Planck Collaboration et al. (2020b)). Likewise, there are two possible approaches towards the alleviation of the S_8 tension, the observational/statistical errors, and the alteration of the cosmological model. The consensus, however, has not yet been reached either. More information about the aforementioned tensions can be found in Abdalla et al. (2022).

Schöneberg et al. (2022) summarised and compared the most common 17 theories proposed to resolve the Hubble tension and among them, the EDE theory is one of the few that carries both theoretical capability and observational evidence. The basic idea of EDE is to introduce a scalar field that behaves like dark energy before the recombination and dilutes faster than the radiation such that the post-recombination evolution remains to be Λ CDM. This extra component decreases the physical sound horizon r_s by slightly increasing the cooling rate of the Universe. As a result, the corresponding H_0 inferred from CMB is increased accordingly.

The most direct observational evidence of EDE by far comes from Poulin et al. (2021); Hill et al. (2022), in which they analysed the CMB temperature power spectrum data from the Wilkinson Microwave Anisotropy Probe (WMAP), ACT and Planck Telescope.

* E-mail: wylu@bao.ac.cn (NAOC)

Two-dimensional models of core-collapse supernova explosions assisted by heavy sterile neutrinos

Kanji Mori,^{1,*} Tomoya Takiwaki,¹ Kei Kotake,^{2,3} and Shunsaku Horiuchi^{4,5}

¹*National Astronomical Observatory of Japan, 2-21-1 Osawa, Mitaka, Tokyo 181-8588, Japan*

²*Research Institute of Stellar Explosive Phenomena,
and Department of Applied Physics, Fukuoka University,
8-19-1 Nanakuma, Jonan-ku, Fukuoka-shi, Fukuoka 814-0180, Japan*

³*Institute for Theoretical Physics, University of Wrocław, 50-204 Wrocław, Poland*

⁴*Center for Neutrino Physics, Department of Physics, Virginia Tech, Blacksburg, VA 24061, USA*

⁵*Kavli IPMU (WPI), UTIAS, The University of Tokyo, Kashiwa, Chiba 277-8583, Japan*

(Dated: February 23, 2024)

Core-collapse supernovae can be a copious source of sterile neutrinos, hypothetical particles that mix with active neutrinos. We develop two-dimensional stellar core-collapse models that incorporate the mixing between tau neutrinos and heavy sterile neutrinos—those with the mass of 150–200 MeV—to investigate signatures of sterile neutrinos in supernova observables. We find that the decay channel of a sterile neutrino into a pion and a tau neutrino can enhance the explosion energy and the synthesized nickel mass. Although the inclusion of sterile neutrinos considered in this study slightly reduce the neutrino and gravitational-wave signals, we find that they are still detectable for a Galactic event. Furthermore, we point out that if sterile neutrinos are as massive as ~ 200 MeV, they produce high-energy tau antineutrinos with energies of ~ 80 MeV, the detection of which can be a smoking signature of the sterile neutrinos and where Hyper-Kamiokande should play a pivotal role.

I. INTRODUCTION

In the Standard Model of particle physics, neutrinos are treated as massless left-handed fermions. However, observations of neutrino oscillations [e.g., 1, 2] reveal that the neutrino masses are nonzero. Although the origin of the neutrino masses is under debate, introducing heavy right-handed particles called sterile neutrinos [3, 4] naturally leads to finite masses of active neutrinos through the seesaw mechanism [5–7].

Apart from the theoretical motivation above, there are experimental hints of sterile neutrinos. For example, electron antineutrino fluxes from reactors are anomalously smaller than theoretical expectations [8–10]. This deficit could be explained by oscillations into sterile neutrinos [11]. Also, sterile neutrino with mass \sim keV work as a candidate of dark matter [12–14]. Interestingly, x-ray observations of galaxy clusters and galaxies with the XMM-Newton and Chandra satellites detected a 3.5 keV line, which can be interpreted as a signature of the radiative decay of 7.1 keV-mass sterile neutrino dark matter [15–17]. Although the sterile neutrino interpretation for these signatures is under debate [e.g., 10, 14, 18–23], these studies motivate experimental and astronomical explorations of the particle.

Core-collapse supernovae are a useful laboratory for sterile neutrinos because neutrinos play essential roles in the supernova explosion mechanism. Sterile neutrinos can be produced in supernova events through mixing

with active neutrinos and can affect the energy transfer inside. Indeed, the effects of sterile neutrinos on supernovae have been investigated for various sterile neutrino masses $m_s = \mathcal{O}(\text{eV})$ [24–34], $\mathcal{O}(\text{keV})$ [35–45], and $> \mathcal{O}(\text{MeV})$ [46–52]. Although these studies have gradually refined the microphysics, they nonetheless have only adopted spherically-symmetric supernova models. This is despite the fact that, multi-dimensionality is essential to the supernova explosion mechanism. Also, it is not possible to predict gravitational wave signals with one-dimensional models. In this study, we hence develop two-dimensional supernova models coupled with sterile neutrinos.

We focus on a heavy sterile neutrino model with $m_s = 150\text{--}200$ MeV and Lagrangian [47, 51],

$$\mathcal{L} = \mathcal{L}_{\text{SM}} + i\bar{\nu}_s \not{\partial} \nu_s - y_\nu \bar{L} \tilde{H} \nu_s + \frac{m_s}{2} \bar{\nu}_s^c \nu_s + \text{h.c.}, \quad (1)$$

where \mathcal{L}_{SM} is the Standard Model Lagrangian, y_ν is a Yukawa coupling constant, H is the $\text{SU}(2)_L$ Higgs doublet, and L is the lepton doublet. The Yukawa coupling term leads to a Dirac mass term below the electroweak scale and diagonalization of the Dirac and Majorana mass terms provides the masses of active and sterile neutrinos through the seesaw mechanism. We assume that sterile neutrinos mix with ν_τ ,

$$\begin{aligned} \nu_\tau &= \cos \theta_{\tau 4} \nu_1 + \sin \theta_{\tau 4} \nu_2 \\ \nu_s &= -\sin \theta_{\tau 4} \nu_1 + \cos \theta_{\tau 4} \nu_2, \end{aligned} \quad (2)$$

where ν_1 and ν_2 are the mass eigenstates and $\theta_{\tau 4}$ is the mixing angle. Heavy sterile neutrinos that mix with ν_e and ν_μ have been strongly excluded by terrestrial experiments [53–55], but mixing with ν_τ is less constrained. Core-collapse supernovae can provide a unique way to

* kanji.mori@nao.ac.jp; Research Fellow of Japan Society for the Promotion of Science

The Jiao Tong University Spectroscopic Telescope Project

JUST Team ^{*1,2}, Chengze Liu^{2,1}, Ying Zu^{2,1}, Fabo Feng^{1,2}, Zhaoyu Li², Yu Yu², Hua Bai^{3,4}, Xiangqun Cui^{3,5}, Bozhong Gu³, Yizhou Gu^{1,2}, Jiaxin Han², Yonghui Hou^{3,5}, Zhongwen Hu^{3,5}, Hangxin Ji³, Yipeng Jing^{1,2}, Wei Li⁶, Zhaoxiang Qi⁷, Xianyu Tan¹, Cairang Tian⁶, Dehua Yang³, Xiangyan Yuan^{3,4}, Chao Zhai⁸, Congcong Zhang⁷, Jun Zhang², Haotong Zhang⁹, Pengjie Zhang^{1,2}, Yong Zhang⁹, Yi Zhao⁶, Xianzhong Zheng¹⁰, Qingfeng Zhu⁸ and Xiaohu Yang^{1,2}

1. Tsung-Dao Lee Institute, Shanghai Jiao Tong University, Shanghai 200240, China;
2. Department of Astronomy, School of Physics and Astronomy, Shanghai Jiao Tong University, Shanghai 200240, China;
3. Nanjing Institute of Astronomical Optics & Technology, Chinese Academy of Sciences, Nanjing 210042, China;
4. University of Chinese Academy of Sciences, Nanjing 211135, China;
5. University of Chinese Academy of Sciences, Beijing 101408, China;
6. Lenghu Technology Innovation Industrial Park Management Committee, Lenghu 817400, China;
7. Shanghai Astronomical Observatory, Chinese Academy of Sciences, Shanghai 200030, China;
8. Department of Astronomy, University of Science and Technology of China, Hefei 230026, China;
9. National Astronomical Observatories, Chinese Academy of Sciences, Beijing 100012, China;
10. Purple Mountain Observatory, Chinese Academy of Sciences, Nanjing 210023, China.

Abstract: The Jiao Tong University Spectroscopic Telescope (JUST) is a 4.4-meter $f/6.0$ segmented-mirror telescope dedicated to spectroscopic observations. The JUST primary mirror is composed of 18 hexagonal segments, each with a diameter of 1.1 m. JUST provides two Nasmyth platforms for placing science instruments. One Nasmyth focus fits a field of view of $10'$ and the other has an extended field of view of 1.2° with correction optics. A tertiary mirror is used to switch between the two Nasmyth foci. JUST will be installed at a site at Lenghu in Qinghai Province, China, and will conduct spectroscopic observations with three types of instruments to explore the dark universe, trace the dynamic universe, and search for exoplanets: (1) a multi-fiber (2000 fibers) medium-resolution spectrometer ($R=4000-5000$) to spectroscopically map galaxies and large-scale structure; (2) an integral field unit (IFU) array of 500 optical fibers and/or a long-slit spectrograph dedicated to fast follow-ups of transient sources for multi-messenger astronomy; (3) a high-resolution spectrometer ($R\sim 100000$) designed to identify Jupiter analogs and Earth-like planets, with the capability to characterize the atmospheres of hot exoplanets.

Keywords: Astronomical instrumentation(799) — Optical telescopes(1174) — Large-scale structure of the universe(902) — Redshift surveys(1378) — Time domain astronomy(2109) — Exoplanet astronomy (486)

Color-flavor locked strange stars with a mirror-dark-matter core and the observations of compact stars

S.-H. Yang,^{a,1} and C.-M. Pi^{b,c}

^aInstitute of Astrophysics,
Central China Normal University,
Luoyu Road, Hongshan District, Wuhan, China

^bSchool of Physics and Mechanical & Electrical Engineering,
Hubei University of Education,
Hi-Tech 2 Road, East Lake Hi-Tech Zone, Wuhan, China

^cResearch Center for Astronomy,
Hubei University of Education,
Hi-Tech 2 Road, East Lake Hi-Tech Zone, Wuhan, China

E-mail: ysh@ccnu.edu.cn

Abstract. We investigate the structure and the tidal deformability of the color-flavor locked strange stars with a mirror-dark-matter core. Assuming the stars in the GW170817 event have a mirror-dark-matter core, the observations of the central compact object within the supernova remnant HESS J1731-347 and the compact objects in the GW190814 and GW170817 events could be explained simultaneously with a pairing gap much smaller than 200 MeV, while a pairing gap larger than about 200 MeV must be employed without the consideration of a mirror-dark-matter core. More importantly, we find that for the case of the quartic coefficient $a_4 < 0.589$, if the mirror-dark-matter core in the compact stars of GW170817 is large enough (e.g., the mass fraction of the mirror-dark-matter core is larger than 22.8% for $a_4 = 0.55$), the minimum allowed value of the pairing gap could be less than 46.5 MeV (i.e., one half of the value of the strange quark mass which is taken as 93 MeV in this paper), which leads to the result that all astrophysical observations mentioned above could be satisfied without violating the conformal bound or the recently proposed positive trace anomaly bound.

Keywords: dark matter, strange star, tidal deformability

¹Corresponding author.

Velocity reconstruction with graph neural networks

Hideki Tanimura* and Jia Liu

*Center for Data-Driven Discovery, Kavli IPMU (WPI), UTIAS,
The University of Tokyo, Kashiwa, Chiba 277-8583, Japan*

Albert Bonneau

École Normale Supérieure de Lyon, 15 parvis René-Descartes 69342 Lyon Cedex 07, France

Sanmay Ganguly

*ICEPP, The University of Tokyo. Hongo, Bunkyo-ku, Tokyo 113-0033, Japan and
Indian Institute of Technology Kanpur, Kalyanpur, Kanpur 208016, Uttar Pradesh, India*

(Dated: February 23, 2024)

In this work, we seek to improve the velocity reconstruction of clusters by using Graph Neural Networks—a type of deep neural network designed to analyze sparse, unstructured data. In comparison to the Convolutional Neural Network (CNN) which is built for structured data such as regular grids, GNN is particularly suitable for analyzing galaxy catalogs. In our GNNs, galaxies are represented as nodes that are connected with edges. The galaxy positions and properties—stellar mass, star formation rate, and total number of galaxies within $100 h^{-1}\text{Mpc}$ —are combined to predict the line-of-sight velocity of the clusters. To train our networks, we use mock SDSS galaxies and clusters constructed from the Magnetism hydrodynamic simulations. Our GNNs reach a precision in reconstructed line-of-sight velocity of $\Delta v=163$ km/s, outperforming by $\approx 10\%$ the perturbation theory ($\Delta v=181$ km/s) or the CNN ($\Delta v=179$ km/s). The stellar mass provides additional information, improving the precision by $\approx 6\%$ beyond the position-only GNN, while other properties add little information. Our GNNs remain capable of reconstructing the velocity field when redshift-space distortion is included, with $\Delta v=210$ km/s which is again 10% better than CNN with RSD. Finally, we find that even with an impressive, nearly 70% increase in galaxy number density from SDSS to DESI, our GNNs only show an underwhelming 2% improvement, in line with previous works using other methods. Our work demonstrates that, while the efficiency in velocity reconstruction may have plateaued already at SDSS number density, further improvements are still hopeful with new reconstruction models such as the GNNs studied here.

I. INTRODUCTION

The velocity field of the large-scale structure is a useful probe of cosmological and astrophysical parameters. Reconstructing the velocity field was an essential step in previous works to e.g. sharpen the baryon acoustic oscillations (BAO) peaks [1–3] and to extract the kinematic Sunyaev-Zel’dovich (kSZ) [4] via cross-correlations with the Cosmic Microwave Background (CMB) measurements [5–17]. The BAO signal originates from the acoustic density waves in the primordial plasma. It is used as a standard ruler to measure the expansion history of the universe [18–36]. The kSZ signal originates from the scattering of CMB photons off coherently moving electrons. Because the kSZ effect is a particularly powerful probe of the electron distribution in under-dense regions, it was used to investigate the “missing baryon problem” [12, 37–39] and to constrain baryonic feedback [9, 15, 40–43].








In the past, the velocity field was typically reconstructed by solving the linearized continuity equation on the galaxy density field [14, 44–48]. While the method works well on large scales where density fluctuation is small (“linear”), three issues complicate the procedure on small scales ($\lesssim 30 h^{-1}\text{Mpc}$). First, structure formation becomes nonlinear on these scales and hence is not fully captured in the linearized continuity equation [49, 50]. Second, to obtain the underlying matter

field, we need to correct the galaxy bias, which becomes nonlinear on small scales and often requires numerical simulations to calibrate [51–56]. Finally, the line-of-sight (LOS) positions of the galaxies are measured in redshift, and hence we need to correct for redshift-space distortion (RSD) to obtain the comoving distance [57, 58].

In this work, we use the Graph Neural Network (GNN)—a deep neural network particularly suitable to sparse, heterogeneous data—to reconstruct the velocity field. The application of machine learning to velocity reconstruction is not new. Previously, [15, 59–61] performed such tasks using the Convolutional Neural Network (CNN). However, there are several limitations with CNNs in handling galaxy catalogs that motivated us to experiment with the GNN architecture [62]. First, CNNs are optimized for grid-like data but less so for irregularly structured data such as galaxy catalogs. Second, CNNs focus mainly on local features and hence likely to overlook global patterns. Third, CNNs are trained on a single data type, i.e. galaxy positions, and hence unable to incorporate other potentially useful galaxy features such as color, shape, stellar mass, and star formation rate. In comparison, GNNs can handle unstructured data of arbitrary size and complex topology, capture global patterns, and allow us to incorporate multiple data types such as galaxy positions and properties. Thanks to these advantages, GNNs with galaxies have been recently used to predict halo masses [63] and the cosmic matter density Ω_m [64, 65]. In this work, to quantify the performance of GNNs on realistic observations, we reconstruct the velocity fields using GNNs trained on mock galaxies of the Sloan Dig-

* hideki.tanimura@ipmu.jp

Broadband noise and quasi-periodic oscillation characteristics of the X-ray pulsar RX J0440.9+4431

P. P. Li,^{1,2} L. Tao ^{1,*} R. C. Ma,^{1,2} M. Y. Ge ¹ Q. C. Zhao,^{1,2} S. J. Zhao,^{1,2} L. Zhang,¹ Q. C. Bu ³,
L. D. Kong ³ Y. L. Tuo ³ L. Ji ⁴ S. Zhang,¹ J. L. Qu,¹ S. N. Zhang ¹ Y. Huang,¹ X. Ma,¹
W. T. Ye,^{1,2} Q. C. Shui,^{1,2}

¹Key Laboratory of Particle Astrophysics, Institute of High Energy Physics, Chinese Academy of Sciences, 100049 Beijing, People's Republic of China

²University of Chinese Academy of Sciences, Chinese Academy of Sciences, 100049 Beijing, People's Republic of China

³Institut für Astronomie und Astrophysik, Kepler Center for Astro and Particle Physics, Eberhard Karls Universität, Sand 1, D-72076 Tübingen, Germany

⁴School of Physics and Astronomy, Sun Yat-sen University, Zhuhai, 519082, People's Republic of China

Accepted XXX. Received YYY; in original form ZZZ

ABSTRACT

We present a comprehensive timing analysis on the Be/X-ray binary pulsar RX J0440.9+4431 using observations from *NICER* and *Insight*-HXMT during the 2022–2023 outburst. The power density spectrum (PDS) of RX J0440.9+4431 exhibits typical aperiodic variability in X-ray flux across a wide frequency range. During a super-critical accretion state, we detect quasi-periodic oscillations (QPOs) at 0.2–0.5 Hz in the light curves of five pulses for RX J0440.9+4431. The observed QPOs manifest during flares, while the flares appear at the peaks of the pulse profiles on a timescale of seconds and are primarily caused by an increase in hard photons. These flares can be explained by increased material ingestion in the accretion column at a fixed phase, primarily generating hard photons. Alternatively, an increase in accretion rate, independent of phase, may result in highly beamed hard photons within the accretion column, causing the flares. We argue the origin of QPOs to instabilities within the accretion flow. Additionally, we find that the break frequencies in the noise power spectra align well with $\propto L_x^{3/7}$ across three orders of magnitude in the luminosity, which points to a relatively strong magnetic field in RX J0440.9+4431, estimated to be $\sim 10^{13}$ G.

Key words: accretion, accretion disc – X-rays: binaries – stars: neutron-pulsars: individual (RX J0440.9+4431)

1 INTRODUCTION

In the analysis of X-ray pulsars (XRP), the power density spectrum (PDS) serves as a commonly used tool for scrutinizing light curves. It presents the power distribution of signals in the frequency domain, thereby unveiling potential signal structures in observational data (e.g. Tian & Zou 2014; Wang 2016). Within the PDS of XRP, in addition to naturally displaying inherent periodic peaks corresponding to pulse components and their harmonics, there is also a strong aperiodic variability in X-ray flux over a wide frequency range, characterized by band-limited noise and possible quasi-periodic oscillations (QPOs; e.g. Reig 2008; James et al. 2010). The power of band-limited noise increases at lower frequencies and exhibits a flattening towards higher frequencies, approximated by a broken (or double-broken) power law. This phenomenon is similar to what is observed in accreting black holes (BHs; e.g. Stiele & Yu 2015) and active galactic nuclei (AGN; e.g. McHardy et al. 2004).

The aperiodic noise can be naturally explained by the propagating fluctuations model (Lyubarskii 1997; Churazov et al. 2001). According to this model, the initial fluctuations in mass accretion rate occur at different radial coordinates in the accretion disc, and then propagate towards the central object, causing local variations in mass accretion rate at all radii. The variability of the local mass accretion

rate leads to photon flux variability observed from different parts of the accretion disc. The time-scales of the initial fluctuations are comparable to or smaller than the local Keplerian time-scale, while the process of viscous diffusion in the disc effectively suppresses variability above the frequency of the initial fluctuations (Mushtukov et al. 2018, 2019). Therefore, the observed break frequency in the PDS is closely related to the inner disc radius (Revnivtsev et al. 2009). As the X-ray luminosity varies, any corresponding changes in the size of the magnetosphere will result in a corresponding alteration in the break frequency (Revnivtsev et al. 2009; Doroshenko et al. 2020). Even though photons mostly originate from the neutron star (NS) surface, the time-scales of photon diffusion from a hotspot/accretion column and reprocessing of X-ray flux by the atmosphere are much shorter than the Keplerian time-scale at the inner disc radius. Therefore, it is believed that the observed aperiodic variability of X-ray flux replicate fluctuations in mass accretion rate at the inner disc radius (Mushtukov et al. 2019). Consequently, for known magnetic field strength in XRP, we can use the measured break frequency in the PDS to estimate the inner radius of the disc (Bodaghee et al. 2016). For XRP with unknown magnetic field, we can estimate it using the relationship between break frequency and luminosity (Doroshenko et al. 2014; Mönkkönen et al. 2022).

QPOs have been detected in multiple highly magnetized NS systems, only concentrated in the low-frequency range (Devasia et al. 2011), from ~ 10 mHz to ~ 1 Hz, referred to as mHz QPOs. These

* E-mail: taolian@ihep.ac.cn

Interacting light thermal-relic dark matter: self-consistent cosmological bounds

Rui An,^{1,*} Kimberly K. Boddy,^{2,†} and Vera Gluscevic^{1,3,‡}

¹*Department of Physics and Astronomy, University of Southern California, Los Angeles, CA 90089, USA*

²*Texas Center for Cosmology and Astroparticle Physics, Weinberg Institute,*

Department of Physics, The University of Texas at Austin, Austin, TX 78712, USA

³*TAPIR, Mailcode 350-17, California Institute of Technology, Pasadena, CA 91125, USA*

We analyze cosmic microwave background (CMB) data to constrain the mass and interaction strengths of thermally-produced dark matter (DM) in a self-consistent manner, simultaneously taking into account the cosmological effects of its mass and interactions. The presence of a light thermal-relic particle contributes non-negligibly to the radiation density during Big Bang Nucleosynthesis (BBN), altering the light-element yields, as well as the effective number of relativistic particle species. On the other hand, DM interactions with the Standard Model can affect distribution of matter in later universe. Both mass and interactions alter CMB anisotropy on sub-degree scales. To understand and quantify the interplay of these effects, we consider elastic DM-baryon scattering with a momentum-transfer cross section that scales as a power law of the relative velocity between the scattering particles. In the range of thermal-relic DM masses relevant for BBN ($\lesssim 20$ MeV), we find that the reconstruction of the DM mass and the scattering cross section from the CMB data features strong degeneracies; modeling the two effects simultaneously increases the sensitivity of the CMB measurements to both fundamental properties of DM. Additionally, we study the effects of late-time residual annihilation of a light thermal relic and provide improved CMB constraints on the DM mass and annihilation cross section. To examine degeneracy between DM mass, cross section for elastic scattering with baryons, and annihilation cross section, we consider a specific case of DM with an electric and magnetic dipole moments. We present new, self-consistent cosmological bounds for this model and discuss implications for future searches.

I. INTRODUCTION

Dark matter (DM) accounts for a significant fraction of the matter in our Universe [1–5], but its physical nature remains a mystery. Standard cosmology features cold and collisionless DM (CDM), interacting only gravitationally with the Standard Model (SM) of particle physics; however, a range of beyond-CDM paradigms is explored in the literature and can lead to unique observational consequences [6–13].

In the standard thermal freeze-out scenario, DM is in chemical equilibrium with the thermal bath at early times. As the temperature drops below the DM mass, DM becomes nonrelativistic; its equilibrium number density drops exponentially, eventually rendering DM annihilation inefficient for maintaining chemical equilibrium [14–17]. The time of onset of exponential suppression in DM number density is primarily dictated by DM mass, while the freeze-out abundance of DM is governed by its annihilation rate to SM particles. During this decoupling process, the contribution of DM to the entropy density of the Universe is transferred to the thermal bath, slowing down the cooling of the bath. Additionally, DM behavior as a radiation-like or matter-like fluid affects the expansion rate of the Universe.

For high DM masses, $\gtrsim 20$ MeV, the decoupling process occurs sufficiently early in cosmic history that there

are no observable effects on the temperature evolution and expansion rate. For DM masses between 10 keV and 20 MeV, the decoupling process occurs around the time of Big Bang Nucleosynthesis (BBN) and may affect standard BBN predictions through changes to the expansion rate, photon-to-baryon density ratio, and weak-interaction rates. As a result, DM mass can affect the production of light chemical elements [18–20] and the effective number of relativistic particle species [21–23]. For even lower DM masses $\lesssim 10$ keV, the decoupling process does not impact BBN, but the presence of relativistic DM still alters the expansion rate during BBN. These effects that originate during the BBN era can be captured in the cosmic microwave background (CMB) anisotropies [24–29] and provide some of the most stringent bounds on the mass of light thermal-relic DM [22, 23, 30–35].

Apart from its mass, the non-gravitational interactions of DM with baryons can also affect CMB anisotropies in a more direct manner, leading to changes in the CMB power spectra. For example, DM-baryon elastic scattering suppresses the clustering of matter in the Universe through DM-baryon momentum transfer, which is absent in the standard Λ CDM model [36–48]. Additionally, late-time (post freeze-out) residual annihilation of DM into SM particles [5, 49, 50] injects energy into the plasma, potentially altering the recombination history and increasing the optical depth of CMB photons.¹ In summary, the

* Email: anrui@usc.edu

† Email: kboddy@physics.utexas.edu

‡ Email: vera.gluscevic@usc.edu

¹ Late-time annihilation occurs if there is an abundance of both DM and anti-DM particles. This scenario is not applicable to asymmetric DM [9].

Velocity Dispersions of Quiescent Galaxies in IllustrisTNG

JUBEE SOHN,^{1,2} MARGARET J. GELLER,³ JOSH BORROW,⁴ AND MARK VOGELSBERGER⁴

¹*Astronomy Program, Department of Physics and Astronomy, Seoul National University, 1 Gwanak-ro, Gwanak-gu, Seoul 08826, Republic of Korea*

²*SNU Astronomy Research Center, Seoul National University, Seoul 08826, Republic of Korea*

³*Smithsonian Astrophysical Observatory, 60 Garden Street, Cambridge, MA 02138, USA*

⁴*Department of Physics, Kavli Institute for Astrophysics and Space Research, Massachusetts Institute of Technology, Cambridge, MA 02139, USA*

ABSTRACT

We examine the central stellar velocity dispersion of subhalos based on IllustrisTNG cosmological hydrodynamic simulations. The central velocity dispersion is a fundamental observable that links galaxies with their dark matter subhalos. We carefully explore simulated stellar velocity dispersions derived with different definitions to assess possible systematics. We explore the impact of variation in the identification of member stellar particles, the viewing axes, the velocity dispersion computation technique, and simulation resolution. None of these issues impact the velocity dispersion significantly; any systematic uncertainties are smaller than the random error. We examine the stellar mass-velocity dispersion relation as an observational test of the simulations. At fixed stellar mass, the observed velocity dispersions significantly exceed the simulation results. This discrepancy is an interesting benchmark for the IllustrisTNG simulations because the simulations are not explicitly tuned to match this relation. We demonstrate that the stellar velocity dispersion provides measures of the dark matter velocity dispersion and the dark matter subhalo mass.

1. INTRODUCTION

The nature of dark matter is a long-standing puzzle. In the Λ CDM paradigm, dark matter plays a pivotal role in the formation of galaxies and large-scale structures. Many indirect techniques trace the masses of dark matter halos. One approach is to take advantage of correlations between the properties of galaxies within dark matter (sub)halos and the dark matter halo mass. Abundance matching (e.g., Yang et al. 2003; Kravtsov et al. 2004; Conroy et al. 2006; Guo et al. 2010; Behroozi et al. 2013), for example, compares the observed stellar mass distribution of galaxies with the dark matter mass distribution obtained from simulations. Despite its success, connecting galaxies and dark matter properties based on stellar mass is affected by potential systematic uncertainties associated with both observational and simulation-based stellar mass estimates. Stellar mass estimates may have systematic uncertainties of ~ 0.3 dex depending on the model choice (e.g., Conroy et al. 2006; Zahid et al. 2016).

Central stellar velocity dispersion is a complementary observable of galaxies that potentially traces the dark matter halo mass (Wake et al. 2012; Schechter 2015; Zahid et al. 2018). The spectroscopic stellar velocity dispersion is a more direct measure of the gravitational potential than photometric observables (Wake et al. 2012; Zahid et al. 2018). The typical systematic uncertainty in the stellar velocity dispersion for quiescent galaxies is also relatively small (< 0.03 dex, Fabricant et al. 2013; Zahid et al. 2018).

Schechter (2015) suggests that the stellar velocity dispersion of elliptical galaxies is a proxy for the dark matter halo mass. Based on a large sample of quiescent galaxies, Zahid et al. (2016) show that the relation between stellar velocity dispersion and the total mass is consistent with the theoretical relation for dark matter halos (Evrard et al. 2008; Rines et al. 2016). Utsumi et al. (2020) use galaxy-galaxy weak lensing to demonstrate that the stellar velocity dispersion is proportional to the corresponding dark matter velocity dispersion (see also van Uitert et al. 2013).

Cosmological numerical simulations offer a testbed for investigating the relation between observables and the velocity dispersion and mass of the dark matter halo.

Developing an Automated Detection, Tracking and Analysis Method for Solar Filaments Observed by CHASE via Machine Learning

Z. ZHENG ^{1,2} Q. HAO ^{1,2} Y. QIU ³ J. HONG ^{1,2} C. LI ^{1,2,3} AND M.D. DING ^{1,2}

¹*School of Astronomy and Space Science, Nanjing University, Nanjing 210023, China*

²*Key Laboratory of Modern Astronomy and Astrophysics, Ministry of Education, Nanjing 210023, China*

³*Institute of Science and Technology for Deep Space Exploration, Suzhou Campus, Nanjing University, Suzhou 215163, China*

ABSTRACT

Studies on the dynamics of solar filaments have significant implications for understanding their formation, evolution, and eruption, which are of great importance for space weather warning and forecasting. The H α Imaging Spectrograph (HIS) onboard the recently launched Chinese H α Solar Explorer (CHASE) can provide full-disk solar H α spectroscopic observations, which bring us an opportunity to systematically explore and analyze the plasma dynamics of filaments. The dramatically increased observation data require automate processing and analysis which are impossible if dealt with manually. In this paper, we utilize the U-Net model to identify filaments and implement the Channel and Spatial Reliability Tracking (CSRT) algorithm for automated filament tracking. In addition, we use the cloud model to invert the line-of-sight velocity of filaments and employ the graph theory algorithm to extract the filament spine, which can advance our understanding of the dynamics of filaments. The favorable test performance confirms the validity of our method, which will be implemented in the following statistical analyses of filament features and dynamics of CHASE/HIS observations.

Keywords: Solar filaments — Convolutional neural networks — Astronomy image processing

1. INTRODUCTION

Solar filament is one of the typical solar activities in solar atmosphere, which is about 100 times cooler and denser than its surrounding corona (Labrosse et al. 2010). They are observed as dark elongated structures with several barbs, but are seen as bright structures suspended over the solar limb called prominences (Vial & Engvold 2015). Filaments are always align with photospheric magnetic polarity inversion line (PIL), where the magnetic flux cancellation often takes place (Martin 1998; Vial & Engvold 2015). Filaments sometimes undergo large-scale instabilities, which break their equilibria and lead to eruptions. There is a close relationship among the erupting filaments, flares, and coronal mass ejections, which are different manifestations of one physical process at different evolutionary stages (Gopal-swamy et al. 2003). Therefore, the study of the formation, evolution and eruption of filament is not only of

great significance to understand the essence physics of solar activities, but also of practical significance for accurately predicting the hazardous space weather (Chen 2011; Chen et al. 2020).

Filament are usually observed by ground-based solar H α telescopes around the world, such as Meudon, Big Bear, Kanzelhöhe, Kodaikanal, and Huairou. These telescopes have been the work horses of most of the current knowledge on filaments (Chatzistergos, Theodosios et al. 2023). To study the mechanisms of solar eruptions and the plasma dynamics in the lower atmosphere, the Chinese H α Solar Explorer (CHASE; Li et al. 2019, 2022) was launched into a Sun-synchronous orbit on October 14, 2021. The scientific payload onboard CHASE is the H α Imaging Spectrograph (HIS; Liu et al. 2022), which can provide solar H α spectroscopic observations. It brings us an opportunity to systematically explore and analyze the plasma dynamics of filaments in details. At the same time, the data volume of CHASE/HIS observations has dramatically increased, which also brings challenges to efficiently process such huge amount of data.

In order to statistically obtain the filament features, Gao et al. (2002) developed an automated algorithm

Luminosity Outbursts in Interacting Protoplanetary Systems

Aleksandr M. Skliarevskii¹, Eduard I. Vorobyov²

¹ Research Institute of Physics, Southern Federal University, Rostov-on-Don 344090, Russia e-mail: sklyarevskiy@sfned.ru

² Ural Federal University, 19 Mira Str., 620002 Ekaterinburg, Russia

12.02.2024

ABSTRACT

FU Orionis type objects (fuors) are characterized by rapid (tens to hundreds years) episodic outbursts, during which the luminosity increases by orders of magnitude. One of the possible causes of such events is a close encounter between stars and protoplanetary disks. Numerical simulations show that the fuor-like outburst ignition requires a very close encounter ranging from a few to a few tens of au. In contrast, the observed stellar objects in fuor binaries are usually hundreds of au apart. Simple mathematical estimates show that if such a close approach took place, the binary stellar components would have an unrealistic relative velocity, at least an order of magnitude greater than the observed velocity dispersion in young stellar clusters. Thus, the bursts are either triggered with a certain delay after passage of the periastron or their ignition does not necessarily require a close encounter and hence the outburst is not caused by the primordial gravitational perturbation of the protoplanetary disk. In this work, an encounter of a star surrounded by a protoplanetary disk with a diskless external stellar object was modeled using numerical hydrodynamics simulations. We showed that even fly-bys with a relatively large periastron (at least 500 au) can result in fuor-like outbursts. Moreover, the delay between the periastron passage and the burst ignition can reach several kyr. It was shown for the first time by means of numerical modeling that the perturbation of the disk caused by the external object can trigger a cascade process, which includes the development of the thermal instability in the innermost disk followed by the magneto-rotational instability ignition. Because of the sequential development of these instabilities, the rapid increase in the accretion rate occurs, resulting in the luminosity increase by more than two orders of magnitude.

Key words. astrophysics, protostellar disks, protoplanetary disks, luminosity outbursts

1. Introduction

It is known that protostars in young stellar systems can experience a sudden increase in luminosity. The luminosity during such events can change up to several orders of magnitude over timescales from tens to several hundred years. FU Orionis is the first object to successfully observe such an outburst. Subsequently, it formed the basis of a whole class of objects called fuors. Despite the fact that at the moment the number of objects classified as fuors reaches only a few dozen (see, for example, Audard et al. 2014; Magakian et al. 2022), such outbreaks are hardly rare. Young stars can experience up to ten or even several dozen such events during their evolution (Kenyon 1999; Audard et al. 2014; Vorobyov & Basu 2015). Fuor-type outbursts are more likely to occur in the early stages of the evolution of protoplanetary systems, while there is still an accretion disk around the star, and this disk is active and optically thick (Mercer & Stamatellos 2017; Vorobyov & Basu 2015).

Outbursts can affect the evolution of the disk, its structure and, in particular, its thermal characteristics. Even a short-term but significant increase in the luminosity of a star can noticeably heat the disk (Vorobyov et al. 2014, 2020a). In addition, the chemical composition of the disk can also be quite sensitive to both the heating of the disk and changes in the radiative characteristics of the star (Visser et al. 2015; Rab et al. 2017; Molyarova et al. 2018; Wiebe et al. 2019; Vorobyov et al. 2013). In addition to chemical reactions, temperature changes can result in a shift in the position of ice lines, a change in the properties of dust grains (for example, due to more active fragmentation) and, as a consequence, a change in the observed characteristics

of the disk (Banzatti et al. 2015; Schoonenberg & Ormel 2017). For example, in Vorobyov et al. (2022), it was shown that an outburst affects the distribution of spectral indices, and the effect persists for up to several thousand years. Finally, a sharp increase in the luminosity of the central star can serve as a trigger for various instabilities in the disk or change its dynamics. It was shown in Vorobyov et al. (2021) that the types of outbursts can be distinguished based on the dynamic characteristics of the post-outburst disk.

Despite the significance of outbursts for the evolution of the disk and their supposed prevalence, as well as the abundance of scientific works studying this phenomenon, it has still not been possible to reach a consensus in explaining the causes of outbursts. At the moment, many hypotheses have been presented about the physical nature of their origin. It is generally accepted that outbursts are a consequence of an episodic increase in the rate of accretion of matter from the disk onto the star (Audard et al. 2014; Connelley & Reipurth 2018). Magnetorotational instability (MRI) is often considered as a phenomenon that potentially leads to a sufficient increase in the accretion rate (see, for example, Armitage et al. 2001; Vorobyov et al. 2020b). This requires that the temperature in the disk be high enough to thermally ionize the alkali metals. In addition to the MRI, the accretion rate can increase when clumps of matter fall from the disk onto the star under the influence of gravity. Articles Vorobyov & Basu (2010, 2015) show that the accretion rate during such an event and the corresponding energy release during the fall of a massive clump onto a star can reach values characteristic of fuors. It is worth noting that not only clumps formed directly in the disk, but also compacted segments of the molecular cloud,

New evidence on the lost giant Chinguetti meteorite

Robert Warren,¹ Stephen Warren,² and Ekaterini Protopapa³

¹40 Mill Rd, Salisbury, SP2 7RZ, UK

²Astrophysics Group, Imperial College London, Blackett Laboratory, Prince Consort Road, London SW7 2AZ, UK
s.j.warren@imperial.ac.uk

³Department of Physics, University of Oxford, Clarendon Laboratory, Parks Road, Oxford, OX1 3PU, UK

(Dated: February 23, 2024)

Abstract

The giant Chinguetti meteorite that Gaston Ripert reported seeing in 1916 has never been found. A radionuclide analysis by Welten et al (2001) of the 4.5kg mesosiderite that Ripert recovered, supposedly sitting on the larger object, has convinced many that Ripert was mistaken, and interest in the giant meteorite has subsequently faded. Aspects of Ripert’s account of the giant meteorite are nevertheless compelling, particularly his description of ductile metal needles in one area of the surface explored. Several visual searches for the giant meteorite, beginning in 1924, might have failed because the object was already by then covered in sand. Using DEM data we have measured dune heights and established their drift speed. This has allowed us to create a map of locations where the meteorite could lie. The 2004 PRISM-I aeromagnetics surveys, acquired by Fugro for the Mauritanian Government for Mining Sector capacity building purposes, have the necessary area coverage, spatial resolution, and sensitivity to establish if the meteorite exists. In Jan 2023 we requested the PRISM data from the Ministry of Petroleum Energy and Mines, explaining, under Confidentiality, the scientific purpose of the request. To date the data have not been made available to us.

1. Brief history and rationale

This paper concerns the Chinguetti meteorite, a huge 40m-high, 100m-long iron inselberg located in the remote high dunes of the Mauritanian desert, that a French officer, Captain Gaston Ripert, claimed to have seen in 1916. His story reads like a fantasy, complete with an overheard conversation between camel drivers, a furtive mission at night, guided by the local chief, who forbade Ripert to take a compass, and was later poisoned, and a meteorite larger than any known by orders of magnitude, but without an impact crater; and yet Ripert produced a 4.5 kg meteorite he said he found on top – a very interesting object in its own right – and his matter of fact account, his proven scientific expertise, his sincerity, and above all some scientific details in his description of the huge meteorite cannot be reconciled unless the meteorite exists. Multiple searches stretching over 75 years have failed to locate it. The Chinguetti meteorite remains a fascinating mystery that has never been satisfactorily disproved. We are by no means the first to note that what is needed is a magnetometer survey over the entire region where the meteorite could possibly lie.

A comprehensive history of the topic is provided in the book *Le Fer de Dieu* (Monod and Zanda 1992), in French, and most of the details in the brief summary presented in this section are from this source. An excellent account in English, based primarily on the book, and including additional details is given by Marvin (2007). It must be appreciated that the region is extremely remote and was largely unmapped when searches for the meteorite commenced in 1924. Also, communication then was by surface mail (Ripert had moved to Cameroon). Because the mission was undertaken at night, without compass, Ripert could provide few details of the location, save that the trip on camelback took some 10h. A miscommunication meant that searches initially concentrated in the region SW of Chinguetti, but later were extended to all areas to the south. Several searches were undertaken by Théodore Monod starting in 1934 that continued intermittently until the 1980s, and there was one final search by Phil Bland and Sara Russell in the late 1990s, the subject of a Channel 4 documentary. With the exception of the last, these were all visual searches either on camelback or using aerial photography. (In truth in the 1950s the French army employed a crude magnetic device, a declinometer, in a search. Details are sparse, few measurements were made, and the sensitivity of the instrument is not stated.) Ripert described the meteorite as being nearly covered by sand in 1916, and so it could have become buried and thereby been missed by all the visual searches. Bland and Russell carried a magnetometer but took only a few measurements (with no positive results) at one particular location, directed there by a pilot Jacques Gallouédec

Steep-spectrum AGN in eROSITA Final Equatorial-Depth Survey (eFEDS): Their host galaxies and multi-wavelength properties

K. Iwasawa^{1,2}, T. Liu^{3,4,5}, Th. Boller³, J. Buchner³, J. Li⁶, T. Kawaguchi⁷, T. Nagao⁸, Y. Terashima⁸, Y. Toba^{8,9,10}, J. D. Silverman¹¹, R. Arcodia^{3,12}, Th. Dauser¹³, M. Krumpel¹⁴, K. Nandra³, and J. Wilms¹⁵

¹ Institut de Ciències del Cosmos (ICCUB), Universitat de Barcelona (IEEC-UB), Martí i Franquès, 1, 08028 Barcelona, Spain

² ICREA, Pg. Lluís Companys 23, 08010 Barcelona, Spain

³ Max-Planck-Institut für extraterrestrische Physik, Giessenbachstraße 1, 85748 Garching bei München, Germany

⁴ Department of Astronomy, University of Science and Technology of China, Hefei 230026, China

⁵ School of Astronomy and Space Science, University of Science and Technology of China, Hefei 230026, China

⁶ Department of Astronomy, University of Illinois at Urbana-Champaign, Urbana, IL 61801, USA

⁷ Department of Economics, Management and Information Science, Onomichi City University, Onomichi, Hiroshima 722-8506, Japan

⁸ Research Center for Space and Cosmic Evolution, Ehime University, Matsuyama, Ehime 790-8577, Japan

⁹ National Astronomical Observatory of Japan, Mitaka, Tokyo 181-8588, Japan

¹⁰ Institute of Astronomy and Astrophysics, Academia Sinica, Taipei 10617, Taiwan

¹¹ Kavli Institute for the Physics and Mathematics of the Universe, WPI, The University of Tokyo, Kashiwa, Chiba 277-8583, Japan

¹² MIT Kavli Institute for Astrophysics and Space Research, 70 Vassar Street, Cambridge, MA 02139, USA

¹³ Universität Erlangen/Nürnberg, Dr.-Remeis-Sternwarte, Sternwartstraße 7, 96049 Bamberg, Germany

¹⁴ Leibniz-Institut für Astrophysik Potsdam (AIP), An der Sternwarte 16, 14482 Potsdam, Germany

¹⁵ Dr. Karl Remeis-Sternwarte & Erlangen Centre for Astroparticle Physics, Sternwartstraße 7, 96049 Bamberg, Germany

February 23, 2024

ABSTRACT

We selected sources with a steep soft-X-ray-band spectrum with a photon index of $\Gamma > 2.5$ —measured by eROSITA on board the Spectrum-Röntgen-Gamma (SRG)— from the eFEDS AGN catalogue as candidates of highly accreting supermassive black holes, and investigated their multi-wavelength properties. Among 601 bright AGN with 0.2-5 keV counts of greater than 100, 83 sources ($\approx 14\%$) are classified as steep-spectrum sources. These sources have typical 0.5-2 keV luminosities of $L_{\text{SX}} \approx 10^{44}$ erg s⁻¹ and the majority of them are found at redshifts below $z = 1$. In comparison with sources with flatter spectra, these sources have, on average, a UV (or optical) to 2 keV luminosity ratio that is larger by ~ 0.3 dex and bluer optical-to-UV continuum emission. They also appear to be radio quiet based on the detection rate in the FIRST and VLASS surveys. Their host galaxies —at least in the redshift range of $z = 0.2-0.8$, where the AGN–galaxy decomposition results from the Subaru Hyper Suprime-Cam imaging are available— tend to be late-type and have smaller stellar masses ($M_{\star} \sim 10^{10.5} M_{\odot}$) than those of sources with flatter spectra. These properties are similar to those found in nearby narrow-line Seyfert 1 galaxies, in agreement with the picture that they are AGN with elevated accretion rates and are in the early growth phase of black hole and galaxy co-evolution. However, the steep-spectrum sources are not exclusively narrow-line Seyfert 1 galaxies; indeed many are broad-line Seyfert 1 galaxies, as found by a catalogue search. This suggests that these steep-spectrum sources may be black holes generally with high accretion rates but of a wide mass range, including a few objects emitting at $L_{\text{SX}} \geq 10^{45}$ erg s⁻¹, of which black hole masses can be close to $10^9 M_{\odot}$.

Key words. X-rays: galaxies – Galaxies: active – surveys

1. Introduction

The ROSAT All-Sky Survey (Voges et al. 1999) discovered many soft X-ray-bright active galactic nuclei (AGN), and these tend to be classified as narrow-line Seyfert 1 (NLS1) galaxies (Boller et al. 1996; Laor et al. 1997). Following black hole mass measurements of these AGN, a consensus formed that they are likely to harbour highly accreting, smaller black holes compared to broad-line Seyfert galaxies (e.g. Grupe 2004; Xu et al. 2012). NLS1s have typical black hole masses of $\log M_{\text{BH}}/M_{\odot} \approx 6-8$ and Eddington ratios of $\lambda_{\text{Edd}} \approx 0.1-1$ (e.g. Järvelä et al. 2015; Cracco et al. 2016; Rakshit et al. 2017; Paliya et al. 2023). This means that a steep X-ray spectrum could be an indicator that an AGN has a high accretion rate (Brightman et al. 2013; Risaliti et al. 2009; Shemmer et al. 2008). When an accretion rate

approaches the Eddington ratio, an enhanced soft photon field from the accretion disc cools the hot corona, and optically thick Comptonised disc emission at the soft X-ray energies is elevated (e.g. Done et al. 2012). These would lead to a steep X-ray spectrum.

Decades later, eROSITA —on board the Spectrum-Röntgen-Gamma (SRG; Sunyaev et al. 2021; Predehl et al. 2021; Merloni et al. 2012)— started to scan the whole sky in the X-ray band. With the large effective area in the soft X-ray band below 2 keV, eROSITA is expected to be sensitive to such steep-spectrum AGN and should therefore be a good tool with which to look for highly accreting super-massive black holes. This means that, as well as objects similar to local NLS1s, more luminous counterparts at higher redshifts can also be detected in the eROSITA survey. An illustrative example has already been discovered: one of

The Solar Neighborhood LI: A Variability Survey of Nearby M Dwarfs with Planets from Months to Decades with *TESS* and the CTIO/SMARTS 0.9 m

AMAN KAR,^{1,2} TODD J. HENRY,² ANDREW C. COUPERUS,^{1,2} ELIOT HALLEY VRIJMOET,^{3,2} AND WEI-CHUN JAO¹

¹*Department of Physics and Astronomy, Georgia State University, Atlanta, GA 30303, USA*

²*RECONS Institute, Chambersburg, PA 17201, USA*

³*Five College Astronomy Department, Smith College, Northampton, MA 01063, USA*

(Received 18 November 2023; Revised 3 February 2024; Accepted 16 February 2024)

ABSTRACT

We present the optical photometric variability of 32 planet-hosting M dwarfs within 25 parsecs over timescales of months to decades. The primary goal of this project, ATLAS — A Trail to Life Around Stars, is to follow the trail to life by revealing nearby M dwarfs with planets that are also “quiet”, which may make them more amiable to habitability. There are 69 reported exoplanets orbiting the 32 stars discussed here, providing a rich sample of worlds for which environmental evaluations are needed. We examine the optical flux environments of these planets over month-long timescales for 23 stars observed by *TESS*, and find that 17 vary by less than 1% (~ 11 mmag). All 32 stars are being observed at the CTIO/SMARTS 0.9 m, with a median duration of 19.1 years of optical photometric data in the *VRI* bands. We find over these extended timescales that six stars show optical flux variations less than 2%, 25 vary from 2–6% (~ 22 –67 mmag), and only one, Proxima Centauri, varies by more than 6%. Overall, LHS 1678 exhibits the lowest optical variability levels measured over all timescales examined, thereby providing one of the most stable photometric environments among planets reported around M dwarfs within 25 parsecs. More than 600 of the nearest M dwarfs are being observed at the 0.9 m in the RECONS program that began in 1999, and many more planet hosts will undoubtedly be revealed, providing more destinations to be added to the ATLAS sample in the future.

Keywords: Exoplanet systems (484); Habitable planets (695); M dwarf stars (982); Planet hosting stars (1242); Solar neighborhood (1509); Stellar Activity (1580); Surveys (1671); Exoplanet Surface Variability (2023)

1. INTRODUCTION

M dwarfs are the most common type of stars in the solar neighborhood (Henry et al. 2006, 2018) and presumably throughout the Milky Way and other galaxies. They represent 75% of the stars in the solar neighborhood and in fact, provide more aggregate habitable zone (HZ) real estate than any other stellar type (Cantrell et al. 2013), and have been found to have closely-packed sets of terrestrial planets (Shields et al. 2016). They are cooler and dimmer than more massive stars and consume their hydrogen slowly over extraordinarily long timescales, creating enduring stable environments in which life might originate and thrive. Pragmatically, M dwarfs are excellent candidates to search for other worlds because their small stellar radii and masses permit the detection of Earth-size planets, which are anticipated to be common (Dressing & Charbonneau 2015).

With the discovery of thousands of exoplanets, the field of exoplanetary science has rapidly developed in the last few decades, thanks to space missions like *Kepler*, *K2*, and the ongoing Transiting Exoplanet Survey Satellite (*TESS*) effort. Our closest neighbor, the M5.0V star Proxima Centauri, has been reported to host two or three planets (Anglada-Escudé et al. 2016; Damasso et al. 2020; Suárez Mascareño et al. 2020; Artigau et al. 2022), and dozens of other nearby M dwarfs are reported to be orbited by exoplanets, typically terrestrial in nature.

Although M dwarfs are often known to be flare stars, such outbursts are not necessarily unfavorable for the habitability of orbiting planets because most of the (presumed) life-damaging UV radiation affects only the stratosphere where ozone is photolyzed, and thus does not reach the surface of the planet (Tarter et al. 2007; Segura et al. 2010).

Multi-field curved solid: early dark energy and perturbation instabilities

Juan P. Beltrán Almeida,^{1,*} Alejandro Guarnizo,^{2,†} Thiago S. Pereira,^{3,‡} and César A. Valenzuela-Toledo^{4,§}

¹*Universidad Nacional de Colombia, Facultad de Ciencias, Departamento de Física,
Av. Cra 30 # 45-03, Bogotá, Colombia*

²*Departamento de Física, Universidad Antonio Nariño,
Cra 3 Este # 47A-15, Bogotá, Colombia*

³*Departamento de Física, Universidade Estadual de Londrina,
Rod. Celso Garcia Cid, Km 380, 86057-970, Londrina, Paraná, Brazil*

⁴*Departamento de Física, Universidad del Valle,
Ciudad Universitaria Meléndez, Santiago de Cali 760032, Colombia*

(Dated: February 23, 2024)

We introduce a multi-field dark energy model with a non-flat field-space metric, in which one field is dynamical while the others have constant spatial gradients. The model is predictive at the background level, leading to an early dark energy component at high redshifts and a suppressed fraction of late-time anisotropy. Both features have simple expressions in terms of the curvature scale of the field-space, and correspond to stable points in the phase space of possible solutions. Because of the coupling between time and space-dependent scalar fields, vector field perturbations develop tachyonic instabilities at scales below the Hubble radius, thus being potentially observable in the number count of galaxies. Overall, the presence of a non-trivial field-space curvature also leads to the appearance of instabilities on scalar perturbations, which can impact the matter density distribution at large scales.

I. INTRODUCTION

The existence of an unexplained dark sector continues to be one of the main drivers of new ideas in cosmology, forcing us to test the limits of the standard Lambda Cold Dark Matter (Λ CDM) model. Recently this program has gained momentum due to the realization that measurements of critical cosmological parameters, among which H_0 , give different values when done using high or low redshift data [1, 2]. Alongside these facts, there remain numerous large-angle Cosmic Microwave Background (CMB) anomalies which also lack an explanation — fundamental or not — and that contribute to the suspicion that the Λ CDM model is just a first approximation to a more accurate description of the universe.

Among the many potential candidates to explain these problems lies the possibility that dark energy results from new matter degrees of freedom. The most popular and paradigmatic example is the quintessence field and its many avatars [3]. At first sight, the versatility of quintessence models seems to be limited by the imposition of translation invariance arising from the Cosmological Principle, which forces the fields to be homogeneous. However, a closer inspection of the Lagrangian from the simplest quintessence model,

$$\mathcal{L} = -\frac{1}{2}\partial_\mu\phi\partial^\mu\phi - V(\phi),$$

reveals that, as far as the kinetic term is concerned, translation invariance does not require homogeneity of the

fields, but rather the homogeneity of their spatial gradients. The realization of this possibility has led to many interesting implementations known generically as “solid” or “elastic” models, where the dynamics is achieved by means of *space-dependent* scalar fields with constant spatial gradients. To account for a forbidden (symmetry breaking) potential, such models usually rely on a non-canonical Lagrangian capable of reproducing an accelerated expansion. This idea has its roots on effective field-theoretic implementations of solid and elastic media [4, 5], and has since found fertile ground in cosmological applications, being implemented in inflation [6–8], dark matter [9, 10], and dark energy [11, 12].

In the standard applications of solids to cosmology, the internal symmetries of the fields, such as $SO(3)$ and shift invariances, are explored when building phenomenologically viable cosmological models [7, 13]. In this regard, one could also envisage the existence of a curvature in field-space, as is usually done in non-linear sigma models of quantum field theory. In fact, *time-dependent* non-linear sigma models have been long explored in the context of inflation [14–20] and dark energy [21–25]. Recently, the authors of Ref. [22] considered the implementation of dark energy in one such model, showing that a phase of accelerated expansion can be achieved even with steep potentials, provided that trajectories in field-space are sufficiently non-geodesic.

In this work we ask whether a time-dependent field could coexist with a solid, thus bridging a gap between the solid and non-linear multi-field descriptions. Specifically, we introduce a non-linear dark energy model in which one field is dynamical, while three others have constant spatial gradients. The model is predictive at the background level, and can lead to a percent level fraction of early dark energy, as well as a suppressed fraction

* jubeltrana@unal.edu.co

† aguarnizo50@uan.edu.co

‡ tspereira@uel.br

§ cesar.valenzuela@correounivalle.edu.co

The Quasar 3C 47: Extreme Population B Jetted Source With Double-peaked Profile[★]

Shimeles Terefe Mengistue^{1,2,3★★}, Paola Marziani⁴, Ascensión del Olmo⁵, Mirjana Pović^{1,5,6}, Jaime Perea⁵, and Alice Deconto Machado⁵

¹ Space Science and Geospatial Institute (SSGI), Entoto Observatory and Research Centre (EORC), Astronomy and Astrophysics Department, P.O.Box 33679, Addis Ababa, Ethiopia.
e-mail: shimeles11@gmail.com

² Addis Ababa University (AAU), P.O.Box 1176, Addis Ababa, Ethiopia.

³ Jimma University, College of Natural Sciences, Department of Physics, P.O.Box 378, Jimma, Ethiopia.

⁴ Istituto Nazionale di Astrofisica (INAF), Osservatorio Astronomico di Padova, vicolo dell' Osservatorio 5, Padova I-35122, Italy.

⁵ Instituto de Astrofísica de Andalucía (IAA-CSIC), Glorieta de la Astronomía s/n, Granada E-18008, Spain.

⁶ Mbarara University of Science and Technology (MUST), Faculty of Science, Physics Department, P.O. Box 1410, Mbarara, Uganda.

Received XX, 2023; accepted XX, 2023

ABSTRACT

Context. An optically thick, geometrically thin accretion disk (AD) around a supermassive black hole might contribute to broad-line emission in type-1 active galactic nuclei (AGN). However, emission line profiles are most often not immediately consistent with the profiles expected from a rotating disk. The extent to which an AD in AGN contributes to the broad Balmer lines and high-ionization UV lines in radio-loud (RL) AGN needs to be investigated.

Aims. This work aims to address whether the AD can account for the double-peaked profiles observed in the Balmer lines ($H\beta$, $H\alpha$), near-UV ($MgII\lambda 2800$), and high-ionization UV lines ($CIV\lambda 1549$, $CIII]\lambda 1909$) of the extremely jetted quasar 3C 47.

Methods. The low ionization lines (LILs) ($H\beta$, $H\alpha$, and $MgII\lambda 2800$) were analyzed using a relativistic Keplerian AD model. Fits were carried out following Bayesian and multicomponent non-linear approaches. The profiles of prototypical high ionization lines (HILs) were also modeled by the contribution of the AD, along with fairly symmetric additional components.

Results. The LIL profiles of 3C 47 are in very good agreement with a relativistic Keplerian AD model. The disk emission is constrained between $\sim 10^2$ and $\sim 10^3$ gravitational radii, with a viewing angle of ≈ 30 degrees.

Conclusions. The study provides convincing direct observational evidence for the presence of an AD and explains the HIL profiles are due to disk and failed wind contributions. The agreement between the observed profiles of the LILs and the model is remarkable. The main alternative, a double broad line region associated with a binary black hole, is found to be less appealing than the disk model for the quasar 3C 47.

Key words. quasars: individual: 3C 47 – quasars: radio-loud – quasars: emission lines – quasars: supermassive black holes – quasars: accretion disks

1. Introduction

In the current working picture of active galactic nuclei (AGN), the underlying power source is thought to be a supermassive black hole (SMBH). An accretion disk (hereafter AD) around the central SMBH is expected in all the AGN. ADs provide an efficient mechanism for dissipating the angular momentum of the accreting matter via viscous stresses (e.g., Shakura & Sunyaev 1973; Dai et al. 2021; Lasota 2023). In addition, they are regarded as an essential ingredient for the production of relativistic jets, which are observed in a considerable fraction of AGN (e.g., Blandford 1990; Shende et al. 2019; Blandford et al. 2019; Chakraborty & Bhattacharjee 2021; Mizuno 2022). High-density material in an AD may be required for the production of the low-ionization lines (LILs) (Rokaki 1997; Zhang et al. 2019b; Hung

et al. 2020). Emission from the surface of a photoionized, relativistic, Keplerian AD produces profiles of double-peaked lines with two distinctive features: (1) a stronger blueshifted peak due to Doppler boosting; (2) a redward shift - increasing toward the line base - associated with gravitational redshift and Doppler transverse effect (Chen & Halpern 1989, hereafter CH89). In this respect, the most commonly proposed solution for double-peaked emission from the AD is the assumption of an elevated structure around the inner disk that would illuminate the outer disk and drive the line emission (Strateva et al. 2003; Eracleous & Halpern 2003; Ricci & Steiner 2019).

Even if the majority of AGN spectra are single-peaked, there are pieces of evidence about a double-peaked structure that can be acquired from observations of very broad, double-peaked emission lines and identification of asymmetries and substructure in the line profiles (e.g., Popović et al. 2002; Kollatschny 2003; Shapovalova et al. 2004). Miley & Miller (1979) found that powerful radio galaxies and radio-loud (RL) quasars with extended radio morphology have the broadest and most complex Balmer

[★] Based on observations collected at the Centro Astronómico Hispano en Andalucía (CAHA) at Calar Alto, operated jointly by the Junta de Andalucía and Consejo Superior de Investigaciones Científicas (IAA-CSIC).

^{★★} Visiting researcher at the IAA-CSIC, Spain as a PhD fellow.

The origin of the Slow-to-Alfvén Wave Cascade Power Ratio and its Implications for Particle Heating in Accretion Flows

KAUSHIK SATAPATHY,^{1,2} DIMITRIOS PSALTIS,¹ AND FERYAL ÖZEL¹

¹*School of Physics, Georgia Institute of Technology, 837 State St NW, Atlanta, GA 30332, USA*

²*Department of Physics, University of Arizona, 1118 E. Fourth Street, Tucson, AZ 85721*

ABSTRACT

The partition of turbulent heating between ions and electrons in radiatively inefficient accretion flows plays a crucial role in determining the observational appearance of accreting black holes. Modeling this partition is, however, a challenging problem because of the large scale separation between the macroscopic scales at which energy is injected by turbulence and the microscopic ones at which it is dissipated into heat. Recent studies of particle heating from collisionless damping of turbulent energy have shown that the partition of energy between ions and electrons is dictated by the ratio of the energy injected into the slow and Alfvén wave cascades as well as the plasma β parameter. In this paper, we study the mechanism of the injection of turbulent energy into slow- and Alfvén- wave cascades in magnetized shear flows. We show that this ratio depends on the particular ($r\phi$) components of the Maxwell and Reynolds stress tensors that cause the transport of angular momentum, the shearing rate, and the orientation of the mean magnetic field with respect to the shear. We then use numerical magnetohydrodynamic shearing-box simulations with background conditions relevant to black hole accretion disks to compute the magnitudes of the stress tensors for turbulence driven by the magneto-rotational instability and derive the injection power ratio between slow and Alfvén wave cascades. We use these results to formulate a local subgrid model for the ion-to-electron heating ratio that depends on the macroscopic characteristics of the accretion flow.

Keywords: black-hole, accretion, plasma

1. INTRODUCTION

Recent Very Long Baseline Interferometric (VLBI) observations by the Event Horizon Telescope of the horizon-scale environments of the black holes at the centers of the Milky Way (Sgr A*) and M87 galaxies have offered a unique opportunity to study plasma astrophysics in low-luminosity accretion flows (Event Horizon Telescope Collaboration et al. 2019; Akiyama et al. 2022). These systems are categorized as Radiatively Inefficient Accretion Flows (see Narayan & Yi 1995) owing to their low luminosities and the characteristics of their spectra. They are made up of low density plasmas, with mass accretion rates typically less than 10^{-3} times the Eddington rate \dot{M}_{Edd} . The collisional timescales between the ions and the electrons in these flows are much larger than accretion timescale, allowing for the ions and the electrons to co-exist in a two-temperature state. In addition, low densities also cause the cooling processes in these systems to be inefficient, resulting in most of the energy carried by the plasma to be advected into the black hole.

Due to the two-temperature nature of the plasma, a first-principles approach to studying accretion flows involves independently evolving the thermodynamics of the ions and the electrons, incorporating physical models for the partition of heat between the species (Ressler et al. 2015; Sądowski et al. 2017). In these accretion flows, heating mechanisms include collisionless damping due to wave-particle resonances (Quataert 1998; Kawazura et al. 2020), magnetic reconnection

(Ball et al. 2018; Rowan et al. 2019), and heating resulting from instabilities due to velocity-space anisotropies (Sharma et al. 2007). These processes are typically dominant at the length-scales comparable to the gyroradii of the ions and the electrons, which are much smaller than the scale of the system. As a result of the large scale separation, the physics of heating mechanisms studied at the microscopic kinetic scales need to be incorporated as sub-grid prescriptions in global simulations.

Among these dissipation processes, magnetic reconnection is primarily dominant in localized regions of the flow that have current sheets (Ball et al. 2016) and causes episodic dissipation of energy. On the other hand, velocity space anisotropies are believed to be driven by mechanisms connected to the time-evolving large scale magnetic fields. In the absence of current sheets or local mechanisms driving velocity space anisotropies, the turbulent energy cascades down to scales comparable to the ion gyroradius and undergoes collisionless damping. This is a ubiquitous mechanism of dissipation, both spatially and temporally and is expected to be the primary driver of electron and ion heating.

Recent numerical studies show that the partition of heat between ions and electrons resulting from collisionless damping of the turbulent energy (Kawazura et al. 2020) depends on the plasma β (the thermal to magnetic pressure ratio) and the ratio of the driving power of the compressive slow magnetosonic wave cascade to that of the Alfvén wave cascade (P_S/P_A). These studies have been performed in the gyroki-

Diverse Oxygen Abundance in Early Galaxies Unveiled by Auroral Line Analysis with JWST

TAKAHIRO MORISHITA ¹, MASSIMO STIAVELLI ², CLAUDIO GRILLO ^{3,4}, PIERO ROSATI ^{5,6}, STEFAN SCHULDt ^{3,4},
MICHELE TRENTI ^{7,8}, PIETRO BERGAMINI ^{3,5}, KIT BOYETT ^{7,8}, RANGA-RAM CHARY ¹, NICHIA LEETHOCHAWALIT ⁹,
GUIDO ROBERTS-BORSANI ¹⁰, TOMMASO TREU ¹¹ AND EROS VANZELLA ¹²

¹*IPAC, California Institute of Technology, MC 314-6, 1200 E. California Boulevard, Pasadena, CA 91125, USA*

²*Space Telescope Science Institute, 3700 San Martin Drive, Baltimore, MD 21218, USA*

³*Dipartimento di Fisica, Università degli Studi di Milano, Via Celoria 16, I-20133 Milano, Italy*

⁴*INAF - IASF Milano, via A. Corti 12, I-20133 Milano, Italy*

⁵*INAF - OAS, Osservatorio di Astrofisica e Scienza dello Spazio di Bologna, via Gobetti 93/3, I-40129 Bologna, Italy*

⁶*Dipartimento di Fisica e Scienze della Terra, Università degli Studi di Ferrara, Via Saragat 1, I-44122 Ferrara, Italy*

⁷*School of Physics, University of Melbourne, Parkville 3010, VIC, Australia*

⁸*ARC Centre of Excellence for All Sky Astrophysics in 3 Dimensions (ASTRO 3D), Australia*

⁹*National Astronomical Research Institute of Thailand (NARIT), Mae Rim, Chiang Mai, 50180, Thailand*

¹⁰*Department of Astronomy, University of Geneva, Chemin Pegasi 51, 1290 Versoix, Switzerland*

¹¹*Department of Physics and Astronomy, University of California, Los Angeles, 430 Portola Plaza, Los Angeles, CA 90095, USA*

¹²*INAF - OAS, Osservatorio di Astrofisica e Scienza dello Spazio di Bologna, via Gobetti 93/3, I-40129 Bologna, Italy*

Submitted to ApJ

ABSTRACT

We present deep JWST NIRSpec observations in the sightline of MACS J1149.5+2223, a massive cluster of galaxies at $z = 0.54$. We report the spectroscopic redshift of 28 sources at $3 < z < 9.1$, including 9 sources with the detection of the $[\text{O III}]_{\lambda 4363}$ auroral line. Combining these with 16 $[\text{O III}]_{\lambda 4363}$ -detected sources from publicly available JWST data, our sample consists of 25 galaxies with robust gas-phase metallicity measurements via the direct method. We observe a positive correlation between stellar mass and metallicity, with a ~ 0.5 dex offset down below the local relation. Interestingly, we find a larger than expected scatter of ~ 0.3 dex around the relation, which cannot be explained by redshift evolution among our sample or other third parameter. The scatter increases at higher redshift, and we attribute this to the enrichment process having higher stochasticity due to shallower potential wells, more intense feedback processes, and a higher galaxy merger rate. Despite reaching to a considerably low-mass regime ($\log M_*/M_\odot \sim 7.3$), our samples have metallicity of $\log(\text{O}/\text{H}) + 12 \gtrsim 7$, *i.e.* comparable to the most metal poor galaxies in the local Universe. The search of primordial galaxies may be accomplished by extending toward a lower mass and/or by investigating inhomogeneities at smaller spatial scales. Lastly, we investigate potential systematics caused by the limitation of JWST's MSA observations. Caution is warranted when the target exceeds the slit size, as this situation could allow an overestimation of “global” metallicity, especially under the presence of strong negative metallicity gradient.

1. INTRODUCTION

Gas cycle within a galaxy system carries an important role. The ejecta from previously formed stars enrich surrounding gas, some fraction of which is subject to be used in the following star formation cycles, leading to

further enhancement in chemical abundances. The accumulation of stars formed in such a cyclical way represents a major component of galaxies in a later epoch, culminating an established relation of metal contents and other fundamental galaxy properties, such as stellar mass, seen in the local universe (e.g., Tremonti et al. 2004; Gallazzi et al. 2005; Andrews & Martini 2013; Kirby et al. 2013; Curti et al. 2020). Observations have reported the presence of the relationship out to $z \sim 3$,

Primordial magnetic fields: consistent initial conditions and impact on high- z structures

Pranjal Ralegankar,^{*a,b*} Mak Pavičević,^{*a,b*} and Matteo Viel^{*a,b,c,d*}

^{*a*}SISSA - International School for Advanced Studies, Via Bonomea 265, 34136 Trieste, Italy

^{*b*}INFN – National Institute for Nuclear Physics, Via Valerio 2, I-34127 Trieste, Italy

^{*c*}IFPU, Institute for Fundamental Physics of the Universe, via Beirut 2, 34151 Trieste, Italy

^{*d*}INAF, Osservatorio Astronomico di Trieste, Via G. B. Tiepolo 11, I-34131 Trieste, Italy

E-mail: pralegan@sissa.it, mpavicev@sissa.it, viel@sissa.it

Abstract. Primordial magnetic fields (PMFs) can enhance matter power spectrum on small scales (\lesssim Mpc) and still agree with bounds from cosmic microwave background (CMB) and Faraday rotation measurements. As modes on scales smaller than Mpc have already become non-linear today, exploring PMFs' impact on small-scale structures requires dedicated cosmological simulations. Here, for the first time, we perform a suite of hydrodynamical simulations that take into account the different impacts of PMFs on baryons and dark matter. Specifically, in the initial conditions we displace particles according to the Lorentz force from PMFs. We also highlight the large theoretical uncertainty in the peak enhancement of the matter power spectrum due to PMFs, which was not considered in previous studies. We present halo mass functions and show that they can be accurately reproduced using Sheth-Tormann formalism. Moreover, we show that PMFs can generate galaxies with baryon fraction several times larger than the cosmic average at high redshifts. This is simply a consequence of the fact that PMFs enhance baryon perturbations, causing them to be larger than dark matter perturbations. We argue that this scenario could be tested soon by obtaining accurate estimates of the baryon fraction in high redshift galaxies.

ESA Science Programme Missions: Contributions and Exploitation – XMM-Newton Observing Time Proposals

Arvind N. Parmar · Norbert Schartel · Maria Santos-Lleó

Received: date / Accepted: date

Abstract We examine the outcomes of the regular announcements of observing opportunities for ESA's X-ray observatory XMM-Newton issued between 2001 and 2021. We investigate how success rates vary with the lead proposer's gender, "academic age" and the country where the proposer's institute is located. The large number of proposals (10,579) and more than 20 years operational lifetime enable the evolution of community proposing for XMM-Newton to be probed. We determine proposal success rates for high-priority and all proposals using both the numbers of accepted proposals and the amounts of awarded observing time. We find that male lead proposers are between 5–15% more successful than their female counterparts in obtaining XMM-Newton observations. The gender balance and the percentage of successful young proposers are comparable to those of HST after the introduction of dual-anonymous reviewing of HST proposals. We investigate potential correlations between the female-led proposal success rates and the amount of female participation in the Time Allocation Committee. We propose additional investigations to better understand the outcomes presented here.

A. Parmar
Former Head of the Science Support Office
Directorate of Science, ESA, ESTEC
The Netherlands
Present address:
Department of Space and Climate Physics
MSSL/UCL
Dorking
UK
E-mail: arvind.parmar@ucl.ac.uk

N. Schartel
Directorate of Science, ESA, ESAC
Villanueva de la Cañada, Madrid, Spain.

M. Santos-Lleó
Directorate of Science, ESA, ESAC
Villanueva de la Cañada, Madrid, Spain.

Fleeting but not Forgotten: the Imprint of Escaping Hydrogen Atmospheres on Super-Earth Interiors

JAMES G. ROGERS ¹, HILKE E. SCHLICHTING ¹ AND EDWARD E. YOUNG¹

¹*Department of Earth, Planetary, and Space Sciences, The University of California, Los Angeles, 595 Charles E. Young Drive East, Los Angeles, CA 90095, USA*

ABSTRACT

Small, close-in exoplanets are divided into two sub-populations: super-Earths and sub-Neptunes. Most super-Earths are thought to have lost their primordially accreted hydrogen-dominated atmospheres via thermally driven winds. We consider the global chemical equilibrium of super-Earths and the lasting impacts of their fleeting hydrogen atmospheres. We find that hydrogen is efficiently sequestered into the interior, oxidising iron and endogenously producing $\sim 0.5 - 1.0\%$ water by mass. As the atmospheres of super-Earths are continuously sculpted by mass loss and chemical equilibration, they remain hydrogen-dominated by mole (number) fraction but become steam-dominated by mass, which may be observable with *JWST* for planets transitioning across the radius valley. One of the main effects of efficient sequestration of hydrogen into the interior is to produce an under-dense bulk interior compared to that of Earth. We predict bulk densities of super-Earths to be $\sim 5.0 \text{ g cm}^{-3}$ for a $1M_{\oplus}$ planet, which is consistent with high-precision mass measurements and also population-level inference analyses from atmospheric escape models.

Keywords: planets and satellites: atmospheres - planets and satellites: physical evolution - planet star interactions

1. INTRODUCTION

Hydrogen plays a central role in controlling various stages of planetary formation and evolution. For the population of small, close-in exoplanets (super-Earths and sub-Neptunes e.g. Howard et al. 2012; Fressin et al. 2013; Silburt et al. 2015; Mulders et al. 2018; Zink et al. 2019), hydrogen-dominated gas is initially accreted from a planet’s nascent protoplanetary disc to form a primordial atmosphere (e.g. Lee et al. 2014; Ginzburg et al. 2016). As the disc disperses, much of this atmosphere can be lost through a boil-off stage, in which the disc rapidly drains onto its host star, inducing extreme atmospheric escape (Owen & Wu 2016; Ginzburg et al. 2016; Rogers et al. 2023b). Then, once the planet receives direct irradiation from its host star, its remaining hydrogen-dominated atmosphere is bombarded by stellar irradiation, inducing further atmospheric escape via X-ray/EUV (XUV) photoevaporation (e.g. Owen & Wu 2013; Lopez & Fortney 2013) and core-powered mass-loss (e.g. Ginzburg et al. 2018; Gupta & Schlichting 2019; Rogers et al. 2023b).

The loss, or retention, of hydrogen-dominated atmospheres has been used to explain various features in the

exoplanet demographics accurately. Examples include the position and slope of the observed radius gap (e.g. Fulton et al. 2017; Van Eylen et al. 2018; Petigura et al. 2022) as a function of orbital period and stellar mass (e.g. Gupta & Schlichting 2019, 2020; Rogers & Owen 2021; Rogers et al. 2021), the planet mass-radius diagram (e.g. Lopez & Fortney 2014; Chen & Rogers 2016; Kubyschkina & Fossati 2022; Rogers et al. 2023c), as well as the short orbital period Neptune-desert (Owen & Lai 2018). It is also known that many sub-Neptunes require a significant hydrogen atmosphere to reproduce their observed bulk densities (e.g. Jontof-Hutter et al. 2014; Weiss & Marcy 2014; Benneke et al. 2019). Direct observational evidence also exists for the prevalence of hydrogen-dominated atmospheres in the form of Ly- α and H α transit spectroscopy (e.g. Dos Santos 2023), as well as recent atmospheric characterisation of sub-Neptunes with *JWST* (e.g. Madhusudhan et al. 2023; Wogan et al. 2024).

A less well-explored avenue of investigation, however, is the potential impact of hydrogen-dominated atmospheres on the bulk interiors of super-Earths and sub-Neptunes (e.g. Kite et al. 2016; Chachan & Stevenson 2018; Olson & Sharp 2018; Kite et al. 2019, 2020; Licht-

Baryon Acoustic Oscillation Theory and Modelling Systematics for the DESI 2024 results

Shi-Fan Chen^{1*} ‡, Cullan Howlett^{2 †‡}, Martin J. White^{3,4}, Patrick McDonald⁴, Ashley J. Ross⁵, Hee-Jong Seo⁶, Nikhil Padmanabhan⁷, J. Aguilar,⁴ S. Ahlen,⁸ S. Alam,⁹ O. Alves,¹⁰ R. Blum,¹¹ D. Brooks,¹² X. Chen,⁷ S. Cole,¹³ T. M. Davis,² K. Dawson,¹⁴ A. de la Macorra,¹⁵ Arjun Dey,¹¹ Z. Ding,^{16,17} P. Doel,¹² S. Ferraro,^{4,3} A. Font-Ribera,¹⁸ D. Forero-Sánchez,¹⁹ J. E. Forero-Romero,^{20,21} C. Garcia-Quintero,²² E. Gaztañaga,^{23,24,25} S. Gontcho A Gontcho,⁴ M. M. S Hanif,¹⁰ K. Honscheid,^{5,26,27} T. Kisner,⁴ A. Kremin,⁴ A. Lambert,⁴ M. Landriau,⁴ M. E. Levi,⁴ M. Manera,^{28,18} A. Meisner,¹¹ J. Mena-Fernández,²⁹ R. Miquel,^{30,18} A. Muñoz-Gutiérrez,¹⁵ E. Paillas,³¹ N. Palanque-Delabrouille,^{32,4} W. J. Percival,^{31,33,34} F. Prada,³⁵ A. Pérez-Fernández,¹⁵ M. Rashkovetskiy,³⁶ M. Rezaie,³⁷ G. Rossi,³⁸ R. Ruggeri,^{39,2} E. Sanchez,²⁹ D. Schlegel,⁴ J. Silber,⁴ G. Tarlé,¹⁰ M. Vargas-Magaña,¹⁵ B. A. Weaver,¹¹ S. Yuan,⁴⁰ R. Zhou,⁴ and Z. Zhou⁴¹

¹ Institute for Advanced Study, 1 Einstein Drive, Princeton, NJ 08540, USA

² School of Mathematics and Physics, University of Queensland, 4072, Australia

³ Department of Physics, University of California, Berkeley, 366 LeConte Hall MC 7300, Berkeley, CA 94720-7300, USA

⁴ Lawrence Berkeley National Laboratory, 1 Cyclotron Road, Berkeley, CA 94720, USA

⁵ Center for Cosmology and AstroParticle Physics, The Ohio State University, 191 West Woodruff Avenue, Columbus, OH 43210, USA

⁶ Department of Physics & Astronomy, Ohio University, Athens, OH 45701, USA

⁷ Physics Department, Yale University, P.O. Box 208120, New Haven, CT 06511, USA

⁸ Physics Dept., Boston University, 590 Commonwealth Avenue, Boston, MA 02215, USA

⁹ Tata Institute of Fundamental Research, Homi Bhabha Road, Mumbai 400005, India

¹⁰ University of Michigan, Ann Arbor, MI 48109, USA

¹¹ NSF's NOIRLab, 950 N. Cherry Ave., Tucson, AZ 85719, USA

¹² Department of Physics & Astronomy, University College London, Gower Street, London, WC1E 6BT, UK

¹³ Institute for Computational Cosmology, Department of Physics, Durham University, South Road, Durham DH1 3LE, UK

¹⁴ Department of Physics and Astronomy, The University of Utah, 115 South 1400 East, Salt Lake City, UT 84112, USA

¹⁵ Instituto de Física, Universidad Nacional Autónoma de México, Cd. de México C.P. 04510, México

¹⁶ Institute of Astronomy, School of Physics and Astronomy, Shanghai Jiao Tong University, Shanghai 200240, China

¹⁷ Key Laboratory for Particle Astrophysics and Cosmology(MOE)/Shanghai Key Laboratory for Particle Physics and Cosmology, China

¹⁸ Institut de Física d'Altes Energies (IFAE), The Barcelona Institute of Science and Technology, Campus UAB, 08193 Bellaterra Barcelona, Spain

¹⁹ Ecole Polytechnique Fédérale de Lausanne, CH-1015 Lausanne, Switzerland

²⁰ Departamento de Física, Universidad de los Andes, Cra. 1 No. 18A-10, Edificio Ip, CP 111711, Bogotá, Colombia

²¹ Observatorio Astronómico, Universidad de los Andes, Cra. 1 No. 18A-10, Edificio H, CP 111711 Bogotá, Colombia

²² Department of Physics, The University of Texas at Dallas, Richardson, TX 75080, USA

²³ Institut d'Estudis Espacials de Catalunya (IEEC), 08034 Barcelona, Spain

²⁴ Institute of Cosmology & Gravitation, University of Portsmouth, Dennis Sciama Building, Portsmouth, PO1 3FX, UK

²⁵ Institute of Space Sciences, ICE-CSIC, Campus UAB, Carrer de Can Magrans s/n, 08913 Bellaterra, Barcelona, Spain

²⁶ Department of Physics, The Ohio State University, 191 West Woodruff Avenue, Columbus, OH 43210, USA

²⁷ The Ohio State University, Columbus, 43210 OH, USA

²⁸ Departament de Física, Serra Hünter, Universitat Autònoma de Barcelona, 08193 Bellaterra (Barcelona), Spain

²⁹ CIEMAT, Avenida Complutense 40, E-28040 Madrid, Spain

³⁰ Institució Catalana de Recerca i Estudis Avançats, Passeig de Lluís Companys, 23, 08010 Barcelona, Spain

³¹ Department of Physics and Astronomy, University of Waterloo, 200 University Ave W, Waterloo, ON N2L 3G1, Canada

³² IRFU, CEA, Université Paris-Saclay, F-91191 Gif-sur-Yvette, France

³³ Perimeter Institute for Theoretical Physics, 31 Caroline St. North, Waterloo, ON N2L 2Y5, Canada

³⁴ Waterloo Centre for Astrophysics, University of Waterloo, 200 University Ave W, Waterloo, ON N2L 3G1, Canada

³⁵ Instituto de Astrofísica de Andalucía (CSIC), Glorieta de la Astronomía, s/n, E-18008 Granada, Spain

³⁶ Center for Astrophysics | Harvard & Smithsonian, 60 Garden Street, Cambridge, MA 02138, USA

³⁷ Department of Physics, Kansas State University, 116 Cardwell Hall, Manhattan, KS 66506, USA

³⁸ Department of Physics and Astronomy, Sejong University, Seoul, 143-747, Korea

³⁹ Centre for Astrophysics & Supercomputing, Swinburne University of Technology, P.O. Box 218, Hawthorn, VIC 3122, Australia

⁴⁰ SLAC National Accelerator Laboratory, Menlo Park, CA 94305, USA

⁴¹ National Astronomical Observatories, Chinese Academy of Sciences, A20 Datun Rd., Chaoyang District, Beijing, 100012, P.R. China

Accepted XXX. Received YYY; in original form ZZZ

MNRAS **000**, 1–29 (2024)

MNRAS **000**, 1–29 (2024)

Preprint 23 February 2024

Compiled using MNRAS L^AT_EX style file v3.0

ABSTRACT

This paper provides a comprehensive overview of how fitting of Baryon Acoustic Oscillations (BAO) is carried out within the upcoming Dark Energy Spectroscopic Instrument's (DESI) 2024 results using its DR1 dataset, and the associated systematic error budget from theory and modelling of the BAO. We derive new results showing how non-linearities in the clustering of galaxies can cause potential biases in measurements of the isotropic (α_{iso}) and anisotropic (α_{ap}) BAO distance scales, and how these can be effectively removed with an appropriate choice of reconstruction algorithm. We then demonstrate how theory leads to a clear choice for how to model the BAO and develop, implement and validate a new model for the remaining smooth-broadband (i.e., without BAO) component of the galaxy clustering. Finally, we explore the impact of all remaining modelling choices on the BAO constraints from DESI using a suite of high-precision simulations, arriving at a set of best-practices for DESI BAO fits, and an associated theory and modelling systematic error. Overall, our results demonstrate the remarkable robustness of the BAO to all our modelling choices and motivate a combined theory and modelling systematic error contribution to the post-reconstruction DESI BAO measurements of no more than 0.1% (0.2%) for its isotropic (anisotropic) distance measurements. We expect the theory and best-practices laid out to here to be applicable to other BAO experiments in the era of DESI and beyond.

Key words:

1 INTRODUCTION

Constraining the expansion history of the Universe is important both for improving our empirical cosmographical knowledge and for the constraints it places on the constituents of the Universe and our theories of gravity. Within the standard Friedmann–Lemaître–Robertson–Walker (FLRW; Friedmann 1922; Lemaître 1931; Robertson 1935; Walker 1937) model, the scale factor $a(t)$ is the only degree of freedom at the background level, determining distance relations over cosmic history. Constraining its behaviour has been a major goal of cosmology for close to a century. One of the most robust and accurate ways of determining $a(t)$ is through measurements of baryon acoustic oscillations (BAO) in the distribution of galaxies and gas. Oscillations in the baryon-photon fluid prior to decoupling leave an imprint in both the cosmic microwave background and the matter density with a characteristic length scale, related to the distance r_d a sound wave can travel prior to the baryon-drag epoch, just after recombination. Measurements of this scale at low redshift in large-scale structure provide a “standard ruler” for constraining the expansion history of the Universe, both by measuring the angular diameter distance ($D_A(z)$) and the Hubble parameter ($H(z)$) to a specific redshift. This ruler can be made “absolute” by connecting the BAO scale back to early universe physics, e.g. through constraints from the cosmic microwave background (CMB; Peebles & Yu 1970; Sunyaev & Zeldovich 1970; Dodelson & Schmidt 2020; Huterer 2023) or big-bang nucleosynthesis (BBN; Cooke et al. 2018).

The BAO method has become a workhorse of modern cosmology and provides some of our tightest current constraints on the cosmological expansion history (Cole et al. 2005; Eisenstein et al. 2005; Beutler et al. 2011; Blake et al. 2011; Alam et al. 2021). Relying as it does on a feature at large spatial separations that is little affected by non-linear evolution or the complex astrophysics of galaxy formation, it is robust and theoretically well understood. For this reason, it is generally regarded as a low-systematics method for constraining cosmology. Indeed, significant theoretical effort over the past two decades has led to a fairly mature understanding of the effect of the small shifts and modulations to the BAO signal incurred by large-

scale structure physics which we recap and build on in this work (§2).

The purpose of this paper is to use our theoretical understanding to generate a theory and modelling systematics budget, and suggest fitting best practices, for BAO measurements in the Dark Energy Spectroscopic Instrument (DESI). DESI is a Stage-IV spectroscopic instrument (DESI Collaboration et al. 2016, 2022) that will deliver galaxy BAO measurements with unprecedented precision up to $z \approx 2$ from galaxy clustering alone, with even greater reach when Lyman- α data are included at higher redshift. At the end of its five-year run DESI is expected to yield measurements on the (isotropic) BAO scale at a cumulative 0.2% precision (DESI Collaboration et al. 2016, 2023a). Already, galaxies from the early data release (EDR) in the luminous red galaxy (LRG) sample and bright galaxy sample (BGS), representing a small fraction of the total DESI data, yield BAO detections at the few percent level (DESI Collaboration et al. 2023b; Moon et al. 2023).

This paper is part of a set focused on the analysis of clustering in DESI Data Release 1 (DR1; DESI Collaboration 2024a,b), and in support of the key paper presenting the main galaxy BAO measurements for that data set (DESI Collaboration 2024c). The DR1 data further contains BAO information in the Lyman- α forest (DESI Collaboration 2024d), and the cosmological implications of the joint galaxy and Lyman- α BAO measurements are discussed in DESI Collaboration (2024e). Information beyond the BAO — particularly the fullshape information in the galaxy 2-point function—are studied in DESI Collaboration (2024f,g,h). While the aggregate isotropic BAO scale precision from analysis of DR1 is closer to 0.5%, our conclusions and recommendations are somewhat general and aimed towards the full DESI sample. Our understanding of galaxy clustering in the standard model of cosmology (Λ CDM) gives us a baseline of *known* theoretical systematics that need to be considered in order to make robust measurements of the BAO scale, even before *unknown* modifications due to nonstandard physics are considered.

The structure of the paper is as follows: In Section 2 we begin with a broad overview of the BAO signal as observed in large-scale structure simulations. In Sections 3 and 4 we review the theory of the BAO and BAO reconstruction, computing error estimates due to theory systematics, filling in extant gaps in the literature where necessary, and motivating our baseline form for fitting the BAO signal. In Section 5 we introduce a cubic-spline based method for marginalizing over the non-BAO broadband of galaxy clustering and

* E-mail: sfschen@ias.edu

† E-mail: c.howlett@uq.edu.au

‡ Both authors contributed equally to this work.

The Peculiar Bursting Nature of CP Pup

M. Veresvarska,^{1*} S. Scaringi,¹ S. Hagen,¹ D. De Martino,² C. Done,¹ K. Ilkiewicz,^{1,3}
C. Knigge,⁴ C. Littlefield⁵

¹Centre for Extragalactic Astronomy, Department of Physics, Durham University, South Road, Durham, DH1 3LE

²INAF-Osservatorio Astronomico di Capodimonte, Salita Moiariello 16, I-80131 Naples, Italy

³Astronomical Observatory, University of Warsaw, Al. Ujazdowskie 4, 00-478 Warszawa, Poland

⁴School of Physics and Astronomy, University of Southampton, Highfield, Southampton SO17 1BJ, UK

⁵Bay Area Environmental Research Institute, Moffett Field, CA 94035, USA

Accepted XXX. Received YYY; in original form ZZZ

ABSTRACT

The classical nova CP Puppis has been observed to have particularly puzzling and peculiar properties. In particular, this classical nova displays occasional bursts in its long-term *ASAS-SN* light curve. Here we report on 5 sectors of *TESS* data displaying 2 of these rapid bursts, lasting ~ 1 day. Based on the estimated lower energy limits of the bursts we discuss whether the bursts may be examples of micronovae resulting from localised thermonuclear explosion. Furthermore, its orbital period remains uncertain, with several inconsistent periodic signals appearing in spectroscopic and photometric observations at various wavelengths. Although we cannot unambiguously unravel the physical origin of the signals, the previously suggested nature of CP Puppis as a long orbital period system may be a viable explanation. The recurrence time of the bursts in CP Puppis, together with the unexplained variable modulations make it a prime candidate for intense monitoring.

Key words: accretion – accretion discs – novae, cataclysmic variables – individual: CP Pup

1 INTRODUCTION

CP Puppis (CP Pup hereafter) is a well studied cataclysmic variable that has undergone a nova explosion in 1942. It is an unusually bright and fast example of a nova explosion, with the difference in amplitude of apparent magnitude of ~ 17 mag (Payne-Gaposchkin 1964). It is also a particularly fast nova with $t_3 \sim 6.5$ d (Payne-Gaposchkin 1964), where t_3 represents the time it takes for the nova luminosity to decline by 3 magnitudes. It has been reported that since the nova explosion the brightness levels of the nova have yet to return to the pre-burst quiescence level (Schaefer & Collazzi 2010). Similarities can be drawn between CP Pup and V1500 Cyg (Della Valle & Livio 1998), which is also uncharacteristically brighter and has also remained brighter post eruption. CP Pup is also suggested to have a magnetic accretor (Balman et al. 1995; Orio et al. 2009; Mason et al. 2013).

One of the main peculiarities of CP Pup is its elusive orbital period. There have been spectroscopic (Bianchini et al. 1985; Duerbeck et al. 1987; O’Donoghue et al. 1989; White et al. 1993; Bianchini et al. 2012; Mason et al. 2013) and photometric (Warner 1985; O’Donoghue et al. 1989; Diaz & Steiner 1991; White et al. 1993; Bruch 2022) periods reported between 0.06115 days and 0.06834 days. A summary of all these is provided in Bruch (2022). Both spectroscopic and photometric periods reported in literature lie in a similar range, with most of the spectroscopic periods being shorter. Furthermore, the spectroscopic periods have been reported to show large scatter in the folded radial velocity curve (Bianchini et al. 2012).

It is worth noting that the spectroscopic and photometric periods in the literature are inconsistent with each other (Diaz & Steiner 1991). Orio et al. (2009) has further reported 3 periods from *XMM-Newton* data. However, due to the large uncertainty, the periods quoted in Orio et al. (2009) are consistent with each other, as well as consistent with previously reported spectroscopic and photometric periods (see summary by Bianchini et al. (2012) and Bruch (2022)).

If taken at face value as the orbital period, all the reported values are short for known classical novae and non-magnetic nova-likes in general (~ 3 hours), making CP Pup one of a handful of novae with a potential period reported below the period gap (Bianchini et al. 1985; Marelli et al. 2018). It has thus been suggested that CP Pup is a system whose disc is always hot and bright, and often exhibits superhumps, persisting in a state similar to SU UMa type dwarf novae during superoutburst (Warner 1985; Patterson & Warner 1998; Patterson et al. 2013).

Further interpretations of the period assigned it to the spin of the magnetic white dwarf, suggesting a white dwarf slightly out of spin-orbit synchronism (Warner 1985; Diaz & Steiner 1991; Balman et al. 1995). Asynchronous polars are not the only option for the magnetic interpretation of CP Pup. Orio et al. (2009) and Mason et al. (2013) consider the hypothesis of CP Pup being an intermediate polar. However, there is a lack of conclusive evidence for either interpretation.

The peculiar nature of CP Pup extends to other observations too. The relatively recent nova explosion, with its characteristics such as peak absolute magnitude, suggests a high mass white dwarf (WD), due to the smaller physical accretor size resulting in higher pressure, making it more favourable to trigger a nova explosion (Priyalnik &

* E-mail: martina.veresvarska@durham.ac.uk

Measuring eccentricity and gas-induced perturbation from gravitational waves of LISA massive black hole binaries

Mudit Garg,^{1*} Andrea Derdzinski,^{1,2,3} Shubhanshu Tiwari,⁴ Jonathan Gair,⁵ and Lucio Mayer¹

¹*Department of Astrophysics, University of Zurich, Winterthurerstrasse 190, CH-8057 Zürich, Switzerland*

²*Department of Life and Physical Sciences, Fisk University, 1000 17th Avenue N., Nashville, TN 37208, USA*

³*Department of Physics & Astronomy, Vanderbilt University, 2301 Vanderbilt Place, Nashville, TN 37235, USA*

⁴*Physik-Institut, Universität Zürich, Winterthurerstrasse 190, 8057 Zürich, Switzerland*

⁵*Max Planck Institute for Gravitational Physics (Albert Einstein Institute), Am Mühlenberg 1, Potsdam 14476, Germany*

Received / Accepted

ABSTRACT

We assess the possibility of detecting both eccentricity and gas effects (migration and accretion) in the gravitational wave (GW) signal from LISA massive black hole binaries (MBHBs) at redshift $z = 1$. Gas induces a phase correction to the GW signal with an effective amplitude (C_g) and a semi-major axis dependence (assumed to follow a power-law with slope n_g). We use a complete model of the LISA response, and employ a gas-corrected post-Newtonian in-spiral-only waveform model TAYLORF2ECC. By using the Fisher formalism and Bayesian inference, we explore LISA's ability to constrain C_g together with the initial eccentricity e_0 , the total redshifted mass M_z , the primary-to-secondary mass ratio q , the dimensionless spins $\chi_{1,2}$ of both component BHs, and the time of coalescence t_c . We find that simultaneously constraining C_g and e_0 leads to worse constraints on both parameters with respect to when considered individually. Assuming a standard thin viscous accretion disc, for $M_z = 10^6 M_\odot$, $q = 8$, $\chi_{1,2} = 0.9$, and $t_c = 4$ years, we can confidently measure (with a relative error of < 50 per cent) an Eddington ratio as small as $f_{\text{Edd}} \sim 0.1$ for a circular binary while for an eccentric system only $f_{\text{Edd}} \gtrsim 1$ can be inferred. The minimum measurable eccentricity is $e_0 \gtrsim 10^{-2.75}$ in vacuum and $e_0 \gtrsim 10^{-2}$ in the presence of a circumbinary disc. A weak environmental perturbation ($f_{\text{Edd}} \lesssim 1$) to a circular binary can be mimicked by an orbital eccentricity during in-spiral, implying that an electromagnetic counterpart would be required to confirm the presence of an accretion disc.

Key words: methods: data analysis – methods: statistical – black hole physics – gravitational waves – accretion, accretion discs.

1 INTRODUCTION

The prospect of the observation of gravitational waves (GWs) in the mHz band in the 2030s looks promising following the adoption by ESA of the Laser Interferometer Space Antenna (LISA; Amaro-Seoane et al. 2017; Barack et al. 2019) and with other projects, such as TianQin (Wang et al. 2019) and Taiji (Gong et al. 2021), being developed. One of the primary expected extragalactic sources for LISA are massive black hole binaries (MBHBs) with primary-to-secondary mass ratios $q \lesssim 10$ and total masses between $10^4 M_\odot$ and $10^8 M_\odot$, which LISA will be able to observe up to redshift $z \sim 20$ (Amaro-Seoane et al. 2017). Another expected source are intermediate/extreme mass ratio inspirals (I/EMRIs; Babak et al. 2017; Amaro-Seoane 2018) with $q \gtrsim 10^2$, which can be observed up to $z \lesssim 2$. MBHBs, with their high signal-to-noise

ratios (SNRs; Amaro-Seoane et al. 2017), provide exciting opportunities to not only measure source properties with high accuracy but also place constraints on the properties of their environments.

The main formation channel for MBHBs is via galaxy mergers (Begelman et al. 1980). To shrink these binaries from a large scale to the coalescence phase within a Hubble time requires an environmental perturbation that could come from either gas or stars (see, e.g. Amaro-Seoane et al. 2023). In this paper, we will be primarily concerned with the dynamical effects of gas, as they can non-negligibly perturb both the semi-major axis and eccentricity of MBHBs in the LISA regime more strongly than stellar interactions, given the tight separations. Therefore, when we refer to an environment we will always mean a gas accretion disc. MBHBs are often observed to be accompanied by an accretion disc at the center of active galactic nuclei (AGN) galaxies, especially beyond $z \gtrsim 1$ and up to $z \lesssim 7$ (Padovani et al. 2017). Therefore, as galaxy

* E-mail: mudit.garg@ics.uzh.ch

Detection of Diffuse Hot Gas Around the Young, Potential Superstar Cluster H72.97–69.39

TRINITY L. WEBB,¹ JENNIFER A. RODRIGUEZ,¹

THESE AUTHORS CONTRIBUTED EQUALLY TO THIS WORK.

LAURA A. LOPEZ,^{1,2,3} ANNA L. ROSEN,^{4,5} LACHLAN LANCASTER,^{6,3,*} OMNARAYANI NAYAK,⁷ ANNA F. MCLEOD,^{8,9}
PAARMITA PANDEY,^{1,2} GRACE M. OLIVIER¹⁰

¹*Department of Astronomy, The Ohio State University, 140 W. 18th Ave., Columbus, OH 43210, USA*

²*Center for Cosmology and AstroParticle Physics, The Ohio State University, 191 W. Woodruff Ave., Columbus, OH 43210, USA*

³*Center for Computational Astrophysics, Flatiron Institute, 162 5th Avenue, New York, NY 10010, USA*

⁴*Department of Astronomy, San Diego State University, 5500 Campanile Dr, San Diego, CA 92182, USA*

⁵*Computational Science Research Center, San Diego State University, 5500 Campanile Dr, San Diego, CA 92182, USA*

⁶*Department of Astronomy, Columbia University, 550 W 120th St, New York, NY 10025, USA*

⁷*Space Telescope Science Institute, 3700 San Martin Drive, Baltimore, MD 21218, USA*

⁸*Centre for Extragalactic Astronomy, Department of Physics, Durham University, South Road, Durham DH1 3LE, UK*

⁹*Institute for Computational Cosmology, Department of Physics, University of Durham, South Road, Durham DH1 3LE, UK*

¹⁰*Department of Physics and Astronomy and George P. and Cynthia Woods Mitchell Institute for Fundamental Physics and Astronomy, Texas A&M Univeersity, 4242 TAMU, College Station, TX 77843-4242 USA*

ABSTRACT

We present the first Chandra X-ray observations of H72.97–69.39, a highly-embedded, potential super-star cluster (SSC) in its infancy located in the star-forming complex N79 of the Large Magellanic Cloud. We detect particularly hard, diffuse X-ray emission that is coincident with the young stellar object (YSO) clusters identified with JWST, and the hot gas fills cavities in the dense gas mapped by ALMA. The X-ray spectra are best fit with either a thermal plasma or power-law model, and assuming the former, we show that the X-ray luminosity of $L_X = (1.5 \pm 0.3) \times 10^{34}$ erg s⁻¹ is a factor of ~ 20 below the expectation for a fully-confined wind bubble. Our results suggest that stellar wind feedback produces diffuse hot gas in the earliest stages of massive star cluster formation and that wind energy can be lost quickly via either turbulent mixing followed by radiative cooling or by physical leakage.

Keywords: Young star clusters — HII regions — Stellar wind bubbles

1. INTRODUCTION

Massive stars are born in clustered environments (Krumholz et al. 2019), depositing substantial energy and momentum to the surrounding interstellar medium (ISM) through a variety of feedback mechanisms. In particular, fast, line-driven stellar winds (with velocities of $v_w \sim 10^3$ km s⁻¹) sweep up surrounding gas and create low-density cavities shock-heated to $\sim 10^7$ K temperatures (Castor et al. 1975; Weaver et al. 1977; Cantó et al. 2000; Stevens & Hartwell 2003; Harper-Clark & Murray 2009). Diffuse X-ray emission associated with these fast stellar winds has been detected from numerous massive star clusters (MSCs) in the Milky Way (Moffat et al. 2002; Yusef-Zadeh et al. 2002; Townsley et al. 2003;

Muno et al. 2006; Townsley et al. 2011) and the Magellanic Clouds (Townsley et al. 2006; Lopez et al. 2011, 2014). Although the integrated kinetic energy carried in the stellar winds is comparable to the kinetic energy delivered by supernova explosions (Agertz et al. 2013), the actual dynamical impact of the stellar wind feedback and how it evolves over time remains uncertain.

One open issue is the role of winds in the early evolution of MSCs, and the study of young, embedded sources can provide important insights. Toward this end, the highly embedded N79 star-forming complex in the southwestern region of the Large Magellanic Cloud (LMC; see Figure 1), which has an accelerating star-formation rate of ~ 2 times that of the starburst region 30 Doradus (hereafter 30 Dor; Ochsendorf et al. 2017), is an ideal target to study the role of stellar wind feedback at the onset of star cluster formation. The N79 region spans across ~ 500 pc and has three giant molecular cloud (GMC) complexes - N79 East, N79 West, and N79 South (see Figure 1; Wong et al. 2011;

Corresponding author: Trinity Webb
webb.916@osu.edu

* Simons Fellow

Taking the pulse of the outer Milky Way with HOWVAST: an RR Lyrae density profile out to >200 kpc

Gustavo E. Medina^{1,2*}, Ricardo R. Muñoz³, Jeffrey L. Carlin⁴, A. Katherina Vivas⁵, Eva K. Grebel², Clara E. Martínez-Vázquez⁶, and Camilla J. Hansen⁷

¹David A. Dunlap Department of Astronomy & Astrophysics, University of Toronto, 50 St George Street, Toronto ON M5S 3H4, Canada

²Astronomisches Rechen-Institut, Zentrum für Astronomie der Universität Heidelberg, Mönchhofstr. 12-14, 69120 Heidelberg, Germany

³Departamento de Astronomía, Universidad de Chile, Camino El Observatorio 1515, Las Condes, Santiago, Chile

⁴AURA/Rubin Observatory Project Office, 950 North Cherry Avenue, Tucson, AZ 85719, USA

⁵Cerro Tololo Inter-American Observatory/NSF's NOIRLab, Casilla 603, La Serena, Chile

⁶Gemini Observatory/NSF's NOIRLab, 670 N. A'ohoku Place, Hilo, HI 96720, USA

⁷Goethe University Frankfurt, Institute for Applied Physics, Max-von-Laue Str. 11, 60438 Frankfurt am Main, Germany

Accepted XXX. Received YYY; in original form ZZZ

ABSTRACT

In order to constrain the evolutionary history of the Milky Way, we hunt for faint RR Lyrae stars (RRLs) using Dark Energy Camera data from the High cadence Transient Survey (HiTS) and the Halo Outskirts With Variable Stars (HOWVAST) survey. We report the detection of ~500 RRLs, including previously identified stars and ~90 RRLs not yet reported. We identify 9 new RRLs beyond 100 kpc from the Sun, most of which are classified as fundamental-mode pulsators. The periods and amplitudes of the distant RRLs do not place them in either one of the two classical Oosterhoff groups, but in the Oosterhoff intermediate region. We detect two groups of clumped distant RRLs with similar distances and equatorial coordinates, which we interpret as an indication of their association with undiscovered bound or unbound satellites. We study the halo density profile using spheroidal and ellipsoidal ($q = 0.7$) models, following a Markov chain Monte Carlo methodology. For a spheroidal halo, our derived radial profile is consistent with a broken power-law with a break at $18.1^{+2.1}_{-1.1}$ kpc separating the inner and the outer halo, and an outer slope of $-4.47^{+0.11}_{-0.18}$. For an ellipsoidal halo, the break is located at $24.3^{+2.6}_{-3.2}$ kpc and the outer slope is $-4.57^{+0.17}_{-0.25}$. The break in the density profile is a feature visible in different directions of the halo. The similarity of these radial distributions with previous values reported in the literature seems to depend on the regions of the sky surveyed (direction and total area) and halo tracer used. Our findings are compatible with simulations and observations that predict that the outer regions of Milky Way-like galaxies are mainly composed of accreted material.

Key words: Galaxy: halo – Galaxy: structure – Galaxy: stellar content – stars: variables: RR Lyrae – surveys

1 INTRODUCTION

In the currently favoured cosmological framework, the Λ cold dark matter (Λ -CDM) model, galaxies assemble hierarchically through the accretion of smaller systems. The Milky Way (MW) and similar massive disc galaxies likely experienced numerous mergers in their early history as part of their hierarchical formation (see, e.g., Press & Schechter 1974; Blumenthal et al. 1984; Bullock & Johnston 2005; Montalbán et al. 2021). The stellar halos of these galaxies provide key information to help reconstruct their formation conditions. For the MW, in particular, compelling evidence for past and ongoing accretion events have been identified in present-day inner and outer halo stellar populations, unveiling details of gravitational interactions with massive satellites such as the Sagittarius stream (e.g.,

Ibata, Gilmore, & Irwin 1994; Majewski et al. 2003; Vivas & Zinn 2006), Gaia-Sausage-Enceladus (GSE; e.g., Belokurov et al. 2018b; Helmi et al. 2018; Haywood et al. 2018), and the infall of the Magellanic Clouds (e.g., Mathewson, Cleary, & Murray 1974; Besla et al. 2007; Zaritsky et al. 2020; Erkal et al. 2021).

The accretion history of a particular halo is also imprinted in the shape of its stellar density profile (e.g., Bullock & Johnston 2005; Cooper et al. 2013), as the mass distribution is sensitive to properties such as the halo formation time, the amount of stellar mass accreted, and how long ago the last mergers took place (see e.g. Pillepich et al. 2014). The slope of the number density profile of outer halo stars, in particular, has been shown to be a parameter of cosmological significance, closely related to the accretion history of MW-like galaxies (Jurić et al. 2008; Pillepich et al. 2014; Merritt et al. 2016; Slater et al. 2016).

However, well-characterized MW stars with precisely determined distances and reliable classifications at large distances are rare, espe-

* E-mail: gustavo.medina@astro.utoronto.ca

On the initial spin period distribution of neutron stars

SHEN-SHI DU ^{1,2} XIAO-JIN LIU ^{2,3} ZU-CHENG CHEN ^{2,3,4,5} ZHI-QIANG YOU ^{2,3,6} XING-JIANG ZHU ^{2,7} AND
ZONG-HONG ZHU¹

¹*School of Physics and Technology, Wuhan University, Wuhan, Hubei 430072, China*

²*Advanced Institute of Natural Sciences, Beijing Normal University, Zhuhai 519087, China*

³*Department of Astronomy, Beijing Normal University, Beijing 100875, China*

⁴*Department of Physics and Synergetic Innovation Center for Quantum Effects and Applications, Hunan Normal University, Changsha, Hunan 410081, China*

⁵*Institute of Interdisciplinary Studies, Hunan Normal University, Changsha, Hunan 410081, China*

⁶*Henan Academy of Sciences, Zhengzhou 450046, Henan, China*

⁷*Department of Physics, Faculty of Arts and Sciences, Beijing Normal University, Zhuhai 519087, China*

ABSTRACT

We derive the initial spin period distribution of neutron stars by studying the population of young pulsars associated with supernova remnants. Our hierarchical Bayesian approach accounts for the measurement uncertainties of individual observations and selection effects. Without correcting for selection effects, as done in previous studies, we find that pulsar initial spin periods follow a Weibull distribution, peaking at 40 ms, which is favoured against the lognormal distribution with a Bayes factor of 200. The known selection effects in radio pulsar surveys, including pulse broadening and a period-dependent beaming fraction, have been quantitatively investigated. We show that, based on measurements of pulsar luminosity and spin period from the ATNF Pulsar Catalogue, the impact of pulse broadening on the inference of pulsar initial period distribution is likely to be insignificant. Correcting for the beaming selection effect, a Weibull distribution remains to be the preferred model, while its peak slightly shifts to longer periods at 50 ms. Our method will prove useful in constraining the birth properties of neutron stars in the Square Kilometre Array era.

Keywords: Neutron stars(1108) — Supernova remnants(1667) — Bayesian statistics(1900)

1. INTRODUCTION

Pulsars are fast rotating, highly magnetized neutron stars (NSs). Since the first discovery (Hewish et al. 1968), the number of observed pulsars has grown to over 3500 (see the Australia Telescope National Facility (ATNF) Pulsar Catalogue¹, Manchester et al. 2005), a majority of which are detected in the radio band. Among them, pulsars observed in association with supernova remnants (SNRs) are of particular interest, since their ages are independently informed by observations of SNRs. The Crab pulsar is the best known

example. Firmly established as the remnant star of supernova 1054, its initial spin period is around 20 ms, close to its current spin period of 33 ms. This is widely used as a proxy for pulsar initial spin periods in the community (e.g., Johnston & Karastergiou 2017).

The astrophysical processes that give rise to NS spins are poorly understood. A range of spin periods from milliseconds to seconds are predicted in a variety of processes during supernova explosions. Newborn NSs could inherit the angular momentum of progenitor stars from the collapsing iron cores (Heger et al. 2005; Ott et al. 2006), where the angular momentum transport and mass loss in single stars play a significant role (Fuller et al. 2014, 2015, 2019; Ma & Fuller 2019; Eggenberger et al. 2019). For instance, Ott et al. (2006) found that an NS could be born with periods of tens to hundreds of milliseconds if the spin periods of iron cores are around 50–100 s. NS spins could also stem from the natal kicks

Corresponding author: Xing-Jiang Zhu
zhuxj@bnu.edu.cn

Corresponding author: Zong-Hong Zhu
zzh@whu.edu.cn

¹ <https://www.atnf.csiro.au/research/pulsar/psrcat/>